Sede Amministrativa: Università degli Studi di Padova

Dipartimento di Scienze Biomediche

CORSO DI DOTTORATO DI RICERCA IN: SCIENZE BIOMEDICHE SPERIMENTALI

CICLO XXXII

Relationship between mitochondrial ROS formation catalyzed by monoamine oxidase and autophagy in diabetic cardiomyopathy

Coordinatore: Ch.mo Prof. Paolo Bernardi

Supervisore: Ch.mo Prof. Fabio Di Lisa

Co-Supervisore: Dr. Nina Kaludercic

Dottorando: Carmen Troiano

Alla mia famiglia…

INDEX

ABBREVIATIONS

ACTB	Actin beta
ADP	Adenosine di-phosphate
AKT (PKB)	Protein Kinase B
AMP	Adenosine monophosphate
AMPK	Adenosine monophosphate-activated protein kinase
AMVMs	Adult mouse ventricular myocytes
ANGPTL4	Angiopoietin Like 4
ANP	Natriuretic Peptide A
ATG	Autophagy-related genes
ATP	Adenosine triphosphate
BNIP3L	Mitochondrial BCL2 Interacting Protein 3 Like L
CAD	Coronary artery disease
CAMKII	Calcium activates Ca2+/calmodulin-dependent protein kinase II
CMA	Chaperone-mediated autophagy
CQ	Chloroquine
CVD	Cardiovascular disease
DCM	Diabetic Cardiomyopathy
DKA	Diabetic ketoacidosis
DMEM	Dulbecco's modified Eagle's medium
DRP1	Dynamin-related protein 1
ECM	Extra-cellular matrix
ERK	Extracellular signal regulated kinase
ES	Enrichment score
ETC	Electron transport chain
FAD	Flavin adenine dinucleotide
FAO	Fatty acids oxidation
FBS	Fetal bovine serum
GAPDH	Glyceraldehyde-3-Phosphate Dehydrogenase
GLUT	Glucose transporter
GLUT4	Glucose Transporter Type 4, Insulin-Responsive
GO	Gene ontology

GSEA	Gene Set Enrichment Analysis
GSK-3 β	Glycogen Synthase Kinase-3β
H_2O_2	Hydrogen peroxide
HF	Heart failure
HG	High glucose
HHS	Hyperglycaemic hyperosmolar state
HIF1α	Hypoxia Inducible Factor 1 Subunit Alpha
HM	High mannitol
I/R	Ischemia/reperfusion
IMM/OMM	Inner/Outer Mitochondrial Membrane
IR	Insulin receptor
IRS	Insulin receptor substrates
LAMP-2A	Lysosome-associated membrane protein type 2A
LSD1	Histone lysine-specific demethylase 1
LV	Left ventricle
MAOs	Monoamine Oxidases
MAP1LC3 (LC3)	Microtubule-associated protein 1A/1B light chain 3
MAPK	Mitogen-activated protein kinase
MFF	Mitochondrial fission factor
MFN1-2	Mitofusins 1-2
mPTP	Mitochondrial permeability transition pore
mTOR	Mammalian target of rapamycin
mTORC1	Mammalian target of rapamycin complex 1
NAD	Nicotinamide adenine dinucleotide
NG	Normal glucose
NLRP3	Nucleotide-binding oligomerization domain-like receptors with pyrin domain
NOX	NADPH oxidase
OPA1	Optic atrophy protein-1
PAD	Peripheral artery disease
PAS	Phagophore assembly site
PDK1	Pyruvate Dehydrogenase Kinase 1
PDK4	Pyruvate Dehydrogenase Kinase 4

PI3K	Phosphoinositide 3-kinase
PINK1	PTEN-induced putative kinase1
PIP2	Phosphatidylinositol 4,5-bisphosphate
PIP3	Phosphatidylinositol 3,4,5-trisphosphate
RGS2	Regulator Of G Protein Signaling 2
ROS	Reactive oxygen species
RPL4	Ribosomal Protein L4
SGLT	Na^+/glucose cotransporter family
STZ	Streptozotocin
T1D	Type 1 diabetes
T2D	Type 2 diabetes
TBP	TATA-Box Binding Protein
TGF-B	Transforming growth factor-β
TXNIP	Thioredoxin Interacting Protein
XO	Xanthine oxidase
ΔΨm	Mitochondrial membrane potential

SOMMARIO

In questo studio, l'obiettivo era di indagare le variazioni di espressione indotte dal diabete nel cuore e se la generazione delle specie reattive dell'ossigeno (ROS) dipendente dalle monoammine ossidasi (MAO) influisse sul trascrittoma cardiaco nel diabete di tipo 1 (T1D). Inoltre, abbiamo studiato il significato biologico e funzionale di tali cambiamenti nell'espressione genica. Il profilo di espressione genica è stato valutato mediante microarray nel tessuto cardiaco ottenuto da un modello murino di T1D indotto con streptozotocina (STZ), mentre il coinvolgimento delle MAO è stato valutato con un approccio farmacologico, usando la pargilina. Sono stati esaminati i seguenti gruppi: (i) topi di controllo, (ii) topi trattati con STZ, (iii) topi di controllo trattati con pargilina, (iv) topi STZ trattati con pargilina. L'analisi dei geni differenzialmente espressi ha messo in luce gruppi in cui i campioni sono raggruppati in modo peculiare e gerarchico. L'analisi ha mostrato che il profilo dei cuori diabetici formava un gruppo distinto e si posizionava separatamente dagli altri gruppi. Il profilo dei cuori diabetici trattati con pargilina era simile a quello dei cuori di controllo. Successivamente, i geni sono stati raggruppati in base a specifici modelli di espressione e abbiamo focalizzato la nostra attenzione su quelli in cui la pargilina previene tali cambiamenti indotti dal diabete.

I geni scelti sono stati classificati in base al vocabolario di Gene Ontology (GO) e sono state prese in considerazione solo definizioni arricchite. Le classi GO più rappresentate nei geni iporegolati nel diabete erano quelle per nucleo, citoscheletro e membrana plasmatica. Le categorie GO più rappresentate tra i geni sovraregolati erano quelle per nucleo, mitocondrio, citoscheletro e vacuolo. La Gene Set Enrichment Analysis e ulteriori analisi hanno mostrato che i geni sovraespressi con il valore più alto di arricchimento appartengono alle categorie dei mitocondri, della matrice extracellulare, e dei processi catabolici. La pargilina ha prevenuto tali variazioni.

Considerando i precedenti lavori pubblicati in laboratorio e i risultati trascrittomici, abbiamo ipotizzato che le ROS mitocondriali indotte dal diabete e l'attività delle MAO possano influire sull'autofagia. L'incremento di LC3 (catena leggera proteica 3 associata ai microtubuli)-II osservato nei cuori diabetici è prevenuto dal trattamento con la pargilina che causa anche un aumento dei livelli di p62, suggerendo una riduzione del flusso autofagico. Ulteriori analisi sui cambiamenti nel flusso autofagico sono stati condotti in cardiomiociti di topo adulti trattati con alto glucosio in assenza o presenza di pargilina e / o inibitore della degradazione lisosomiale clorochina.

Le cellule mantenute in alto glucosio e pargilina hanno mostrato una riduzione drammatica del flusso autofagico che non si è verificata nel controllo. Inoltre, la fosforilazione della proteina chinasi attivata da AMP ha mostrato un andamento decrescente in cardiomiociti trattati con alto glucosio e pargilina. Inoltre, abbiamo osservato un aumento dei livelli del fattore di fissione mitocondriale nelle cellule esposte ad alto glucosio. Questo evento è stato drasticamente ridotto con l'inibizione delle MAO. È interessante notare che anche la fosforilazione di DRP1 su Ser616 ha mostrato un andamento decrescente.

In aggiunta agli studi precedenti, i risultati attuali suggeriscono che il diabete comporta profondi cambiamenti trascrittomici nel cuore di topi T1D e l'inibizione delle MAO previene tali modificazioni, influenzando i mitocondri, la matrice extracellulare ed i processi catabolici. Inoltre. la formazione delle ROS MAO-dipendente, innescata dall'alto glucosio, agisce come un segnale che determina l'attivazione dell'autofagia. In conclusione, i nostri risultati forniscono la prima evidenza che la formazione delle ROS mitocondriali e, soprattutto, l'attività delle MAO modulino l'autofagia cardiaca nella cardiomiopatia diabetica.

SUMMARY

Diabetic cardiomyopathy (DCM) represents the major and leading cause of morbidity and mortality in diabetic patients. This study aimed at investigating changes in the gene expression profile induced by diabetes in the cardiac tissue and whether monoamine oxidases (MAO)-dependent reactive oxygen species (ROS) generation affects the transcriptome in type 1 diabetes (T1D) hearts. Moreover, we investigated the biological and functional significance of such changes in gene expression focusing on autophagy. Gene expression profile was evaluated by microarray in the cardiac tissue from a mouse model of T1D induced by treatment with streptozotocin (STZ), while MAO involvement were evaluated through a classical pharmacological approach, using pargyline as an inhibitor for both MAO-A and MAO-B. The following groups were examined: (i) control mice, (ii) STZ-treated mice, (iii) control mice treated with pargyline, (iv) STZ mice treated with pargyline. The analysis of differentially expressed genes showed that profile of samples from STZ-mice formed a distinct group and positioned itself separately from all the other groups. Notably, the expression profile of diabetic hearts treated with pargyline was similar to the expression profile of control hearts. Importantly, pargyline treatment did not affect the gene expression profile of control mice. Subsequently, genes were clustered based on specific expression patterns and we focused on genes in which pargyline prevents changes in gene expression induced by diabetes.

Chosen genes were classified according to the Gene Ontology (GO) vocabulary and only enriched definitions were considered. Most represented GO classes in downregulated genes in diabetic conditions were those for nucleus, cytoskeleton and plasma membrane. Notably, the most represented GO categories within upregulated genes were those for nucleus, mitochondrion, cytoskeleton and vacuole. Gene Set Enrichment Analysis and the leading-edge analysis showed that overexpressed genes with the highest enrichment score belong to mitochondria, extracellular matrix (ECM), and catabolic processes. Pargyline administration prevented these changes.

Considering our previous studies and the transcriptomic results, we hypothesized that mitochondrial ROS formation induced by diabetes and MAO activity could affect autophagy. The increase in LC3 (microtubule-associated protein light chain 3)-II occurring in diabetic hearts was prevented by pargyline that also caused an increase in p62 levels suggesting a reduction in the autophagic flux. Further analysis of changes

in the autophagy flux was performed in adult mouse cardiomyocytes (AMVMs) cultured with high glucose (HG) in the absence or presence of pargyline and/or inhibitor of lysosomal degradation chloroquine. Cells cultured in presence of HG and pargyline displayed a dramatic reduction in the autophagy flux that was not affected in control. Moreover, phosphorylation of AMP-activated protein kinase showed a trend to decrease in AMVMs treated with HG and pargyline. Moreover, regarding mitochondrial dynamics, we observed increased levels of mitochondrial fission factor in cells exposed to HG. This event was dramatically reduced upon MAO inhibition. Interestingly, phosphorylation of dynamin-related protein 1 on Ser616 also showed a decreasing trend.

In addition to previous studies from laboratory of Prof. Di Lisa, the present results suggest that diabetes leads to profound transcriptomic changes in STZ-treated mice heart and MAO inhibition prevents such changes affecting mitochondria, ECM, and catabolic processes. Furthermore, MAO-dependent ROS formation triggered by HG acts as a signal that leads to autophagy activation. Finally, mitochondrial fission is likely reduced upon MAO inhibition in AMVMs exposed to HG. Taken together, our results provide the first evidence that mitochondrial ROS formation and specifically MAO activity modulate cardiac autophagy in DCM.

I. INTRODUCTION

1.1Diabetes

Diabetes is a chronic metabolic condition associated with cellular dysfunction in the transport and utilization of glucose. Diabetes causes a high human, social and economic cost.

In healthy condition, pancreatic β-cells release the hormone insulin in the blood stream that increases the uptake of glucose in adipose tissue and muscle. The absence of insulin or the inability of the cells to respond to insulin leads to high levels of glucose in the blood, or hyperglycaemia, which is one of the hallmarks of diabetes. Hyperglycaemia, if left unchecked over a long period, can cause damage to various body organs, leading to the development of disabling and life-threatening health complications such as cardiovascular disease, neuropathy, nephropathy, and retinopathy[1,2] (Figure 1).

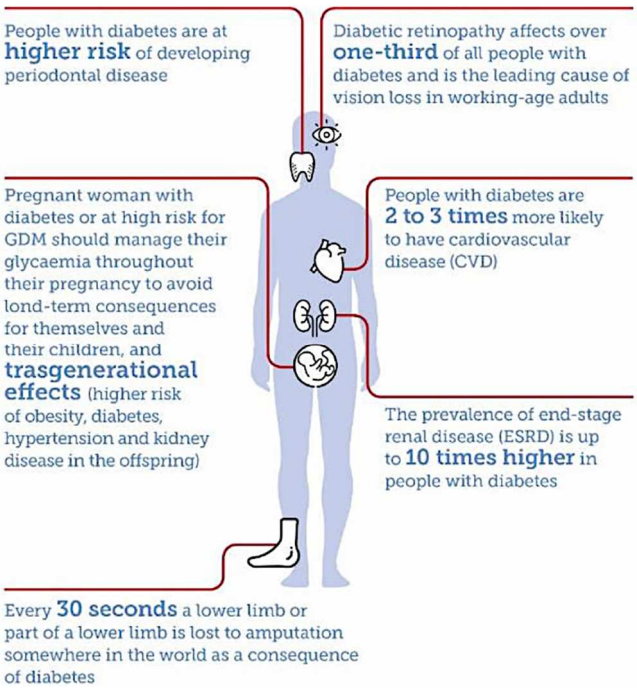

Figure 1: Diabetes complications. People with diabetes have an increased risk of developing a number of serious life-threatening health problems. Persistently high blood glucose levels cause generalized vascular damage affecting the heart, eyes, kidneys and nerves. Diabetes is one of the leading causes of cardiovascular disease, blindness, kidney failure and lower-limb amputation (*International Diabetes Federation, 2017.* http://www.diabetesatlas.org)[2].

There are two main types of diabetes, type 1 diabetes (T1D) and type 2 diabetes (T2D). T1D is characterized by insulin deficiency as a primary result of an autoimmune response

against pancreatic β-cells. In contrast, hallmarks of T2D are peripheral insulin resistance and pancreatic β-cell failure during the later course of the disease[3].

Diabetes is characterized by three central metabolic disturbances: (i) hyperlipidemia; (ii) hyperinsulinemia and pancreatic β-cell failure; and (iii) hyperglycemia. These abnormalities and other pathological mechanisms including reactive oxygen species (ROS) formation and abnormal cardiac fuel usage are believed to act synergistically and exacerbate the cardiac phenotype present in diabetes[1]. In addition, diabetes is characterized by increased fatty acids oxidation (FAO) and decreased glucose oxidation in the heart as described for T1D[4,5] and T2D patients[6,7], and several rodent models[3].

1.1.1 Insulin signaling

Glucose transport is mediated by two families of glucose transporters, facilitative glucose transporter family (GLUT) and Na^+/glucose cotransporter family (SGLT)[8]. GLUT4 is the insulin-sensitive transporter and its role has been extensively studied in diabetes. Glucose transport in cardiac tissue is mediated via GLUT4 as in skeletal muscle, liver, and fat tissue.[8–12].

Briefly, insulin activates the insulin receptor (IR, Figure 2) tyrosine kinase which phosphorylates and recruits insulin signaling/docking molecule insulin receptor substrate (IRS)-1/2. Phosphorylated IRS activates the downstream phosphoinositide 3-kinase (PI3K) that converts phosphatidylinositol 4,5-bisphosphate (PIP_2) to phosphatidylinositol 3,4,5-trisphosphate (PIP_3). PIP_3 recruits two protein kinases to the plasma membrane: protein kinase B (Akt or PKB) and phosphoinositide dependent protein kinase (PDK1), and this leads to the activation of Akt[12] (Figure 2). Activated Akt1,2 migrates to the cytosol and intracellular membranes, where it phosphorylates AS160, which catalyzes the inactivation of Rab GTPases, responsible for the regulation of vesicle fission, destination, and fusion that are crucial for GLUT4 translocation to the sarcolemma[13]. GLUT4 can be mobilized also in relation to exercise. Indeed, muscle contraction induces glucose uptake leading to the phosphorylation of AS160 by adenosine monophosphate-activated protein kinase (AMPK). AS160 is a protein that may act as one site of convergence between insulin- and contraction- stimulated glucose uptake[14]. Muscle contraction raises intracellular concentrations of Ca^{2+} along with an increase in AMP/adenosine triphosphate (ATP) ratio leading to AMPK activation. Calcium activates Ca^{2+}/calmodulin-dependent protein kinase II (CAMKII), which then contributes to

AMPK activation[15]. Muscle glycogen suppresses AMPK signaling, thus providing a negative feedback mechanism for AMPK-mediated glucose uptake[15].

Besides insulin and muscle contraction, several other stress signals are also known to enhance glucose uptake. For instance, hypoxia, inhibitors of glycolysis and electron transport chain, and uncoupling of oxidative phosphorylation increase glucose uptake at least partially through AMPK and modulation of the AMP/ATP ratio[16].

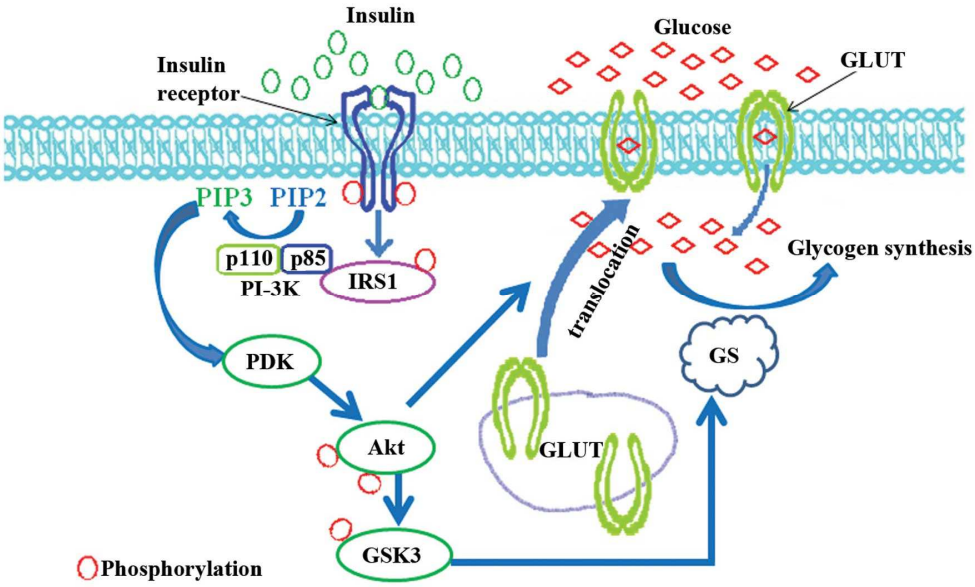

Figure 2: Glucose transport and insulin signaling. Schematic representation of insulin signaling pathway in the regulation of glucose transport. Insulin binds to the insulin receptor (IR) and promotes its autophosphorylation at tyrosine residues. Activated receptor recruits IR substrate (IRS) and enhances its activation by mediating its phosphorylation. Phosphorylated IRS activates PI3K and subsequently activates PDK1. As the upstream kinase of Akt, PDK1 promotes the phosphorylation of Akt. Activated Akt regulates glucose metabolism in two pathways. One is promoting GLUT translocation to the membrane, which mediates glucose uptake; another one is repressing the function of glycogen synthesis kinase 3 (GSK3) enhancing the activation of glycogen synthase and promoting glycogen synthesis (*Yu & Chai,* Int J Mol Med. *2015;35:305-10)*[17].

An additional branch of the insulin signaling pathway is the mitogen-activated protein kinase (MAPK) pathway, which is activated independently of PI3K/Akt. MAPKs are important modulators insulin-mediated anabolic response. Downstream of the IR, a protein-protein interaction is stimulated leading to the activation of a cascade of protein kinases (i.e. MAPK) that eventually results in the phosphorylation of transcription factors responsible for protein synthesis.

1.2Diseases associated with diabetes

Diabetes can lead to complications in many organs and tissues, resulting in frequent hospitalisations and early death. People with diabetes are at increased risk of cardiovascular disease (CVD) compared with people without diabetes. More than two-thirds of diabetic patients die from cardiovascular complications including diabetic cardiomyopathy (DCM) and heart failure[12,18].

A hallmark clinical feature of insulin-resistant individuals and T2D patients is reduced clearance of glucose from the blood, and this is mainly due to impaired insulin-stimulated glucose transport into muscle and adipocytes[11]. Persistently hyperglycaemia causes generalized vascular damage affecting all organs, especially those dependent on oxygen availability (i.e. the heart, eyes, kidneys, and nerves).

Diabetes complications can be divided into acute and chronic complications. Acute complications include, diabetic ketoacidosis (DKA), hyperglycaemic hyperosmolar state (HHS), hyperglycaemic diabetic coma, seizures or loss of consciousness[2]. The long-term vascular complications associated with diabetes are divided into two groups, (i) microvascular disease and (ii) macrovascular disease. Microvascular complications, resulting from the damage of small blood vessels, are nephropathy, neuropathy and retinopathy, whereas chronic macrovascular complications, resulting from the damage of the arteries, are coronary artery disease (CAD), peripheral artery disease (PAD), diabetic encephalopathy and stroke. In addition, diabetes has also been associated with increased rates of cancer, physical and cognitive disability, tuberculosis, and depression[2].

1.2.1 Diabetic cardiomyopathy

A prominent role in disease associated with diabetes is played by DCM that is responsible for higher incidence of sudden cardiac death and represents the leading cause of morbidity and mortality among the diabetic patients[19]. Data from experimental, epidemiologic, and clinical investigations have collectively demonstrated that DCM results in alterations in myocardial function, structure, and dimension[1]. DCM is an early complication, initially presenting as diastolic dysfunction with preserved ejection fraction in the absence of coronary atherosclerosis, hypertension, and valvular heart disease. Subsequently, diastolic dysfunction can progress to compromised systolic function resulting in heart failure with reduced ejection fraction[1,20].

Hyperglycaemia and systemic insulin resistance are associated with an increase in left ventricle mass (LV) and LV-mass to LV end-diastolic volume ratio[1,12,21].

DCM is a multi-factorial disease. Multiple factors may collectively contribute to the development and progression of DCM, but still the underlying exact cellular and molecular mechanisms are not entirely clear[1,3,22,23] (Figure 3). Several mechanisms, including oxidative stress, inflammation, mitochondrial dysfunction, metabolic derangements, autophagy, apoptosis and fibrosis have been proposed to trigger diabetes-induced cardiac damage[20]. Among various mechanisms proposed to contribute to the higher risk of heart failure in diabetic patients, oxidative stress that results from uncontrolled generation of ROS has received significant experimental and clinical evaluation[1,19]. Another candidate mechanism is autophagy that is induced by ROS upon nutrient deprivation[24].

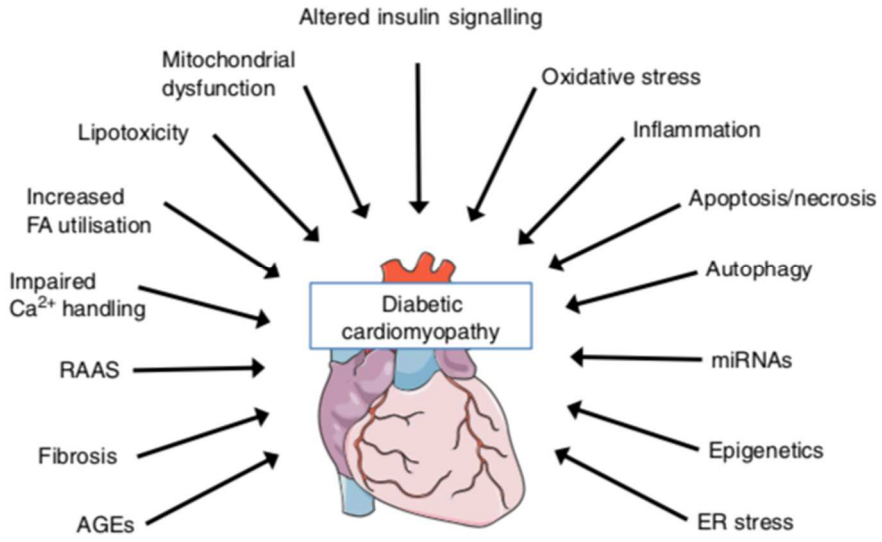

Figure 3: Schematic depiction of the multiple potential mechanisms that have been implicated in the pathophysiology of diabetic cardiomyopathy. Although depicted as separate mechanisms, these pathways interact with each other in complex ways (*Bugger & Abel, Diabetologia 2014, 57:660–671*)[20].

1.3 Reactive oxygen species and their sources

The complete reduction of O_2 inevitably implies the formation of partially reduced intermediates. These partially reduced forms of oxygen (superoxide anion, hydroxyl radical) are commonly referred to as reactive oxygen species (ROS)[25]. The imbalance between excessive formation and insufficient removal of ROS is termed oxidative stress and plays a major role in all cardiac diseases[25,26].

Current consensus is that excess generation of ROS, largely due to hyperglycemia, causes oxidative stress, which further exacerbates the development and progression of diabetes and its complications[26]. Indeed, increased ROS formation is well documented in multiple tissues in both animal and human diabetic subjects[27]. This notion is strongly supported by the ability of various antioxidants to reduce DCM in animal studies[28,29]. Nevertheless, large scale clinical trials using antioxidant therapies have not reproduced the desired results[26].

There are several sources of ROS in human cells, including, NADPH oxidase (Nox), xanthine oxidase (XO), uncoupled nitric oxide synthase (NOS), arachidonic acid and mitochondria, but their effects vary depending on the disease and the tissue[30].

NADPH oxidase is a flavocytochrome b composed of two plasma membrane protein subunits, p22-phox and either p91-phox and cytosolic components (rac, p47phox, p67phox, p40phox). NAD/NADPH oxidase is membrane bound and is the most powerful source of endogenous $O^{\cdot -}_2$ production[31].

Microorganisms can activate NO and promote translocation of its cytosolic components to the plasma membrane to form an active complex that allows transfer of electrons to molecular oxygen to generate superoxide[32]. So far, different isoforms have been described, including NOX1–5, NOX oxidase 1 and 2, NOX organizer 1, and NOX activator 1[32,33].

NOX specifically generate ROS as their primary function and their role as the major cellular ROS sources has been identified in different pathologies including cardiac diseases. Up to now, studies indicate that NOX1 and/or 2-mediated signaling may be detrimental in hypertension, atherosclerosis, cardiac hypertrophy and remodelling[34]. NOX4 may play a protective role in the heart subjected to chronic pressure overload as well as in the vasculature in the setting of hypertension[34].

The contribution of NOX to hyperglycemia-induced ROS production has also been reported[35]. It is well documented that the activity of NOX is increased in cardiomyocytes exposed to high glucose and in the heart of diabetic mice[35–37]. However, no clinical trials have been conducted with the inhibitors of these enzymes because it has not been easy to obtain specific and selective inhibitors for each NADPH oxidase isoform[35].

Xanthine oxidase (XO) is an enzyme that generates superoxide radicals and hydrogen peroxide when it catalyzes the oxidation of hypoxanthine to xanthine, and can further catalyze the oxidation of xanthine to uric acid[32].

Hypoxanthine and XO activity are also increased in diabetic subjects[38]. The role of XO in hyperglycemia-induced oxidative stress is documented by increased ROS formation in the muscle and development of fibrosis of hyperglycemic streptozotocin (STZ)-induced diabetic mice[32,39]. XO inhibition has been proven beneficial in animal studies[23] and humans[39]. Some investigators reported evidence for beneficial vascular effects of XO inhibitors in hypercholesterolemic and diabetic patients[23]. Indeed, in T1D patients XO inhibition reduced the degree of oxidative stress, whereas in T2D patients results in significant improvements in peripheral endothelium-dependent vasorelaxant function[40]. Although XO may represent an important therapeutic target, it is not suitable to treat cardiovascular complications in patients, since human heart does not contain detectable amount of these enzymes[41].

1.3.1 Mitochondrial sources of ROS

ROS are produced at various intracellular sites, yet it is generally accepted that in cardiac myocytes the largest amount of ROS are formed within mitochondria[25,42]. ROS produced by mitochondria have been implicated in the pathogenesis of diabetes and its complications[20]. In addition, mitochondrial dysfunction is a key feature of DCM observed both in cardiac tissue from diabetic patients and animal models of T1D and T2D[3,43].

ROS generation within mitochondria occurs at the level of respiratory chain complexes or is catalyzed by specific enzymes, such as monoamine oxidase (MAO) and $p66^{Shc}$ (Figure 4).

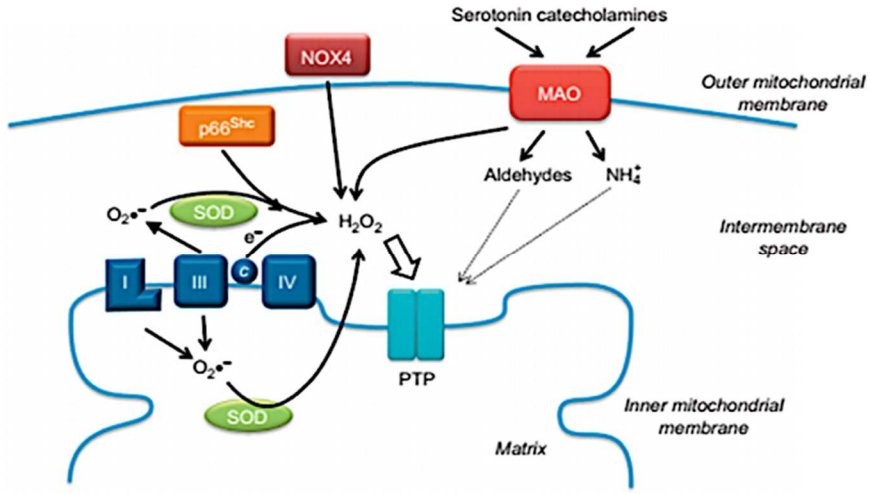

Figure 4: Schematic representation of principal mitochondrial sources of ROS. c: Cytochrome C, I, II, IV: Complexes I/II/IV, MAO: Monoamine Oxidase, NOX4: NADPH Oxidase, PTP: Permeability Transition Pore, SOD: Superoxide Dismutase (*Di Lisa, F. & Scorrano, L., 2012*)[44].

1.3.1.1 The electron transport chain

The electron transport chain (ETC, Figure 5) is the major site of ATP production in mitochondria. At the inner mitochondrial membrane (IMM), complexes of the ETC shuttle electrons to their final acceptor (oxygen) to form water by the transfer of electrons from NADH (Nicotinamide adenine dinucleotide) and $FADH_2$ (Flavin adenine dinucleotide) to oxygen[45]. In parallel, the resulting electrochemical gradient drives the translocations of protons from the mitochondrial matrix uphill across the IMM by means of the F_0F_1-ATP synthase activity[46]. This proton translocation is coupled to the phosphorylation of ADP to generate ATP[42]. At the level of the first three complexes, oxygen is partially reduced into superoxide, especially under conditions that decrease the flow of electrons towards complex IV. Electrons flowing through the respiratory chain can be donated to oxygen at other sites, but in these cases the reduction is not complete, resulting in the release of partially reduced forms.[25,42,47].

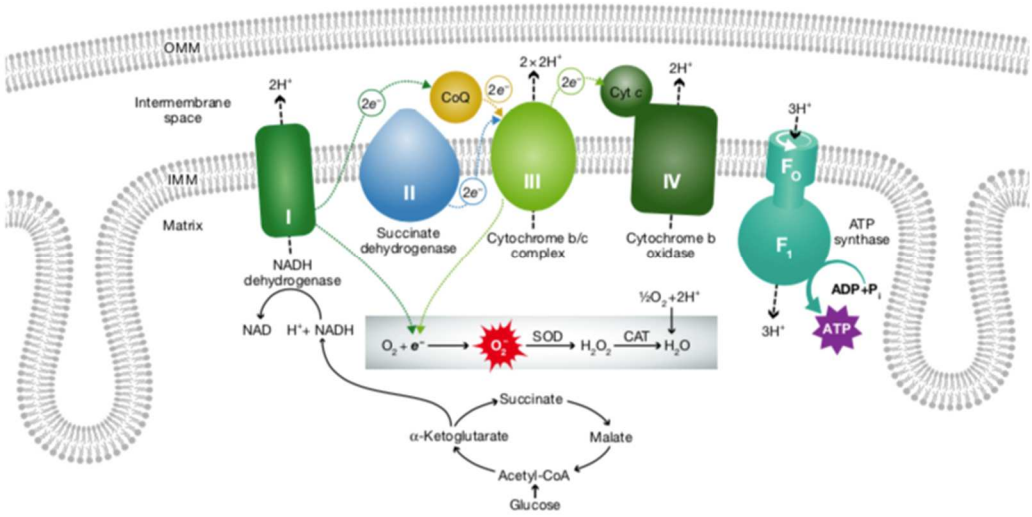

Figure 5: The ETC and its relationship with ROS production. Electrons are transferred between enzymatic complexes of the ETC, promoting proton transport from the matrix to the intermembrane space. Proton flow through F_OF_1-ATP synthase converts ADP to ATP. Normally, O_2 is the terminal electron acceptor from complex IV. Electron leak from complexes I or III of damaged mitochondria can produce toxic reactive O_2 and H_2O_2 (*Gerald W. Dorn II EMBO Mol Med (2015) 7: 865–877*)[48].

Superoxide that does not cross IMM is rapidly dismutated into the freely permeable H_2O_2 by Mn-SOD[49]. It has been shown that Mn-SOD deficient mice develop ROS toxicity and dilated cardiomyopathy[50]. Moreover, increased catalase expression or inhibition of ETC complexes I and II with rotenone and thenoyltrifluoroacetone, respectively, attenuate ROS formation in cardiomyocytes from animals with T1D and T2D[51,52].

Hyperglycemia-induced ROS formation is not observed in rho zero (ρ0) endothelial cells in which mitochondrial DNA is depleted and ETC is not functional. In addition, it is not possible to inhibit the respiratory chain in humans without affecting a wide array of vital functions. Thus, inhibition of the ETC complexes cannot be considered as potential therapeutic strategy for the treatment of this multifactorial disease.

1.3.1.2 p66^{Shc}

p66^{Shc} is a cytosolic adaptor protein present in all vertebrates[25,53–55]. Unlike its splice variants (p52^{Shc} and p46^{Shc}), p66^{Shc} is involved in the intracellular pathway(s) that regulates ROS metabolism and apoptosis[55,56]. Under stress conditions, this enzyme translocates to mitochondria and reacts with cytochrome c[57] sequestering electrons from the ETC to generate H_2O_2[25,53]. Therefore, the increase in mitochondrial ROS formation caused by p66^{Shc} contributes to mitochondrial ROS formation as it has been highlighted in a wide array of physiological and pathological conditions[53,56].

Several studies suggest a pivotal role of $p66^{Shc}$ in cardiovascular pathophysiology[25]. Cells and mice lacking $p66^{Shc}$ show reduction in markers of oxidative stress[56]. Mice lacking $p66^{Shc}$ show a significant reduction in both the occurrence of apoptosis and the degree of hypertrophy[25,58]. Moreover, the lack of $p66^{Shc}$ was shown to protect against diabetic cardiomyopathy by preventing the senescence of cardiac progenitor cells[25]. Cardiac protection was demonstrated in mouse hearts exposed to ischaemia and reperfusion[53,56]. Indeed, cardiac deletion of $p66^{Shc}$ resulted in increased viability and decreased oxidative stress[56]. Although it is widely accepted that mice lacking $p66^{Shc}$ display better functional recovery and decreased damage during reperfusion, studies highlight the potential protective effect of ROS induced by $p66^{Shc}$. Despite the role of $p66^{Shc}$ in severe oxidative stress in the heart is widely accepted, at the moment there are no drugs available that can prevent or modulate ROS forming activity of $p66^{Shc}$.

1.3.1.3 Monoamine oxidases

1.3.1.3.1 The structure of monoamine oxidases

Monoamine oxidases are flavoenzymes located at the outer mitochondrial membrane that catalyze the oxidative deamination of catecholamines and biogenic amines releasing hydrogen peroxide (H_2O_2), aldehydes and ammonia[59–61]. They have been classified in two isoenzymes A (MAO-A) and B (MAO-B) and are distinguished by substrate specificity and sensitivity to inhibitors[62]. The two isoforms (Figure 6) share 70% homology in their primary sequence. Both of them contain the obligatory cofactor FAD, necessary for catalysis, which is covalently bound to cysteine residue, namely Cys406 in MAO-A and Cys397 in MAO-B[61]. Although human MAO-A is monomeric and MAO-B is dimeric, both isoforms display a dimerization in their membrane-bound forms[61,63–70]. Instead rat MAO-A has a dimeric structure that is similar to that of human MAO-B[65,66,71].
The active site of MAOs consists of a hydrophobic cavity (about 500 Å and 700 Å in MAO A and MAO B, respectively) that extends from the core of the globular body in front of the flavin to the protein surface[65,66].
Genes encoding for MAO-A and MAO-B are located side-by-side on the short arm of X-chromosome and have 92% similarity in their sequence. In both genes, exon 12 encodes for the covalent FAD binding site and is the most conserved exon, showing 94% amino acid identity between MAO-A and B[64].

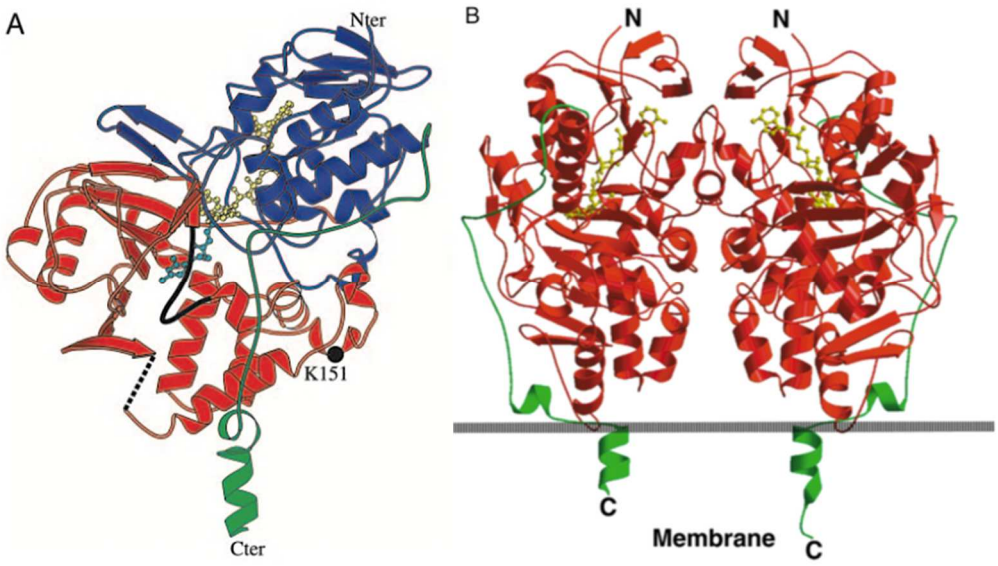

Figure 6: Ribbon structures of hMAO. (A) Overall structure of MAO-A. The FAD-binding domain is in blue; the substrate-binding domain is in red; and the C-terminal membrane region is in green. FAD and clorgyline are depicted in yellow and cyan ball-and-stick representation, respectively. The active site cavity-shaping loop is depicted as black coil (*De Colibus et al. Pnas 2005*)[72]. (B) Monomer A is on the right and monomer B is on the left. The letters 'N' and 'C' indicate the N-terminal and C-terminal amino acids, respectively. Residues 4–460 are in red, and the C-terminal tail is in green. The FAD is shown in ball-and-stick representation and colored in yellow (*Binda et al. Nature Structural Biology 2002*)[67].

1.3.1.3.2 Tissue distribution

During development, MAO-A is expressed before MAO-B, but levels of the latter increase conspicuously in the brain after birth[66]. MAO-A and MAO-B are expressed, at different levels, in many organs[73], and they have been extensively studied in the central nervous system[65]. In the brain, MAO-A has been found prevalently in noradrenergic neurons, whereas MAO-B has been detected in serotoninergic and histaminergic neurons and in glial cells[61]. In particular, MAO activities were detected in the heart of humans and different animals[74–80]. Human heart contains predominantly MAO-A, but MAO-B is also present[61]. In mouse cardiomyocytes, MAO-B is the predominant isoform while, in contrast, rat cardiomyocytes express more MAO-A[61].

1.3.1.3.3 Physiological roles

MAO catalyzes the oxidative deamination of monoamines according to the following reaction:

$$RCH_2NR´R´´ + O_2 + H_2O \rightarrow RCHO + N\,R´R´´ + H_2O_2$$

This reaction occurs in two steps. In the first step, the co-factor of MAO flavin adenine dinucleotide (FAD) is reduced to an aldehyde intermediate and ammonia, while in the second step FAD is re-oxidized and H_2O_2 is produced[25]:

$$RCH_2NH_2 + MAO \rightarrow RCHO + NH_3 + MAO\text{-reduced}$$

$$MAO\text{-reduced} + O_2 \rightarrow MAO + H_2O_2$$

Aldehyde dehydrogenase (ALDH) metabolizes the reactive aldehyde into the corresponding acid to avoid its accumulation and toxicity[61,81].

Serotonin and norepinephrine are preferentially metabolized by MAO-A, while MAO-B catalyzes phenylethylamine and benzylamine[60,61]. Both isoenzymes catalyze the deamination of the other amines (dopamine, tyramine, octopamine and tryptamine), playing an important role in their turnover.

It has been shown that MAO-A and MAO-B knockout (KO) mice display differences in neurotransmitter metabolism and behavior[62]. Shih and coworkers observed that MAO-A KO mice had elevated levels of some amines in the brain and manifest aggressive behaviour. On the other hand, no aggression was observed in MAO-B KO mice. Both MAO-A and MAO-B KO mice show increased reactivity to stress. Studies in MAO-A KO mice also confirmed that maintenance of serotonin levels is important for the normal development of thalamocortical axonal activity[62].

1.3.1.3.4 MAO in cardiovascular diseases

MAO can generate 10-fold higher levels of ROS in human atrial myocardium in comparison to the ETC[61,81,82]. In addition, studies carried out with intact mitochondria suggest H_2O_2 generated during deamination of tyramine by MAO is 48-fold higher than that generated during oxidation of succinate via complex II, again demonstrating the potential contribution of MAOs to cellular ROS levels and signaling[47,83].

MAO has been mostly studied in the brain but several studies have proved a role of these flavoenzymes (more specifically MAO-A) in cardiovascular diseases[65] and in the regulation of cardiac redox balance[25,61].

Pharmacological and genetic inhibition of these flavoenzymes is protective in cardiovascular complications, including I/R injury[56,84,85], pressure overload-induced heart failure[86,87] and streptozotocin (STZ)-induced cardiac dysfunction[43,88].

Parini's group was the first to demonstrate that MAO-A is an important source of ROS in the myocardium[89]. They showed that MAO-A induced ROS trigger signaling pathways that are receptor-independent and lead to cell proliferation and hypertrophy or apoptosis. Moreover, the same group demonstrated that incubation of cardiomyocytes with serotonin

led to an increase in ROS production and hypertrophy that involved the activation of extracellular signal regulated kinase (ERK) 1/2 in a MAO-A dependent manner[89,90].

Kaludercic et al. demonstrated the contribution of MAO-A in maladaptive hypertrophy and myocardial dysfunction in hearts subjected to pressure overload[81]. They showed that triggering MAO-A activity leads to increased ROS formation, oxidative stress, mitochondrial dysfunction, caspase activation and apoptosis in cardiomyocytes. Pharmacological MAO inhibition mediated by clorgyline, a selective inhibitor of MAO-A does not have any side-effects on basal cardiac structure or function in control mice. Moreover, the effect of genetic deletion of MAO-A in cardiovascular setting was further characterized in MAO-A mutant mice (MAO^{neo}) where the expression of a truncated non-functional variant of MAO-A transcript occurred. MAO^{neo} mice showed a complete protection against transverse aortic constriction (TAC)-induced cardiac remodeling compared to wild type mice[81,84,86]. Another study showed that MAO-A KO mice performed worse after aortic banding[91]. Those mice showed cardiomyocyte hypertrophy and LV dilation at baseline, although LV dysfunction was absent and no hemodynamic alterations were observed. This discrepancy should take into account the following elements: primarily, the difference between the two genetic models used in those studies; secondly, the severity of the aortic banding used to induce hypertrophy and heart failure.

MAO-A has been identified as an important source of ROS in STZ-treated rats, suggesting that its inhibition may improve cardiac contractility[88]. These Authors focused on the later stages of DCM, characterized by reduced heart rate and contractility, and likely associated with reduced ejection fraction and dilation.

A mechanistic insight into the deleterious role of MAO-A in DCM was further proposed by Deshwal et al. who provided an unprecedented evidence that diastolic stiffness observed in STZ mice is prevented by the MAO inhibitor pargyline.

They showed that exposure of cardiomyocytes to high glucose and IL-1β cytokine, led to a significant rise in MAO-A- mediated ROS production accompanied by mitochondrial dysfunction and endoplasmic reticulum (ER) stress. *In vivo*, mice treated with the irreversible and non-selective MAO inhibitor pargyline were protected from early diastolic dysfunction, ER stress and fibrosis after STZ administration[43].

The role of MAO-B has also been documented in pressure overload induced heart failure[61]. $MAO\text{-}B^{-/-}$ mice displayed reduced cardiac oxidative stress, LV remodeling and

apoptosis. In addition to this, the absence of MAO-B activity completely prevented LV dilation/pump failure[61].

Studies employing genetically modified mice show that MAO-A$^{-/-}$ and MAO-B$^{-/-}$ display a slight reduction in contractility/relaxation, although fractional shortening and ejection fraction remain unchanged when compared to WT mice[61,86].

Several studies have also investigated the role of MAO in ischemia/reperfusion (I/R) injury[84,92]. MAO inhibition with both clorgyline and pargyline remarkably reduced infarct size in an in vivo rat model of I/R injury[84]. Another independent study also showed that pargyline completely prevented I/R induced injury in isolated Langendorff perfused mouse hearts[56]. The significant contribution of MAO activity to oxidative stress and cardiac dysfunction was supported by in vitro and in vivo models of MAO overexpression[93]. Cardiac overexpression of MAO in mice resulted in the loss of ~50% of cardiomyocytes, fibrosis and heart failure[93]. Moreover, these hearts displayed p53 accumulation and reduced levels of PGC-1α (peroxisome proliferator-activated receptor-γ coactivator-1α), a master regulator of mitochondrial biogenesis. These changes were accompanied by excessive H_2O_2 formation, reduced ATP levels and mitochondrial dysfunction[93].

The involvement and the pivotal role of MAO in cardiovascular injury highlighted by these studies prompt the question whether MAOs could play a role in the oxidative stress and cardiac dysfunction triggered by hyperglycemia. These enzymes can be targeted pharmacologically and this represents an attractive and important therapeutic target for the treatment of diabetic cardiomyopathy. This concept is supported by the recent work showing the protective efficacy of MAO inhibition on diabetes-induced cardiac dysfunction[88].

1.3.1.3.5 Monoamine oxidase inhibitors

Monoamine oxidase inhibitors were first introduced in the 1950s[94–96]. They are a separate class from other antidepressants, treating different forms of depression as well as other nervous system disorders. The antidepressant properties result from selective MAO-A inhibition in the central nervous system, which leads to increased brain levels of dopamine, noradrenalin and serotonin. Even though MAO inhibitors were the first antidepressants introduced, they are not the first choice in treating mental health disorders in the current clinical practice due to important side effects, such as orthostatic hypotension and hypertensive crises[60,94–96]. While the mechanism underlying hypotensive

effects of MAO inhibitors remains unclear, hypertensive crisis, also known as the 'cheese reaction', occurs in patients treated with irreversible MAO-A inhibitors following consumption of food rich in tyramine, such as cheese, red wine, fava beans, soy sauce or chocolate[60]. This side-effect occurs when tyramine and other sympathomimetic amines ingested with food are not degraded in the intestines. They are therefore able to enter the circulation and potentiate sympathetic cardiovascular activity by triggering the release of noradrenaline[60].

Although tyramine-induced MAO inhibitors' reactions are normally not associated with myocardial injury, myocardial infarction events have been reported in patients treated with phenelzine after cheese ingestion[60]. These side effects are due to the irreversible MAO-A inhibition and are resolved by using reversible MAO-A inhibitors and/or MAO-B inhibitors[60]. Indeed, reversible MAO inhibitors are currently used in clinical practice and are devoid of the aforementioned side-effects[60]. MAO inhibitors have been classified in three groups:

- Irreversible and non-selective inhibitors, such as phenelzine, pargyline and tranylcypromine;
- Irreversible and selective inhibitors, such as selegiline for MAO-B and clorgyline for MAO-A;
- Reversible and selective MAO inhibitors, such as moclobemide for MAO-A and safinamide for MAO-B.

Some of the non-selective irreversible inhibitors, such as phenelzine and tranylcypromine, are still in clinical use along with the reversible MAO inhibitors moclobemide, befloxatone, toloxatone and safinamide[66]. As levels of MAO-B are increased in patients with Parkinson's disease, MAO-B inhibitor selegiline has been used as a dopamine sparing agent[81]. In addition to these, safinamide, a reversible MAO-B inhibitor, was licensed by EMA (Emergency medical assistant licensing board) for the treatment of Parkinson's disease in combination with L-DOPA or with other anti-Parkinson drugs in mid-to advanced-stage fluctuating patients[81].

MAO inhbitors such as iproniazid, isocarboxazid, beta-phenylisopropylhydrazine, nialamide and phenelzine, had become not only available in the clinics for the treatment of depression, but they were also evaluated for their potentially beneficial effects in patients with CVD[60]. Because of their hypotensive effects, these MAO inhibitors were successfully used as antihypertensive agents and were considered promising tools for the

treatment of CVD. MAO inhibition can also be the result of an off-target effect. For example, the PPARγ agonist, pioglitazone, used for the treatment of T2D, specifically inhibits MAO-B in a reversible manner, a property that is not shared by other members of the glitazone family[97]. Importantly, this off-target effect may contribute to the beneficial effects of pioglitazone in DCM.

To date, MAO inhibitors have been used in patients to preserve or increase monoamine levels. It remains to be investigated clinically products derived by MAO deamination of biogenic amines[97].

1.4 Autophagy process

Autophagy has acquired a pivotal role in the pathological alterations of diabetes. Depending on the extent of autophagy and its duration, autophagy can have both beneficial and detrimental effects[3].

Autophagy refers to an evolutionarily conserved mechanism of degradation and an adaptive process driven by autophagy-related (ATG) proteins devoted to the intracellular recycling of cytoplasmic element, such as damaged or dysfunctional components, senescent organelles, and unfolded proteins. Autophagy is also known as a self-degradative process contributing to the maintenance of cellular functions and survival in all organisms under basal conditions. Furthermore, this recycling mechanism occurs in response to different forms of stress, including nutrient deprivation, growth factor depletion, infection and hypoxia. It also ensures quality control and regulates the synthesis of new cellular components by providing amino acids, fatty acids and sugars obtained from the turnover of redundant cellular elements[98–104].

Autophagy refers to regulated catabolic processes, all of which deliver cytoplasmic components to the lysosome for degradation, and that are classified at least into three types: macroautophagy, microautophagy and chaperone-mediated autophagy (CMA) (Figure 7). They differ in terms of cargo delivery to the lysosomes.

Macroautophagy, the major catabolic mechanism used by eukaryotic cells, involves the formation of double-membrane vesicles called autophagosomes that engulf damaged, dysfunctional and redundant cytoplasmic components. Then, autophagosomes are trafficked to lysosomes for the degradation of sequestered cargos. On the other hand, microautophagy refers to the direct invagination of the lysosomal or endosomal membrane, resulting in the engulfment of cytoplasmic cargo that is subsequently

degraded by lysosomal proteases. The third pathway is CMA, which consists of proteins containing the KFEQR motif that is recognized by the cytosolic chaperone heat shock cognate 70 (HSC70). The targeted protein is delivered to the lysosomes for degradation with the assistance of the CMA receptor, lysosome-associated membrane protein type 2A (LAMP-2A)[104].

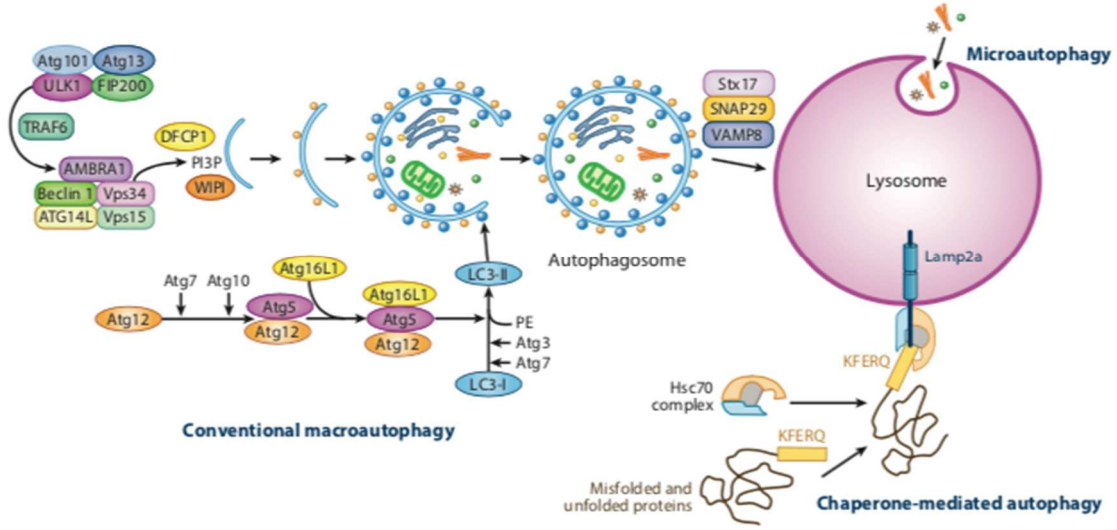

Figure 7: Schematic model of the major pathways in the regulation of the autophagic machinery. These pathways include macroautophagy, microautophagy, and chaperone-mediated autophagy. In macroautophagy, double-membrane vesicles (autophagosomes) sequester cellular components and deliver them to lysosomes for degradation, whereas in microautophagy, lysosomes directly engulf cellular components. In chaperone-mediated autophagy, the chaperone Hsc70 transports target proteins to lysosomes for degradation (*Sciarretta et al. Annu. Rev. Physiol. 2018. 80:7.1–7.26)*[105].

As previously mentioned, induction of autophagy results in recruitment of ATGs to a specific subcellular location termed the phagophore assembly site (PAS) and nucleation of an isolation membrane that forms a structure called the phagophore. Gradual elongation of the curved isolation membrane results in expansion of the phagophore into a sphere around a portion of the cytosol. The isolation membrane closes into a double-membrane vesicle, thereby capturing the engulfed cytosolic material. Then, the outer membrane of the autophagosome fuses with the lysosomal membrane to form an autolysosome [98,100]. The canonical, or conventional, autophagic pathway involves Atg4, Atg5, Beclin1 (Atg6), Atg7, Atg12, and Atg16, that govern these steps.

Increasing lines of evidence suggest that an Atg5/Atg7-independent pathway exist. Nishida et al. revealed that $Atg5^{-/-}Atg7^{-/-}$ double-knockout mouse embryonic fibroblasts (MEF) are still able to form autophagosomes and perform autophagy-mediated protein degradation of substrates inside autolysosomes in response to certain stressors[106].

During this process of Atg5/Atg7-independent autophagy, termed alternative autophagy, lipidation of LC3 does not occur. Instead, Rab9, a small GTPase involved in membrane trafficking and fusion between the trans-Golgi network and late endosomes, plays a critical role in generating autophagosomes by promoting fusion of the phagophore with vesicles derived from the trans-Golgi network and late endosomes.

Although autophagy was originally identified as a non-specific mechanism of degradation, cargo-specific forms of autophagy have also been discovered. For example, mitophagy for mitochondria, lipophagy for lipid droplets, or ERphagy for endoplasmic reticulum[104].

Mitophagy is the best characterized form of selective macroautophagy, and is responsible for the removal of redundant or damaged organelles through their engulfment into autophagosomes[105,107]. Mitophagy guarantees normal cellular metabolism, reduces mitochondrial generation of ROS, and prevent mitochondrial release of pro-apoptotic factors. Thus, maintenance of proper mitochondrial function by mitophagy is crucial for cellular and organismal health[101,102,105,107,108]. Classical hallmarks of mitochondrial dysfunctions, such as membrane potential ($\Delta\Psi m$) collapse, ROS production, and low ATP levels, activate mitophagy.

Mitochondrial fitness is required for normal cell metabolism and to prevent cell damage. Mitochondria grow and divide to control their number and size both in physiological and pathological conditions[109]. Mitochondrial dynamism is linked to mitochondrial quality control through the processes of fission and fusion. Changes in mitochondrial dynamics represent the first step in response to mitochondrial damage, and it is thought that mitochondrial fragmentation is a prerequisite for mitophagy to occur. Mitochondrial dynamics are mediated by several proteins. Firstly, dynamin-related protein 1 (DRP1) and its adaptor proteins human fission protein (hFIS), mitochondrial dynamics proteins (MID49 and MID51), and mitochondrial fission factor (MFF) regulate mitochondrial fission, while mitofusins 1 and 2 (MFN1, MFN2), and optic atrophy protein-1 (OPA1) control mitochondrial fusion[104,105,108]. Thus, proteins that regulate mitochondrial dynamics also play essential roles in autophagy, and both *in vitro* and *in vivo* models have confirmed that mitochondrial dynamics and mitophagy are indeed highly integrated processes[104].

Defective or senescent mitochondria can be degraded either through PTEN-induced putative kinase1 (PINK1)-Parkin dependent or independent pathways. When mitochondria are damaged, PINK1 accumulates in the outer mitochondrial membrane

(OMM), where it promotes recruitment of Parkin, an E3-ubiquitin ligase that ubiquitinates proteins on the OMM of damaged mitochondria[105,108]. Although PINK1 is regarded as a master regulator of mitophagy, basal mitophagy *in vivo* occurs independently of PINK1 in a variety of tissues[110]. Indeed, several PINK1/Parkin-independent mechanisms exist. PINK1/Parkin-independent mitophagy is also mediated by mitochondrial BCL2 Interacting Protein 3 Like L (NIX/BNIP3L) that can directly bind to microtubule-associated protein 1A/1B light chain 3 (MAP1LC3; best known as LC3) to form the mitophagosome[99,102,104].

1.4.1 Autophagy in cardiac pathophysiology

Autophagy has emerged as a major regulator of cardiac homeostasis and function[105,111]. Removal of protein aggregates is particularly important in terminally differentiated cells such as adult cardiomyocytes that have nearly completely lost replicative abilities. Physiological levels of autophagy in baseline conditions or following an acute pathologic insult is generally considered cardioprotective. However, excessive or uncontrolled levels of autophagy activation can trigger cardiac cell death in some circumstances, thus contributing to myocardial injury[105].

Mice with inducible cardiomyocyte-specific Atg5 gene deletion, which serve as a loss-of-function model for general autophagy, show cardiac dysfunction (hypertrophy, left ventricular dilatation, and contractile dysfunction). In particular, at the cellular level, Atg5-deleted cardiomyocytes display protein aggregation and mitochondrial dysfunction[111]. Indeed, partial activation of autophagy is beneficial[111].

Autophagy has been shown to preserve cardiac function during ischemia and starvation by supplying substrates for ATP regeneration and reduces myocardial injury[112–114]. Moreover, studies conducted in animal models of cardiac diseases have shown that activation of autophagy in myocardium limits cardiac senescence, ischemic injury, chronic cardiac remodeling, genetic cardiomyopathy, and heart failure[104,115]. This mostly occurs when mitophagy is stimulated.

Cardiac autophagy is suppressed below physiological levels in failing hearts, contributing to the progression of heart failure (HF), and during aging[108]. On the other hand, autophagy is activated excessively under some conditions, including ischemia/reperfusion (I/R), where autophagy may facilitate myocardial injury[113]. Indeed, cardiac cell death is attenuated by autophagy inhibition in I/R[113] and pressure overload[116].

Autophagy has different roles and consequences during I/R because of clear and distinct pathophysiological mechanisms. Generally, reperfusion is characterized by a rise of ROS that contribute to the progression of myocardial injury[25,104]. While it is now accepted that autophagy plays a relevant role in cardiac pathologies, its contribution to cell death is still controversial.

In this respect, mitophagy could take part into the beneficial effects of autophagy in preventing chronic cardiac stress. Basal mitophagy is greater in the heart than in other organs[117], maybe because of high levels of oxidative phosphorylation, ROS, and mitochondrial damage in cardiomyocytes[107].

Several studies confirmed that impaired mitophagy is one of the concurrent cause of mitochondrial dysfunction, cardiac hypertrophy and heart failure in response to pressure overload[118]. Saito et al. showed that mitophagy during myocardial ischemia was mediated predominantly through alternative autophagy characterized by Rab9-associated autophagosomes, rather than the well-characterized form of autophagy that is dependent on Atg5/Atg7 conjugation system and LC3. This form of mitophagy played an essential role in protecting the heart against ischemia and was mediated by a protein complex consisting of Ulk1, Rab9, Rip1, and Drp1. Mitophagy mediated through the aforementioned complex pathway protected the heart against ischemia by maintaining healthy mitochondria[119].

The functional consequences of impaired cardiac autophagy in T1D and T2D are different. In many models of T2D, cardiac autophagy is inhibited at different levels[105,120,121], but other studies reported an increase[122,123]. Several studies have shown that autophagy is both inhibited in T1D mouse models[122] and increased[120] in the heart. Xu et. al demonstrated that T1D-induced cardiac damage was reduced upon autophagy inhibition in either beclin 1- or Atg16-deficient mice[124]. An interesting additional finding is that the reduction in the canonical autophagy was associated with the activation of the alternative autophagy, thereby maintaining normal levels of mitophagy and limiting diabetic cardiac injury[124]. On the other hand, autophagy inhibition in T2D contributes to cardiac damage[125]. Tong et al. found that deletion of Atg7 diminished autophagy/mitophagy and exacerbated DCM in HFD, highlighting the importance of these processes during DCM[125]. However, the authors did not provide evidence for the activated autophagic pathways in HFD (e.g. the non-canonical alternative autophagy).

1.4.1.1 Signaling pathways involved in autophagy

Due to the great importance that autophagy plays inside the cell both in physiological and pathological contexts, it is not surprising that different signaling pathways participate in the regulation and activation of the process. Among them, mTOR, 5′-AMP-activated kinase (AMPK), ROS, metabolites, and miRNA can be mentioned as important players (Figure 8).

mTOR is a serine/threonine kinase that acts through two multiprotein complexes[108,126]. mTORC1 is a master regulator of several processes, among which there is also autophagy. It is activated by nutrients and growth factors and is inhibited during starvation. mTORC2 regulates cell survival, insulin sensitivity, and cell polarity[105,108]. mTORC1 negatively regulates autophagy through post-translational and transcriptional mechanisms. Forced mTORC1 activation in the heart during myocardial ischemia blunts autophagy activation and dramatically increases ischemic injury[105,127]. Insulin signaling prevents excessive activation of autophagy during postnatal heart development through activation of the mTOR pathway, and mice with disrupted insulin signaling develop cardiomyopathy through unrestrained activation of autophagy[105]. mTORC2 also regulates autophagy indirectly through Akt and mammalian sterile 20–like kinase 1 (Mst1)[126].

Autophagy is also regulated by AMPK and glycogen synthase kinase-3 beta (GSK-3β), serine/threonine kinases whose activity is finely controlled by the energy status. AMPK is mostly activated by an increase in AMP following ATP depletion, but also by ROS, stimulating autophagy. AMPK activates TSC1/2, which inhibit Rheb, an mTORC1 activator and stimulates autophagy. AMPK also directly activates autophagy by phosphorylating Ulk1, thus dissociating Ulk1 frommTORC1[105,128]. AMPK is required for autophagy activation during ischemia in cardiomyocytes[113]. GSK-3β is also stimulated during energy stress leading to mTORC1 inhibition and stimulation of autophagy. GSK-3β is activated and promotes autophagy through inhibition of mTOR during myocardial ischemia, whereas GSK-3β is inhibited during reperfusion, allowing mTORC1 activation and restraining autophagy[105].

A growing amount of evidence indicates ROS as a signal transducer sustaining autophagy. A central role in autophagy activation has been attributed to Atg4[105,129]. Atg4 oxidation inhibits its protease activity, thereby increasing the amount of lipidated LC3

and autophagosome formation. Physiological levels of ROS are required for autophagy activation during nutrient deprivation and ischemia in cardiomyocytes[130]. Therefore, oxidative stress is linked to autophagy through many pathways[24]. In the context of relationships between ROS and autophagy, a role has been attributed also to MAO. Recent work has linked these flavoenzymes with lysosomal dysfunction both in vitro and in vivo[131]. MAO-A dependent ROS formation is likely responsible for the impaired mitochondrial quality control and lysosomal dysfunction, since cardiomyocyte-specific MAO-A overexpression blocked autophagic flux causing accumulation of LC3II, p62 and ubiquitylated proteins, leading to mitochondrial fission and cardiomyocyte necrosis. These effects have been attributed to MAO-A induced inhibition of nuclear translocation of TFEB (transcription factor-EB), a master regulator of autophagy and lysosome biogenesis[131].

Finally, miRNAs have emerged as important regulators of autophagy. miRNA-212/132 promotes cardiomyocyte hypertrophy though down-regulation of FoxO3a and inhibition of autophagy. miRNA-22 is progressively upregulated in the heart during aging, contributing to the aging-induced decline in autophagy through peroxisome proliferator-activated receptor alpha inhibition. miRNA-22 inhibition improves cardiac adaption to chronic myocardial infarction in old mice by stimulating autophagy[132]. miR-19a-3p/19b-3p inhibits autophagy in cardiomyocytes by targeting the TGF-β R II[133]. MiR-30b disrupts autophagy in vascular smooth muscle cells by decreasing autophagy-related genes, such as Atg5 and LC3II[133]. MiR-199a represses autophagy by indirectly activating mTORC1, which leads to cardiac hypertrophy[133].

Considering that, usually, one miRNA targets several genes or several miRNAs target one gene in autophagy regulation, the crosslink between the different pathways needs to be further explored.

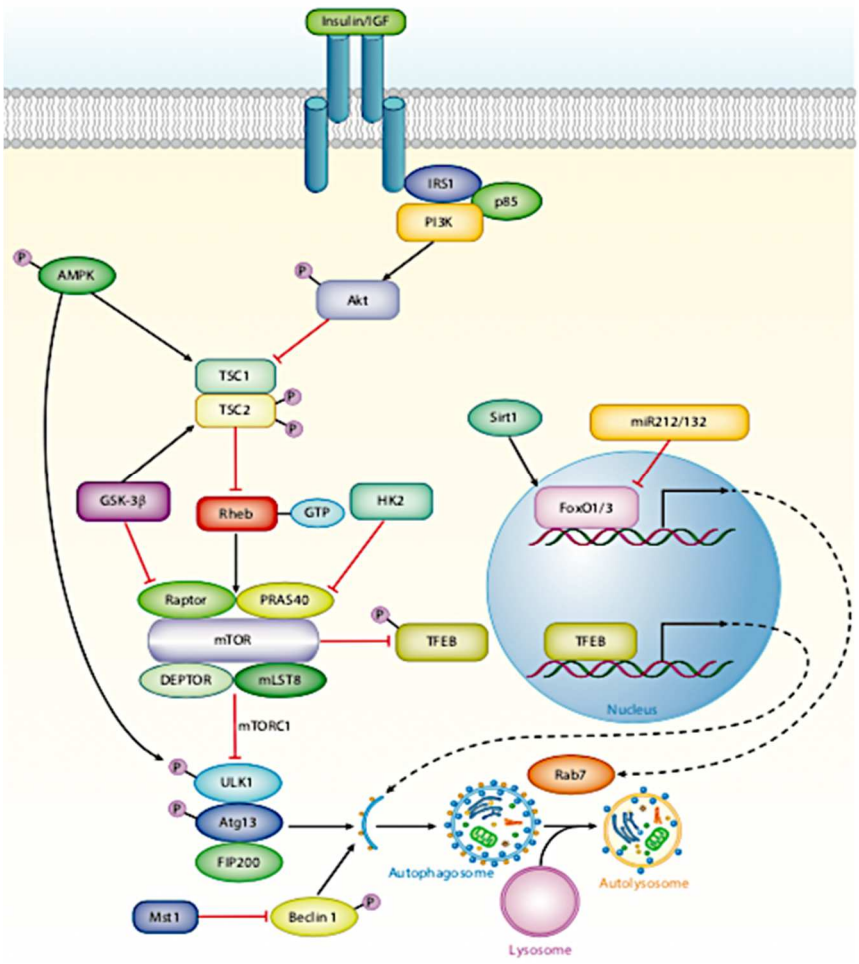

Figure 8: Schematic model of the intracellular signaling mechanisms regulating autophagy. The autophagic machinery is modulated by various signaling pathways and posttranslational modifications. mTORC1 negatively regulates autophagy through both posttranslational and transcriptional mechanisms. AMPK activates both TSC1/2 and ULK1, thereby facilitating initiation of the autophagic machinery. Similarly, GSK-3β phosphorylates and activates TSC1/2, thereby suppressing mTORC1 activity, which in turn activates autophagy. Pro-apoptotic Mst1 attenuates autophagic activity through Beclin 1 phosphorylation. TFEB promotes both lysosome biogenesis and autophagy activation. Activation of FoxO1 stimulates autophagy and enhances autophagic flux through upregulation of Rab7. miR-212/132 downregulates FoxO3a, thereby inhibiting autophagy *(Sciarretta et al. Annu. Rev. Physiol. 2018. 80:7.1–7.26)*[105].

1.5 Transcriptomic analysis of diabetes

Despite remarkable advances in the molecular biology and enormous efforts to elucidate the relationship between obesity, insulin resistance, diabetes, and other metabolic pathologies, the precise link between them largely remains unknown. This is very likely because the etiology of the aforementioned diseases is difficult to explain with a single physiological or genetic endpoint. Rather, multiple susceptibility genes as well as complex relationship between them are involved in the development of these pathological conditions. Considering the polygenic nature of these metabolic disorders, the necessity of using multifaceted genetic approaches has increased. With the advances in high-

throughput technology, it is now possible to identify more susceptible genes and to analyze their complex genetic networks. For instance, recent progress on the identification of insulin resistance susceptibility gene in various model systems using microarray analysis show that (i) in liver, genes involved in lipid synthesis and gluconeogenesis were increased in insulin-resistant animal model; (ii) in adipose tissues, genes involved in fatty acid synthesis and adipogenesis were down-regulated both in insulin-resistant humans and animal models; and (iii) in muscle, overall gene expression was either decreased or unresponsive compared to that of insulin-sensitive control human subject or animals[134].

A recent study in adipose tissue highlighted that glycan biosynthesis, metabolism pathway genes, immune and inflammation pathway genes are strongly upregulated in the T2D subjects. Downregulated genes included those encoding for oxidative phosphorylation components, branched-chain amino acids, and carbohydrate and lipid metabolism among people with T2D[135,136]. Reported transcriptome studies have been performed in T1D patients and non-obese diabetic mouse models analyzing peripheral blood, lymphoid organs and pancreas/islets. In the periphery, the distinctive profiles are inflammatory pathways inducible by IL-1β and IFNs that can help in the identification of new biomarkers. In the target organ, a remarkable finding is the overexpression of inflammatory and immune response genes[137,138].

Despite the efforts made, genomic studies on how mitochondrial ROS generation and, in particular, MAOs activities impact on diabetes have not been performed and requires further investigations.

II. AIM OF THE WORK

The aim of this study was to investigate whether MAO-dependent ROS generation induced by diabetes affects the gene expression profile in T1D cardiac tissue and to characterize the biological significance of such changes.
Previous results from the laboratory of Professor Di Lisa showed that MAO-dependent ROS formation plays a major role and contributes to the development of DCM. Indeed, MAOs activity is involved in the cross-talk between mitochondria, inflammation and ER stress occurring in cardiomyocytes exposed to diabetic milieu.

In this study, we used STZ-induced T1D mice treated or not with pargyline as an inhibitor for both MAO-A and MAO-B. In the in vitro study, diabetic conditions were mimicked with HG in primary cardiomyocytes.

The working hypothesis was that mitochondrial ROS and, in particular, MAO-dependent ROS formation induced by diabetes leads to transcriptomic changes in gene expression profile in the context of cardiac pathophysiology. Previous works from laboratory of Professor Di Lisa demonstrated: (i) the involvement of mitochondrial ROS produced by MAO triggered by hyperglycemia and inflammation in cardiac damage; (ii) the involvement of MAO activity in cardiac fibrosis through mechanisms involving other cardiac cell types. Based upon above mentioned results, we investigated the changes in gene expression profile induced by diabetes and prevented by MAO inhibition in the cardiac tissue from a mouse model of T1D induced by treatment with STZ through microarray technology. Transcriptomic analysis highlighted that degradative processes could be one of the mechanisms involved in the disease and we hypothesized that MAO activity might affect autophagy leading to mitochondrial and cellular derangements in diabetic conditions.

Taking into account that MAO inhibitors are readily available and used in the clinic for the treatment of depression and Parkinson's disease, characterizing in depth the effects of MAO inhibition in the heart is a pressing task in order to consider it as a possible therapeutic strategy for DCM.

III. MATERIALS AND METHODS

3.1 Animal model of T1D

All the animal studies were performed using male C57BL6/J mice (6-7 weeks of age and at least 20 g in weight; Charles River Laboratories, UK). T1D was induced with Streptozotocin (STZ) (50 mg/kg/day in citrate buffer pH 4.5) administered intraperitoneally for five consecutive days. STZ is a glucosamine-nitrosourea compound toxic to pancreatic β-cells. Mice were then randomized to receive either vehicle or MAO inhibitor pargyline (50 mg/kg/day) for 12 weeks. Blood glucose levels were measured twice a month using glucose meter (OneTouch Ultra 2) and mice with blood glucose levels ≥17 mM were considered diabetic.

3.2 Microarray data analysis

Gene expression profiling is by far the most common use of microarray technology. The process of analysing gene expression data generally involves the steps represented in Figure 9.

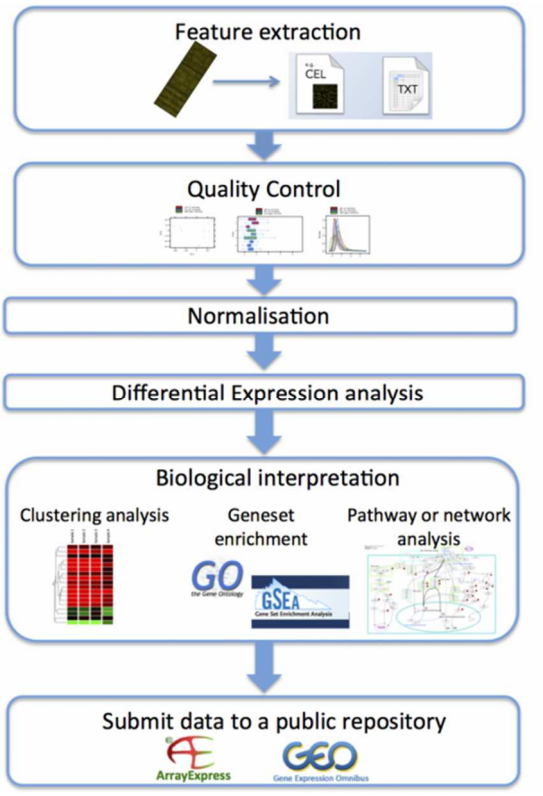

Figure 9: Overview of the microarray data analysis pipeline
(https://www.ebi.ac.uk/training/online/course/functional-genomics-ii-common-technologies-and-data-analysis-methods/analysis-microarray-data).

Briefly, RNA is extracted from hearts and then reverse transcribed into cDNA by using a reverse transcriptase and a nucleotide labelled with fluorescent dyes. Once the samples have been labelled, they are purified and allowed to hybridize onto the microarray glass slide. Hybridization step allows the hybridization of each labeled cDNA to specific complementary oligonucleotides (spot probes) placed on specific positions of the microarray. Each oligonucleotide identifies a specific gene and the amount of cDNA bound to a spot will be directly proportional to the initial number of RNA molecules present in the sample. Following the hybridization step the microarray slide was washed and then scanned to recover the fluorescence of each probe from the slide. The amount of fluorescence emitted upon excitation corresponds to the amount of bound nucleic acids. Thus, what is seen at the end of the experimental stage is an image of the microarray, in which each spot, that corresponds to a gene, has an associated fluorescence value representing the expression level of that gene[139]. A schematic representation of what microarrays are and how do they work is shown in Figure 10.

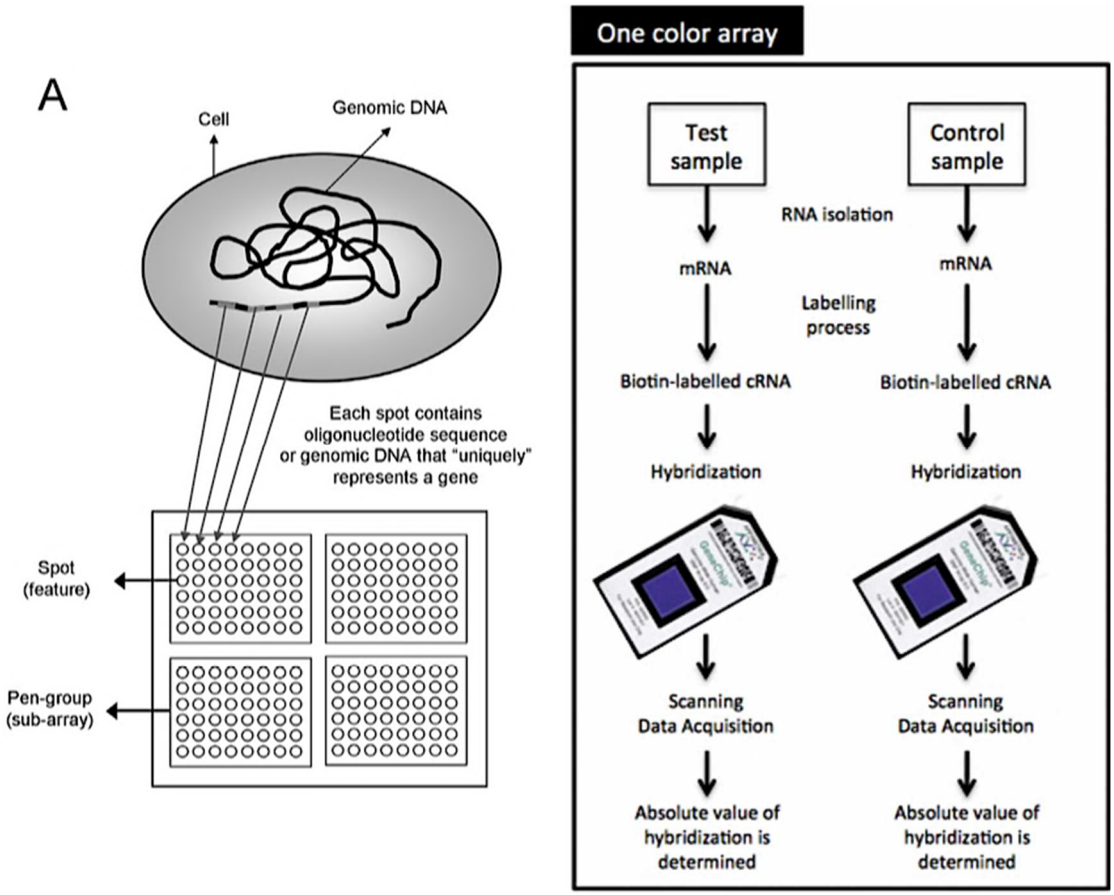

Figure 10: What are microarrays and how do they work. A microarray may contain thousands of probes (spots). Each spot contains many copies of the same DNA sequence (oligonucleotides) that uniquely represents a gene from an organism. On the right an example of an experimental protocol to study differential expression of genes. The organism is grown in two different conditions (a reference condition and a test condition). RNA is extracted from the two cells and is labelled with the same dye (Cy3 in our case) during the synthesis of cDNA by reverse transcriptase. Following this step, cDNA is hybridized onto different microarrays, where each cDNA molecule representing a gene will bind to the spot containing its complementary DNA sequence. The microarray slide is then scanned to detect the fluorescence associated to each spot. The final image is stored as a file for further analysis[139]. On the right the schematic representation of one colour microarrays. In this kind of microarrays, each sample is labelled and hybridized to a separate microarray and an absolute value of fluorescence for each probe is obtained.

A major design consideration in a microarray experiment is whether to measure the expression levels from each sample on separate microarrays (one-colour array, what we have done) or to compare relative expression levels between a pair of samples on a single microarray (two-colour array or microarray based on a competitive hybridization). The overall performance of one-colour and two-colour arrays is similar, but the majour problem of the competitive hybridization is the impossibility of performig a different experimental design of the one already performed because data are referred to the control sample co-hybridized with the test sample.

In the experiments performed to evaluate the effects of pargyline on gene expression, labelled RNA was used to hybridize onto microarrays. RNA labeling was performed using the Low Input Quick Amp Labeling Kit (Agilent) according to manufacturer instructions.

To remove the residual primers and nucleotides, cRNA was purified with the RNeasy Mini Ki (Qiagen) according to the manufacture's manual. Resulting cRNA was quantified with Nanodrop ND-1000 spectrophotometer (Celbio).

About 800 ng of labelled sample were mixed with 5 µl of 10X Blocking Agent (Agilent Technologies) and water to a final volume of 25 µl. Samples were denatured at 95°C for 2 min and added to 25 µl of 2X GEx Hybridization Buffer HI-RPM (Agilent Technologies). 40 µl of prepared mix was dispensed onto the array. Slides were loaded into the Agilent SureHyb chambers and hybridization was performed in a hybridization oven at 65°C for 17 hours with 10 rpm rotation. Finally, slides were washed using Wash Buffer Kit (Agilent Technologies) and dried at room temperature.

Microarray slides were scanned using G2505C scanner (Agilent Technologies) at 3 µm resolution. Probes features were extracted using the Feature Extraction Software v. 10.7.3.1 with GE_1_Sep09 protocol (Agilent Technologies). Intra-array normalizations were directly performed by the Feature Extraction Software. Inter-array normalization of

expression levels was performed with quantile method[140] and the values for within-arrays replicate spots were then averaged. Quantile normalization makes the assumption that the different biological samples have roughly the same distribution of RNA abundance, and transform the intensities so that the bulk of the intensity distribution is the same for all assays in an experiment, typically with some differences in the distribution tails (which might reflect actual biological differences)[141].

Feature Extraction Software, which provided spot quality measures, was used to evaluate the quality and reliability of the hybridization. In particular, the flag "glsFound" (set to 1 if the spot had an intensity value significantly different from the local background and to 0 when otherwise) was used to filter out unreliable probes: the flag equal to 0 was noted as "not available (NA)." Probes with a high proportion of NA values were removed from the dataset in order to carry out a more solid and unbiased statistical analyses. 45% of NA was used as the threshold in the filtering process.

To identify differentially expressed probes in at least one condition analysis was performed using a threshold p-value ≤ 0.05 Bonferroni corrected[142].

3.3 Hierarchical clustering and Self-Organizing Trees Analysis

Hierarchical clustering is the most widely used method for the analysis of patterns of gene expression. It produces a representation of the data with the shape of a binary tree, in which the most similar patterns are clustered in a hierarchy of nested subsets.

The Self-Organising Tree Algorithm (SOTA) is a neural network that grows adopting the topology of a binary tree[143,144]. The result of the algorithm is a hierarchical cluster obtained with accuracy and robustness. Genes whose expression was statistically different were used to search specific expression clusters according to SOTA[144] as implemented in MultiExperiment Viewer version 4.8.1 (tMev) of the TM4 Microarray Software Suite[145].

A common method of visualising gene expression data is to display it as a heatmap (Figure 11). The heatmap may also be combined with clustering methods which group genes and/or samples together based on the similarity of their gene expression pattern.

In heat maps the data is displayed in a grid where each row represents a gene and each column represents a sample. The colour and intensity of the boxes is used to represent changes (not absolute values) of gene expression.

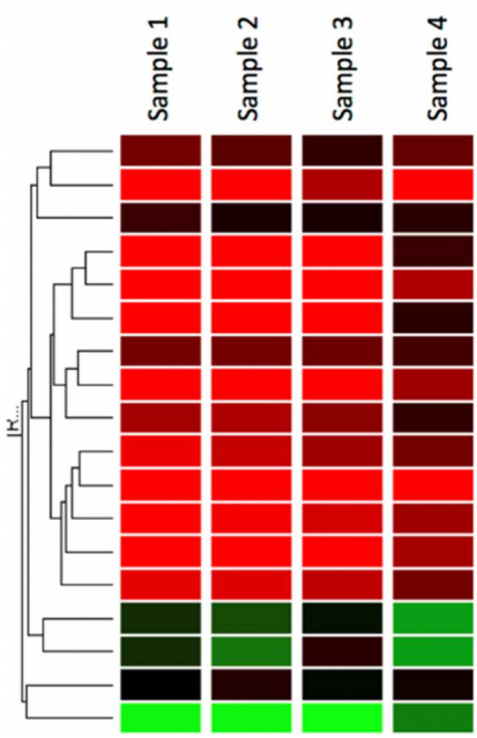

Figure 11: An example of a heatmap in which genes have been grouped based on their pattern of gene expression. In the example below, red represents up-regulated genes and green represents down-regulated genes. Black represents unchanged expression (https://www.ebi.ac.uk/training/online/course/functional-genomics-ii-common-technologies-and-data-analysis-methods/biological-0).

3.4 Gene onthologies

Genes were categorized according to gene ontology (GO) classes using GoMiner, a downloadable free program package that organizes lists of 'interesting' genes from a microarray experiment for biological interpretation. One of the main uses of the GO is to perform enrichment analysis on gene sets. For example, given a set of genes that are upregulated under certain conditions, an enrichment analysis will find which GO terms are over-represented (or under-represented) using annotations for that gene set. GoMiner has been used to provide quantitative and statistical output files[146].

Firstly, genes were analyzed using GO vocabulary (molecular function, biological process, cellular component) and the selected GO aspect has been chosen for our analysis. The results page displays a table that lists significant enriched GO terms used to describe the set of genes under analysis, and p-value that is an indication of the probability that the particular result can be due to chance.

3.5 Gene Set Enrichment Analysis

Gene Set Enrichment Analysis (GSEA) evaluates microarray data at the level of gene sets. The gene sets are based on a prior biological knowledge, e.g. published information about biochemical pathways or co-expression in previous experiments. The goal of GSEA is to determine whether members of a gene set S tend to occur toward the top (or bottom) of the list L, in which case the gene set is correlated with the phenotypic class distinction. GSEA acts through three steps:

1. Calculation of an enrichment score
2. Estimation of significance level of enrichment score
3. Adjustment for multiple hypothesis testing

A schematic representation of the main steps of the mentioned computational method is shown in Figure 12.

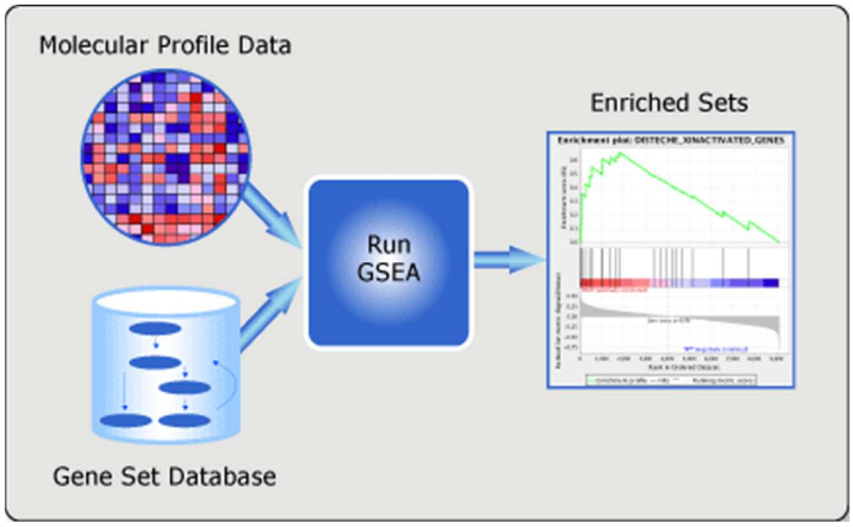

Figure 12: Schematic representation of GSEA (http://software.broadinstitute.org/gsea/index.jsp).

The primary result of the gene set enrichment analysis is the enrichment score (ES), which reflects the degree to which a gene set is overrepresented at the top or bottom of a ranked list of genes (Figure 13). The ES reflects the degree to which a set *S* is overrepresented at the extremes (top or bottom) of the entire ranked list *L*. The score is calculated by scrolling down the list *L*, increasing a running-sum statistic when we encounter a gene in *S* and decreasing it when we encounter genes not in *S*. The magnitude of the increment depends on the correlation of the gene with the phenotype[147].

The ES is the maximum deviation from zero encountered in scrolling the list. A positive ES indicates gene set enrichment at the top of the ranked list; a negative ES indicates gene set enrichment at the bottom of the ranked list.

The top portion of the plot shows the running ES for the gene set as the analysis scrolls down the ranked list. The score at the peak of the plot (the score furthest from 0.0) is the ES for the gene set.

The estimated significance has then been adjusted to account for multiple hypothesis testing. Subsequently, the ES has been normalized for each gene set to account for the size of the set, yielding a normalized enrichment score (*NES*). The detection of false positives has been carried out by calculating the false discovery rate (FDR). The FDR is the estimated probability that a set with a given *NES* represents a false positive finding.

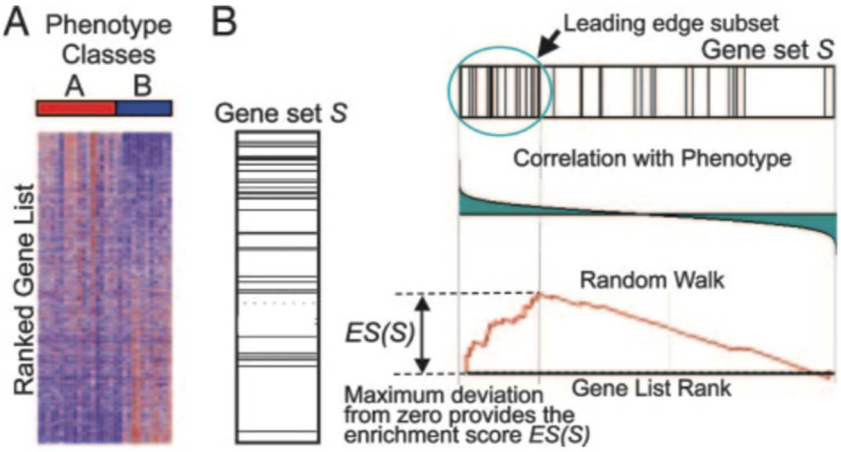

Figure 13: GSEA overview. (*A*) An expression data set sorted by correlation with phenotype, the corresponding heat map, and the ‘‘gene tags,’’ i.e., location of genes from a set *S* within the sorted list. (*B*) Plot of the running sum for *S* in the data set, including the location of the maximum enrichment score (*ES*) and the leading-edge subset[147].

3.6 Leading Edge Analysis

The leading-edge subset in a gene set are those genes that appear in the ranked list at or before the point at which the running sum reaches its maximum deviation from zero. The leading-edge subset can be interpreted as the core that accounts for the gene set’s enrichment signal[147].

After running the gene set enrichment analysis, the leading-edge analysis was used to examine the genes that are in the leading-edge subsets of the enriched gene sets. A gene

that is in many of the leading-edge subsets is more likely to be of interest than a gene that is in only a few of the leading-edge subsets.

3.7 cDNA synthesis and real time-PCR

To validate the expression patterns of selected genes based on the microarray analysis, relative quantification of mRNA was performed by Real-Time PCR (qRT-PCR) using Power SYBR Green PCR Master Mix and a StepOnePlus™ Real-Time PCR System (Thermo Fisher Scientific).

Total RNA was extracted from the heart tissue using TRIzol reagent (Thermo Fisher Scientific), a monophasic solution of phenol and guanidine isothiocyanate, according to the manufacturer instructions. Tissue was homogenized using a TissueLyser II (QIAGEN) for 3' at 30Hz/s of frequency.

The total RNA concentration of each sample was determined using a *NanoDrop* Fluorospectrometer (Thermo Fisher Scientific) prior to sample storage at – 80°C. The ratio of absorbance values at 260 and 280 nm (Abs 260/280) was used to assess purity of total RNA samples. All samples used in these studies had Abs 260/280 ratios > 1.9. In addition, the RNA integrity and quality of each sample was determined using an Agilent 2100 Bioanalyzer following the protocol provided by the manufacturer. All samples used in the present study had RNA integrity number (RIN)>6.5.

To avoid amplification of genomic DNA sequences, all RNA samples were treated with DNase I and reverse transcription reactions were performed using 1 µg of RNA.

After addition of dNTPs (10 mM) and random hexamers (50 µM) to prime the first strand for cDNA synthesis, RNA was denatured at 65°C for 5 min and then placed on ice. Next, 4 µl of 5X RT buffer, 1 µl of DTT (0.1 M), and RNaseOUT were added to the mix. Superscript IV Reverse Transcriptase (Thermo Fisher Scientific) was added to the mixture which was further incubated at 25°C for 5 min and then heated to 50°C for 15 min. At the end of the retrotranscription the enzyme was inactivated at 70°C for 15 min. The cDNA was diluted in nuclease-free water (Thermo Fisher Scientific) and used as a template in the qPCR assays.

Primer pairs were bioinformatically designed using the tool Primer3 (http://biotools.umassmed.edu/bioapps/primer3_www.cgi) or searched in PrimerBank (https://pga.mgh.harvard.edu/primerbank/). Each primer couple was tested with the on-

line oligo analysis tool (http://www.operon.com/tools/oligo-analysis-tool.aspx; http://unafold.rna.albany.edu/?q=mfold/RNA-Folding-Form2.3) for their ability to form hairpins, homo- and hetero-dimers. Finally, selected primers were in silico tested to verify their amplification specificity using the tool in-Silico-PCR implemented in the UCSC Genome Browser (https://genome.ucsc.edu/cgi-bin/hgPCR).

Each PCR reaction was performed in a 20 µl volume combining 20 ng of cDNA, 0.5 or 0.25 µM of forward and reverse primers and 10 µl of SYBR green 2X PCR master mix (Thermo Fisher Scientific).

The qRT-PCR was performed using the following settings: 15 min at 95°C for denaturation of cDNA/RNA hybrid, followed by 40 cycles of 30 s at 95°C and 60°C for 1 min, followed by one step and hold cycle starting to determine the melting curve data. Each primer pair yielded a single peak in the melting curve.

Nuclease-free water (Life Technologies), instead of cDNA template, was added to the no-template control qPCR. The mix used for qRT-PCR was prepared as follows (mix described is for one well):

Component	Volume µl	Volume µl
H_2O DNase/RNase *free*	5	4
primer Forward (10 µM)	0.5	1
primer Reverse (10 µM)	0.5	1
Power SYBR Green PCR Master Mix	10	10
cDNA (20 ng/µl)	4	4
Total volume	20	20

Table 1: Mix used for real-time PCR

The cycle threshold (Ct) was used to calculate relative amounts of target RNA.

Table 2 summarizes the sequences and sources of primers used in this study. Samples that do not reach the threshold line are considered not above background.

We used at least three biological and three technical replicates.

The Cts of target genes were normalized to the levels of four housekeeping genes ACTB, TBP, GAPDH and RPL4 resulting in the same pattern. Here, we show data normalized to TATA box binding protein (TBP) as endogenous controls in each group. Reference genes were chosen according to their homogeneous expression in analyzed samples. The average Ct for each gene is calculated by subtracting the Ct of the sample RNA from that

of the control RNA for the same time measurement. This value is known as the ΔCt and reflects the relative expression of the treated sample compared with the control and becomes the exponent in the calculation for amplification 2ΔCtcont-ΔCtsample, equivalent to fold change in expression.

Target gene	**Primer sequence**
Actb	F-5' GGCTGTATTCCCCTCCATCG 3' R-5' CCAGTTGGTAACAATGCCATGT 3'
Angptl4	F-5' ACAGTGACTTTGGTTGTGGC 3' R-5' CTCGAGCCCATGTTTTCTGG 3'
Anp	F-5' GTGCGGTGTCCAACACAGAT 3' R-5' TCCAATCCTGTCAATCCTACCC 3'
Gapdh	F-5'CATGGCCTTCCGTGTTCCTA 3' R-5'GCTTCACCACCTTCTTGAT 3'
Glut4	F-5'GTGACTGGAACACTGGTCCTA 3' R-5'CCAGCCACGTTGCATTGTAG 3'
Pdk4	F-5' AGGGAGGTCGAGCTGTTCTC 3' R-5'GGAGTGTTCACTAAGCGGTCA 3'
Prdx4	F-5' CTCAAACTGACTGACTATCGTGG 3' R-5' CGATCCCCAAAAGCGATGATTTC 3'
Rgs2	F-5' ACCTGCCCACTGAGAAATCA 3' R-5' GCTGTTTGGCCCTGTAACTT 3'
Rpl4	F-5' GCCCAGAAATCCAAAGAGCC 3'

	R-5’ GCCTGGCGAAGAATGGTATT 3’
Tbp	F-5’ AAGGGAGAATCATGGACCAG 3’ R-5’ CCGTAAGGCATCATTGGACT 3’
Txnip	F-5’CCTGTGAAGGGTTGTGGTTG 3’ R-5’CCATCAGCTCGCAGACATTC 3’
Hif1α	F-5’GATGCAGCAAGATCTCGGC 3’ R-5’GGTGAGCCTCATAACAGAAGC 3’

Table 2. Sequences of primers used for real-time PCR

Before performing qRT-PCR experiments primers were experimentally tested to verify their amplification efficiency. Serial dilutions from 20 to 1,25 ng/µl of cDNA (final concentration in 20 µl reaction volume) were used to calculate primers efficiency. In the table below are indicated results for each primer pair amplifying tested genes. cDNA was synthesized as previously described using a pool of RNAs derived from whole heart tissues. We indicated primer concentration, R^2 for the linear regression in the graph representing $\log_2$[cDNA] vs C_t, the y-intercept, melting temperature (T_m), and the efficiency of the amplification calculated as $10^{-1/m}$ where m is the angular coefficient of the straight line interpolating points of the graph.

Gene	Primer concentration (nM)	R^2	y-intercept	T_m (°C)	Efficiency
Actb	500	0.99	24	82.4	84%
Angptl4	500	0.98	31.8	81.8	97%
Anp	500	0.98	28	62	95%
Gapdh	500	0.99	20	80.7	86%
Pdk4	500	0.98	32	84.6	82%
Prdx4	500	0.99	28.8	75.7	101%

Rgs2	250	0.99	31.8	76	86%
Rpl4	500	0.99	24.3	79.5	90%
Tbp	250	0.99	28.3	80.6	84%
Txnip	500	1	26	83.6	101%
Hif1 α	500	0.99	25.2	78.5	90%

Table 3. Parameters of primers amplification efficiency

3.8 Isolation and culture of adult mouse ventricular cardiomyocytes

Adult mouse ventricular myocytes (AMVMs) were isolated from the hearts of 12-weeks old C57Bl6/J mice as previously described[87]. In brief, mice were injected intraperitoneally (i.p.) with 1,000U heparin 30 min before the isolation procedure to prevent coagulation of blood in the arteries. Hearts were quickly cut out and the aorta cannulated. Hearts were then perfused with perfusion buffer (PB, in mM: NaCl 120, KCl 14.75, KH_2PO_4 0.6, Na_2HPO_4 0.3, $MgSO_4$ 1.2, HEPES 10, $NaHCO_3$ 4.6, taurine 30, BDM 10, glucose 5.5, pH 7.4) for 2 min to remove the blood. Next, hearts were perfused with PB containing 1.2 mg/ml collagenase type II (Worthington) and 0.05 mg/ml protease type XIV (Sigma) for 3 min at 2 ml/min and then for 8 min at 1.5 ml/min. After perfusion, hearts were placed into 5 ml of PB added with 10% FBS and 12.5 µM $CaCl_2$, cut into smaller pieces and cardiomyocytes dissociated by gentle pipetting. The suspension was filtered through 100 µm mesh, centrifuged at 180 g for 1 min and resuspended in PB containing increasing Ca^{2+} concentration. Ca^{2+} concentration was gradually increased from 0.25 mM to 1 mM to avoid Ca^{2+} overload and hypercontracture. After each step cardiomyocytes were allowed to sediment by gravity for 10 min. Cells were plated at non-confluent density (at least 25,000 rod-shaped cells/ml) on 6-well plates pre-coated with laminin (20 µg/ml) in DMEM supplemented with 5.5 mM glucose, 5% FBS, 1% penicillin/streptomycin, 25 µM blebbistatin and kept at 37°C in presence of 5% CO_2. After 1h medium was changed to DMEM supplemented with 5.5 mM glucose, 25 µM blebbistatin, 1% penicillin/streptomycin.

3.9 Treatment of primary cardiomyocytes

AMVMs were treated in culture media with following additions: normal glucose (NG, 5 mM), high glucose (HG, 25 mM) or high mannitol (HM 25 mM, osmotic control) for 6h. To inhibit MAO activity cells were pre-treated with 100 µM pargyline (Sigma) for 30 min. Autophagic flux was assessed after 4 h of incubation with 50µM cloroquine (CQ). After indicated incubation, samples were collected to assess levels of markers of autophagy or related catabolic processes by western blotting.

3.10 Western blot

AMVMs were plated in 6 well-plates at density from 25.000 to 50.000 cells/well. Cells were homogenized in 50 µl RIPA lysis buffer (Merck Millipore) containing protease (cOmplete mini protease inhibitor cocktail, Roche) and phosphatase (PhosSTOP, Roche) inhibitors. Cells were then detached using a cell scraper. Homogenized samples were sonicated (Labsonic P Braun Biotech International), centrifuged at 12000 x g for 20 min at 4°C and then the pellet was discarded. Protein concentration was determined using PierceTM BCA Protein Assay Kit (Thermo Fisher Scientific) following the manufacturer's protocol. Samples were mixed with NuPAGE™ LDS sample buffer 4X (Thermo Fisher Scientific) and β-mercaptoethanol (3%) in order to denaturate and solubilize the proteins. Samples were heated at 90°C for 5 minutes and then loaded on the gel or aliquoted and stored at -20°C.

Proteins were separated on NuPAGE™ 4-12% gradient Bis-Tris (Thermo Fisher Scientific) SDS-PAGE using the MES running buffer (50 mM MES, 50 mM Tris Base, 0.1% SDS, 1 mM EDTA, pH 7.3) at 130 V and transferred to the nitrocellulose membrane 0,45 µm (Amersham Protran) or PVDF membrane using transfer buffer (25 mM Bicine, 25 mM Bis-Tris, 1mM EDTA, 20% methanol, pH 7.2) at 400 mA for 70 min. At the end of the transfer, the membrane was incubated with Red Ponceau dye (Sigma-Aldrich) to stain all the proteins on the membrane, destained with diluited NaOH 0,1M, washed and saturated using 3% BSA dissolved in TBS-T (Tris buffered saline solution, 0.1% Tween 20), composed of 50 mM Tris-HCl, 85 mM NaCl, pH 7.6). After 1 h of blocking at room temperature, membranes were incubated at 4°C overnight with primary antibody diluted in 3% BSA. Antibodies used in this study to detect proteins of interest are listed in Table 4.

Primary antibody	Manufacturer	Dilution
Anti-β-Actin (SPM161)	SC-56459	1:1000
Anti-LC3B	CST2775	1:1000
Anti-MFF	Abcam (ab81127)	1:500
Anti-p62/SQSTM1	Sigma P0067	1:1000
Anti-pAMPKα (Thr172) (D79.5E)	CST4188	1:1000
Anti-AMPKα	CST2532	1:1000
Anti-pDRP1 S616 (D9A1)	CST4494	1:1000
Anti-DLP1 (DRP1)	BD Biosciences	1:1000

Table 4: List of primary antibodies used in the study

Following incubation with primary antibodies, membranes were washed three times for 10 min with the washing buffer TBS-T and incubated with secondary antibodies for 1 h at room temperature. Secondary antibodies used were:

Anti-mouse (Santa Cruz Biotechnology, SC-516102), dilution 1:3000

Anti-rabbit (Santa Cruz Biotechnology, SC-2357), dilution 1:3000

Secondary antibody is conjugated to reporter enzyme horseradish peroxidase (HRP). After incubation with secondary antibody, membrane was washed three times (10 min each). Immunoreactive bands were visualized and digitalized with the Alliance Mini HD9 UVITEC imaging system (Eppendorf), using LiteAblot luminol solutions (EuroClone). Bands were detected using Alliance (Uvitec) and analyzed using ImageJ software. This program allows the quantification of the optical density of bands or dots that is directly proportional to the protein content.

3.11 Statistical analysis

All values are expressed as mean ± SEM.

To correlate and compare microarray data and relative mRNA expression of selected genes, the Pearson correlation coefficient was calculated to measure the linear correlation between two variables. Pearson's r can range from -1 to 1. An r of -1 indicates a perfect negative linear relationship between variables, an r of 0 indicates no linear relationship between variables, and an r of 1 indicates a perfect positive linear relationship between variables. Comparisons between two groups were performed using non paired two-tailed Student's t-test. A value of $p<0.05$ was considered significant.

IV. RESULTS

4.1 The expression profile of diabetic hearts differs from all the other groups

Transcriptional regulation is a complex process that plays a pivotal role in reprogramming cellular states in response to internal or external changes that occur in physiological growth and pathological conditions. Hence, measuring and analyzing transcriptional changes provide crucial information on mediators and pathways involved in cellular responses to physiological and pathological stimuli[141]. Functional genomics involves the simultaneous analysis of large datasets of information derived from various biological experiments. Microarray technology is now a consolidated methodology for transcription profiling and large-scale genomics studies[139,148].

Microarray is a small chip that contains thousands of probes fixed to its surface, which can hybridize with fluorescently labeled RNA samples (the targets). Hybridization intensities, represented by the amount of fluorescent emission, give an estimate of the amounts of the different transcripts that are present in the RNA sample. A single microarray experimental assay, like most high-throughput technologies, records the transcript levels of all the genes in a given condition, for a particular cell type or mixture, at a specific time. One of the goals of microarray data analysis is to cluster genes or samples with similar expression profiles together, to make meaningful biological inference about the set of genes or samples.

To have a better insight of the deregulated gene and the mRNA expression, we conducted the microarray analysis in the cardiac tissue from a mouse model of T1D induced by treatment with STZ, while MAO involvement and contribution were evaluated through a classical pharmacological approach, using pargyline as an inhibitor for both MAO-A and MAO-B. The following groups were examined: (i) control mice (n=3), (ii) STZ-treated mice (n=3), (iii) control mice treated with MAO inhibitor pargyline (n=3), (iv) STZ mice treated with pargyline (n=3).

Clustering is one of the unsupervised approaches to classify data into groups of genes or samples with similar patterns that are characteristic of the group[139]. The analysis of differentially expressed genes grouped samples in a peculiar manner. Biological replicates within each experimental group were similar to each other and samples from

STZ-mice formed a distinct group separated from all the other groups. Interestingly, diabetic hearts treated with pargyline were more similar to control hearts than untreated ones (Figure 14).

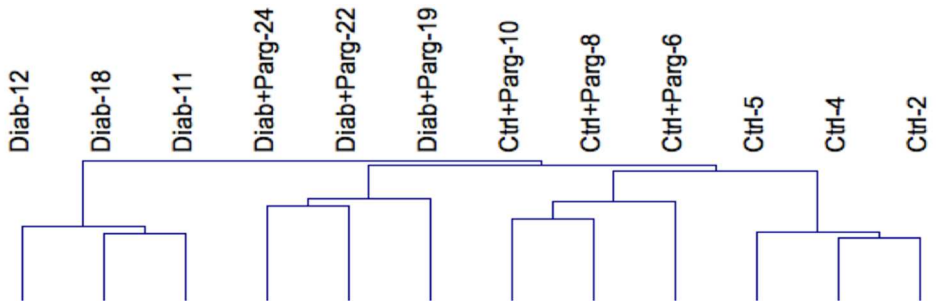

Figure 14: Hierarchical organization of samples based on gene expression profile. Hierarchical clustering of samples from cardiac tissue of mice belonging control (ctrl, n=3), diabetic hearts (diab, *n*=3), treated or not with pargyline (each of them n=3). Data were analyzed through Pearson clusterization with average linkage algorithm. Biological replicates within each group are similar to each other and gene expression profile of samples from diabetic mice formed a distinct group. The expression profile of diabetic hearts treated with pargyline is more similar to those of control.

4.2 SOTA analysis groups genes in peculiar clusters

Subsequently to the identification of differentially expressed genes, we carried out the SOTA analysis to group genes according to common expression profiles to identify interesting expression patterns that may explain the activity of pargyline. The algorithm identified 11 clusters that are represented in Figure 15.

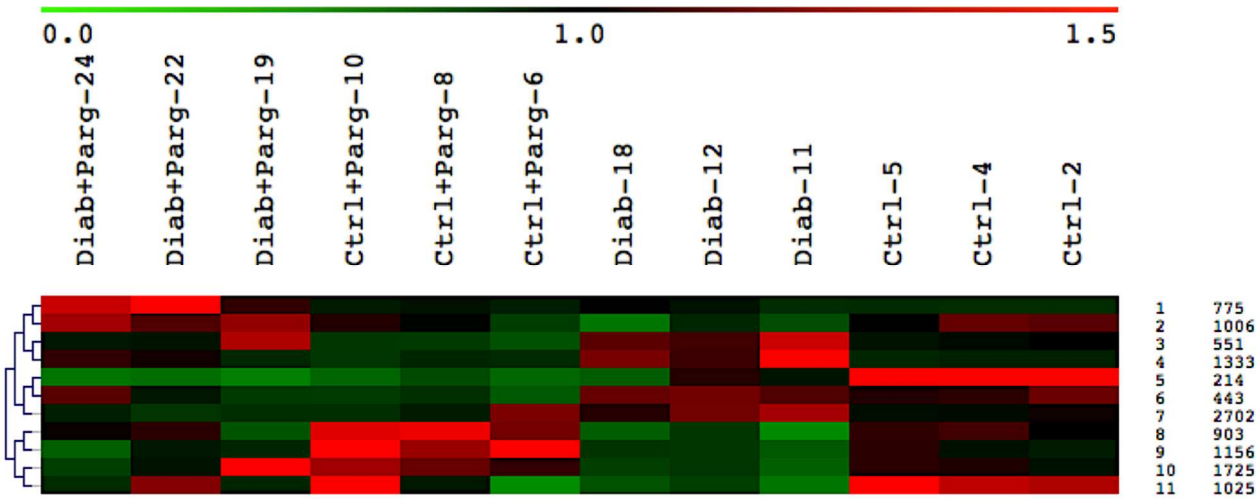

Figure 15: Gene expression clusters of differentially expressed genes according to SOTA analysis. Eleven clusters were identified. Numbers on the right are for cluster number and genes belonging to the respective cluster. Red indicates the over-expression while green the under-expression.

We were interested in the identification of transcriptomic changes induced by diabetes, MAO activity and its inhibition by pargyline. In fact, we excluded clusters in which pargyline alone affected the gene expression profile of controls and/or does not prevent the transcriptomic changes induced by diabetes. Among the clusters, genes belonging to clusters 5 and 6 showed similar effect of pargyline on gene expression profile. Furthermore, results concerning clusters 8 and 10 are similar. For further analyses, we considered genes included within clusters 4 and 7 and those in clusters 2 and 11 (containing up- or down-regulated genes in diabetic hearts, Table 5), since pargyline normalized the gene expression profile in those clusters and their analysis could provide clues on the biological function of genes affected by pargyline in diabetic hearts.

We found 4035 differentially expressed mRNAs upregulated and 2031 downregulated in diabetes with respect to control condition in which treatment with pargyline prevented gene expression changes.

A detailed description of gene clusters identified with SOTA analysis is shown in Table 5

Cluster	
1	Activated genes in diabetic condition in which pargyline does not prevent the pattern
2-11	Downregulated genes in diabetic condition in which pargyline prevents the pattern
3	Upregulated genes in diabetic condition compared to control in which pargyline has no effect.
4-7	Activated genes in diabetic condition in which pargyline reverts the expression profile to baseline levels. Pargyline treatment does not affect the gene expression profile of control mice.
5-6	Downregulated genes in diabetic condition. Pargyline treatment affects the gene expression profile in control condition resulting in downregulation
8-10	Genes that are not affected by pargyline treatment. These genes are downregulated in diabetic condition compared to control condition even after pargyline treatment
9	Pargyline treatment affects gene expression profile of control condition

Table 5: Description of gene clusters identified with SOTA analysis

4.3 GO categories

In gene-expression microarray studies, lists of hundreds or thousands of genes that differ in expression between samples are generally obtained. To interpret this huge amount of data, bioinformatic algorithms have been developed with the task to reorganize biological information into networks that are easy to be visualized and understood[149]. Genes were categorized in GO classes. GO organizes genes into hierarchical categories based on biological process, molecular function and subcellular localization[146,149]. GoMiner is a bioinformatic tool that organizes lists of 'interesting' genes for biological interpretation.

To understand the function of chosen genes, they were classified according to the GO vocabulary using the GoMiner algorithm. However, only enriched definitions were considered because GO terms described with GoMiner having the FDR<0.05 (false discovery rate) were considered redundant terms using Categorizer algorithm.

Interestingly, the most represented GO categories (Figure 16) among 388 GO terms for cellular component within upregulated genes in diabetic condition were those for nucleus (GO:005634, 8,46%), mitochondrion (GO:0005739, 3,10%), cytoskeleton (GO:0005856, 2,96%) and vacuole (GO:0005773, 2,26%).

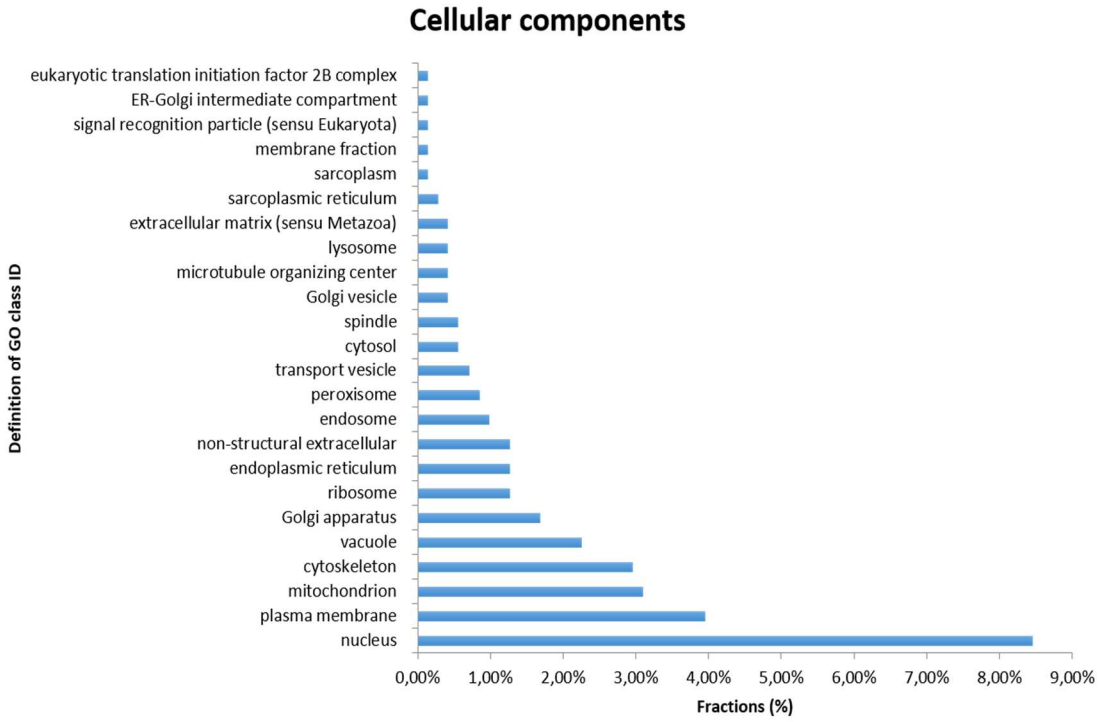

Figure 16: GO description of the transcriptome of overexpressed genes in diabetic condition. Histogram illustrating the percentage of fractions in the cluster of overexpressed genes in diabetic hearts in

which pargyline is able to prevent the effect on gene expression profile and GO terms for Cellular Component categories. The most represented GO categories were those for nucleus, mitochondrion, cytoskeleton, and vacuole. FDR<0.05

Among 222 GO terms, the most represented for cellular component of downregulated genes in diabetes were those for nucleus (GO:005634, 10,93%), cytoskeleton (GO:0005856, 4,10%) and plasma membrane (GO:0005886, 3,55%) as shown in Figure 17.

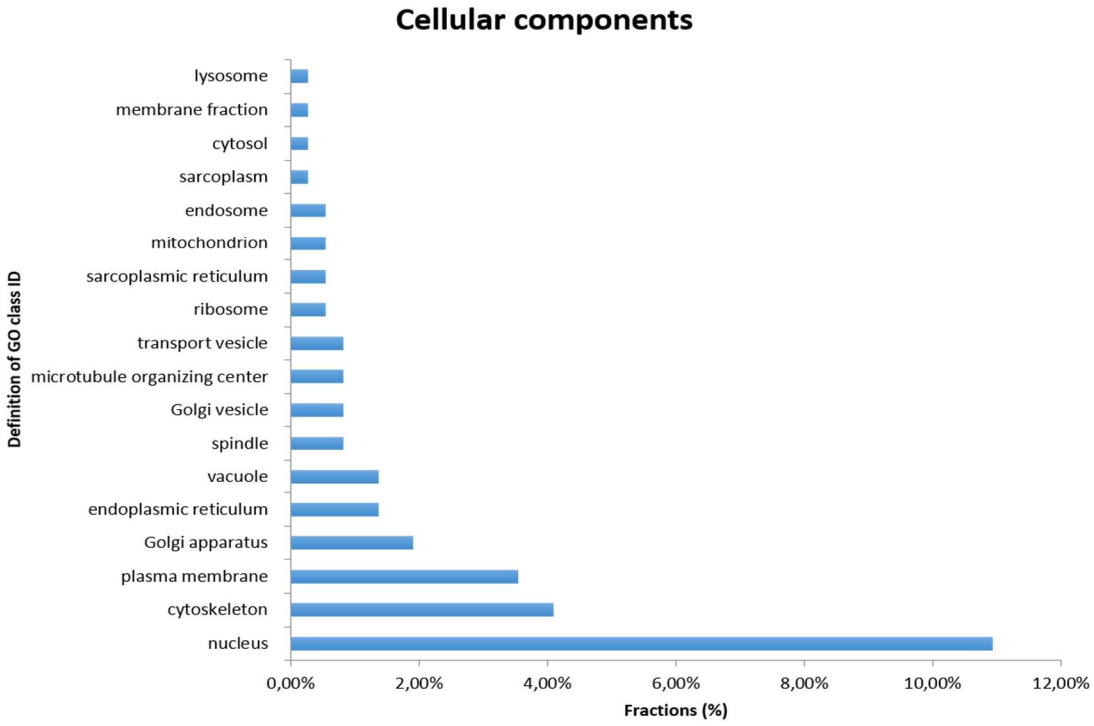

Figure 17: Gene ontology description of the transcriptome of downregulated genes in diabetic condition. Histogram illustrating the percentage of fractions in the cluster of downregulated genes in diabetic hearts in which pargyline is able to prevent the effect on gene expression profile and GO terms for Cellular Component categories were those for nucleus, cytoskeleton and plasma membrane. FDR<0.05

4.4 ECM and mitochondria are the mostly enriched classes in the upregulated genes cluster

A common method of visualizing gene expression data is to display it as a heatmap. In heat maps the data is displayed in a grid where each row represents a gene and each column represents a sample. The color and intensity of the boxes is used to represent changes (not absolute values) of gene expression.

Our results showed that most genes involved in the ECM synthesis are upregulated in diabetes and this is prevented by pargyline treatment (Figure 18). Examples for genes described in the heatmap are: Ctgf (Connective Tissue Growth Factor), Tgfb

(Transforming Growth Factor Beta), Fgf12 (Fibroblast Growth Factor 12), Col15A1 (Collagen Type XV Alpha 1 Chain), Fgf16 (Fibroblast Growth Factor 16), Col5A2 (Collagen Type V Alpha 2 Chain), Lum (Lumican), Col11A1 (Collagen Type XI Alpha 1 Chain), Col13A1 (Collagen Type XIII Alpha 1 Chain).

Cardiac fibrosis is one of the underlying causes of diastolic dysfunction and a major feature of DCM[43]. In a previous work published in the laboratory of Prof. Di Lisa it has been observed that STZ-treated hearts displayed 4-fold increase in collagen deposition as compared to normal hearts[43]. Interestingly, pargyline treatment prevented the modification, demonstrating the efficacy of MAO inhibitors to prevent fibrosis progression in T1D animals and in pressure overload[43,86,87]. Our result supports and extends what has been previously showed.

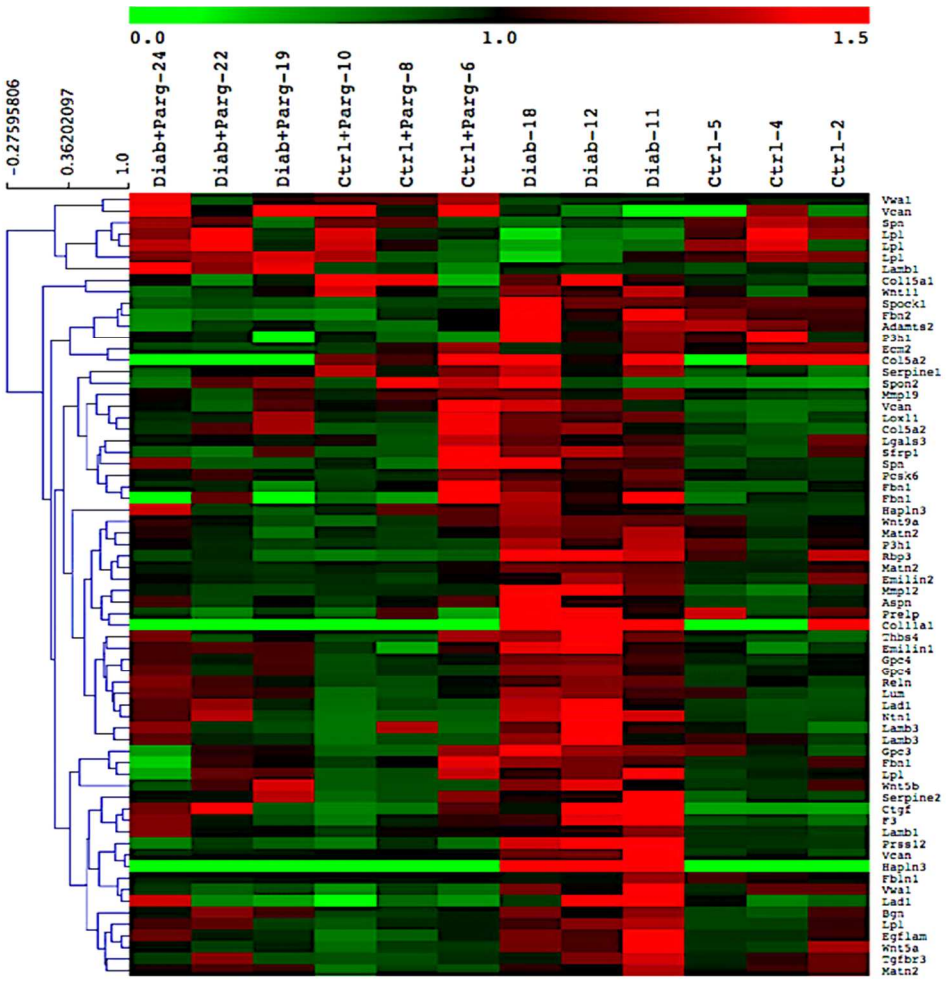

Figure 18: Heatmap and hierarchical clustering of genes based on the DE genes belonging to upregulated genes in diabetic condition. Heatmap of ECM-related genes was generated from a subset of differentially expressed genes. Most up-regulated genes in diabetes were involved in ECM synthesis. Columns represent samples, while rows represent genes. The relative value for each gene is depicted by color intensity, with red indicating upregulated and green indicating downregulated genes. mRNA expression profile between the groups with expression 0 < fold change < 1,5.

In association with GO analysis, we performed the GSEA to evaluate the association between functional pathways and differential expression. GSEA is a powerful analytical and computational method, that considers a group of genes related to their involvement in a specific pathway, or genes that share a chromosomal location or a specific function.[147,148]. Gene sets are defined based on prior biological knowledge, e.g., published information on biochemical pathways or co-expression in previous experiments. GSEA was initially used to discover metabolic pathways altered in diabetes[147,150] and was subsequently applied to discover processes involved in several pathological conditions[147,151].

GSEA analysis showed that overexpressed genes with highest enrichment score belong to ECM (Figure 19) and mitochondria (Figure 21) categories. T1D induced a variation in the expression profile of genes involved in these functions and this change was prevented by pargyline.

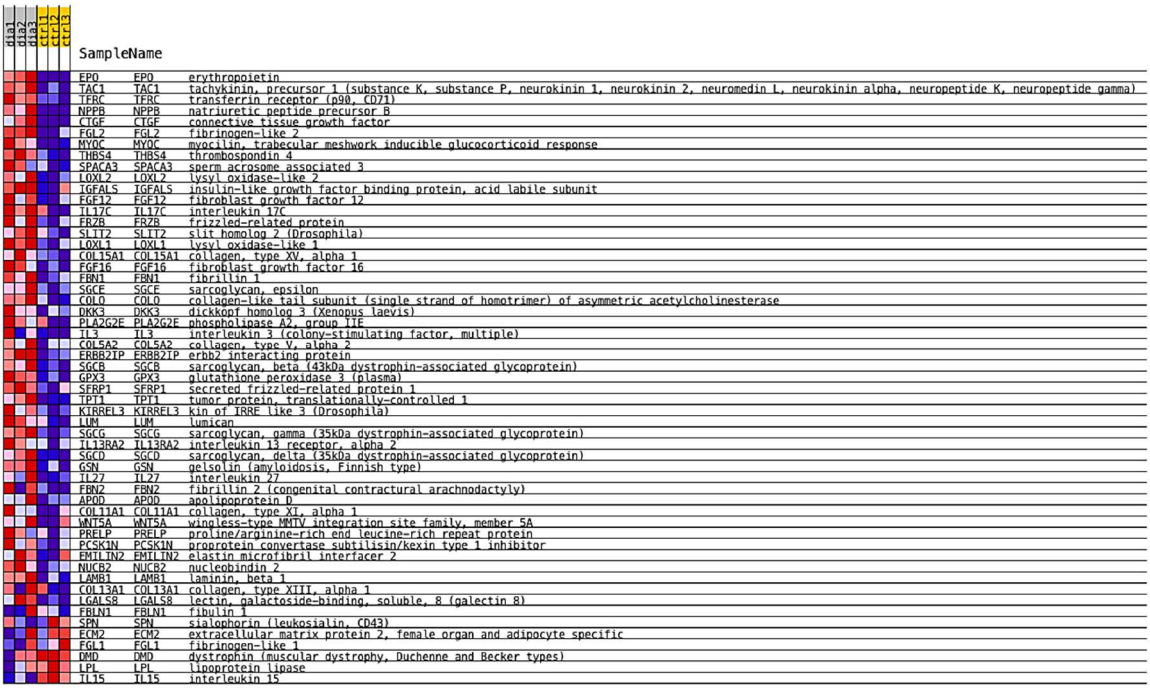

Figure 19: Normogram of the down-and up-regulated gene sets enriched for ECM molecules in the array dataset. Heat map of the gene set 'dia vs ctrl' containing all genes found significantly up-regulated among differentially expressed ones when comparing STZ-treated mice versus the control ones. Colors range from dark red to dark blue representing respectively the highest and lowest expression of a gene.

In the same cluster, components of organelles, nucleus, and Golgi apparatus were enriched. Among the organelles, mitochondrial components are mostly affected (Figure 20). The genes affected to the greatest extent were as follows (Figure 21): Mfn2

(Mitofusin 2), Atp5g3 (ATP Synthase Membrane Subunit C Locus 3), Atp5β (ATP Synthase F1 Subunit β), Atp7b (ATPase Copper Transporting Beta), Ndufv1 (NADH:Ubiquinone Oxidoreductase Core Subunit V1).

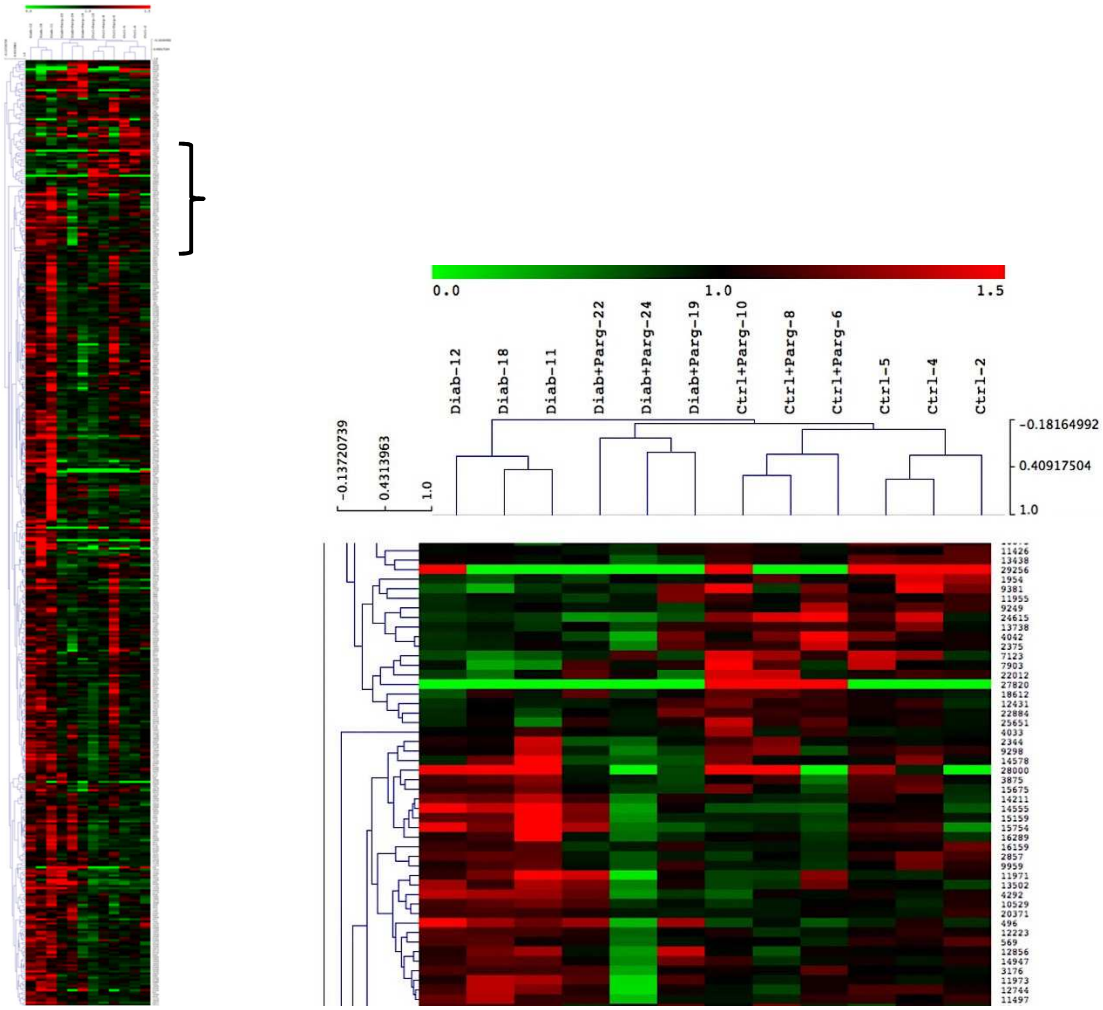

Figure 20: Heatmap and hierarchical clustering of all samples based on the differentially expressed genes belonging to upregulated genes in diabetic condition. Heatmap of ECM-related genes was generated from a subset of differentially expressed genes. Most up-regulated genes in diabetes were involved in mitochondrial function. Columns represent samples, while rows represent genes. The relative value for each gene is indicated by color intensity, with red indicating upregulated and green indicating downregulated genes. On the right, a magnification of the selected section as representative. mRNA expression profile between the groups with expression 0 < fold change < 1,5.

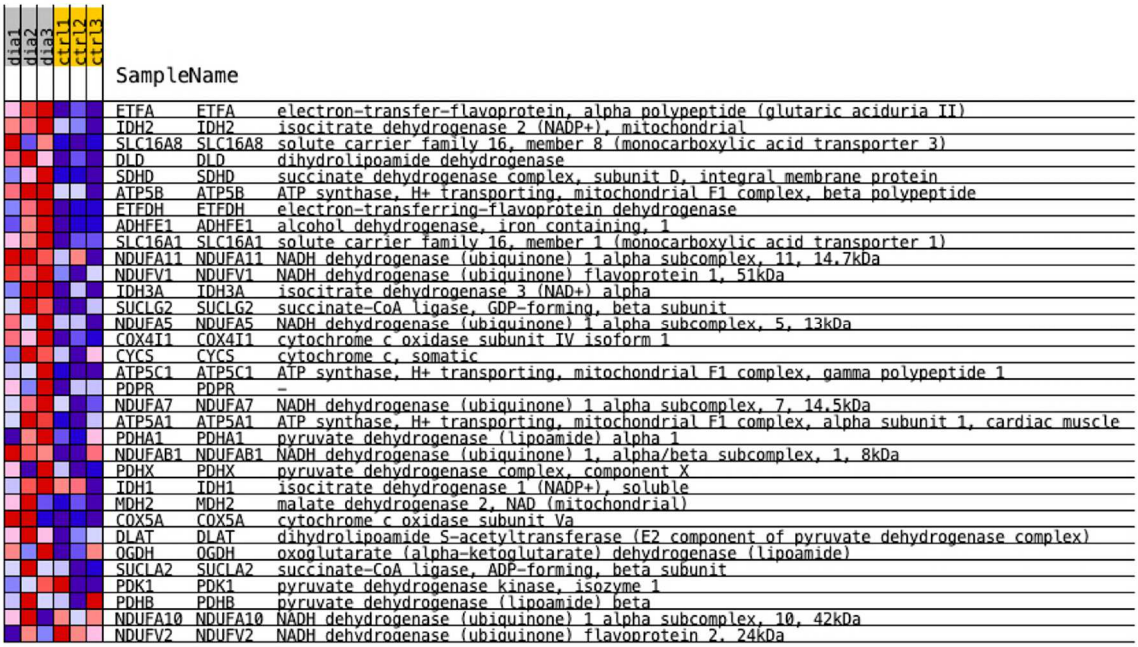

Figure 21: Normogram of the down-and up-regulated gene sets enriched for mitochondrial components in the array dataset. Heat map of the gene set 'dia vs ctrl' containing all genes found significantly up-regulated among differentially expressed ones when comparing STZ-treated mice versus the control ones. Colors range from dark red to dark blue representing respectively the highest and lowest expression of a gene.

4.5 Genes belonging to catabolic processes and mitochondria categories are upregulated in diabetes in a MAO-dependent manner

A leading-edge analysis was carried out on the cluster of overexpressed genes in diabetic hearts in which pargyline administration prevented changes in the expression values.

To determine which genes have the highest impact on the biological process under study, a portion of the GSEA was dedicated to performing leading edge analysis of the differentially expressed genes. The leading edge analysis allows the GSEA to determine which subsets (referred to as the leading edge subset) of genes contributed the most to the enrichment signal of a given leading edge subset or core enrichment[147]. The leading-edge analysis is determined from the enrichment score, defined as the maximum deviation from zero[147]. Remarkably, the analysis based on cellular function performed on the cluster of genes overexpressed in T1D showed that the highest enrichment score belongs to catabolic processes (GO: 0030163; ES=8,36, p=8,28E-11) and mitochondria (GO:0005739; ES=7,64, p=7,37E-12) categories. Pargyline prevented changes in gene expression profile of these categories.

The GSEA analyses allowed to uncover transcriptomic changes induced in diabetes in a MAO-dependent manner and identified mitochondria, degradative processes and ECM as categories that were mostly affected. Taken together, these results demonstrate that changes in the gene expression profile occurring in T1D can be completely prevented by pargyline. The present findings confirm and extend the characterization of mitochondrial dysfunction and MAO involvement in DCM described previously.

4.6 Validation of gene expression profiles by means of qRT-PCR

Due to the limited sample size of the majority of experiments involving microarray analysis, statistical tools simply work like a filter that highlights the significant differentially expressed genes, but do not represent the ultimate validation of the differential expression. Transcripts detected by statistical analysis need to be validated by other approaches to confirm their differential expression[148].

Since differences in the gene expression profile can be generated by false positives, alternative techniques such as qRT-PCR are required to validate microarray results. Among the four housekeeping genes (ACTB, TBP, GAPDH and RPL4) we used, here we show data normalized to TBP as endogenous controls in each group since it appeared as the most stable gene among all samples (Figure 22).

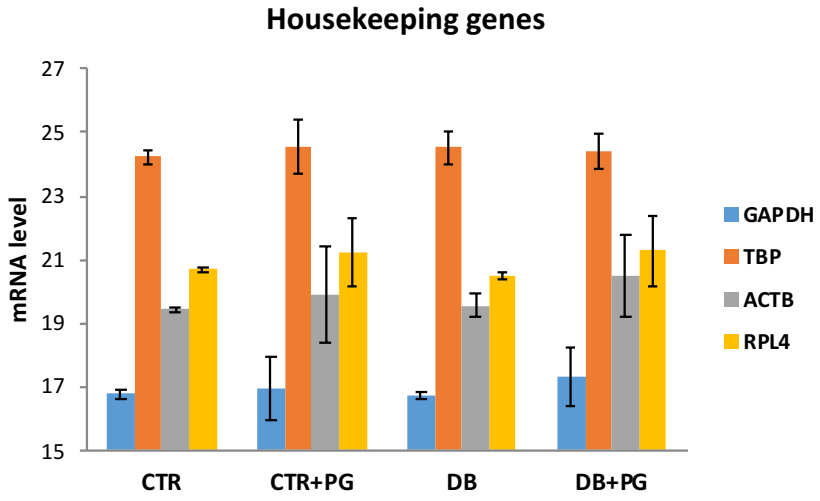

Figure 22: mRNA of four housekeeping genes. Trend of expression of four housekeeping genes. Reference gene were chosen according to their homogeneous expression in analyzed samples. mRNA level is expressed as mean ± SEM. GAPDH: Glyceraldehyde-3-Phosphate Dehydrogenase, TBP: TATA binding protein, ACTB: actin beta, RPL4: Ribosomal Protein L4.

The validation of the microarray was carried out on a series of randomly selected genes (Figure 23). The microarray validation involved the following genes: atrial natriuretic peptide (ANP), pyruvate dehydrogenase lipoamide kinase isozyme 4 (PDK4), glucose transporter type 4 (GLUT4), hypoxia-inducible factor 1α (HIF1α), thioredoxin-interacting protein (TXNIP), peroxiredoxin 4 (PRDX4), angiopoietin-like 4 (ANGPTL4), regulator of G-protein signaling 2 (RGS2). The RT-PCR data had comparable expression pattern as the microarray results for most of the randomly selected genes as confirmed by Pearson correlation coefficient (r). A strong correlation ($r \geq 0,7$) was observed for TXNIP (r=0,77), ANGPTL4 (r=0,82), ANP (r=0,99), PDK4 (r=0,99), PRDX4 (r=0,70) and RGS2 (r=0,71); HIF1α (r=0,57) and GLUT4 (r=0,63) showed a trend and a moderate correlation ($0,5 < r < 0,7$).

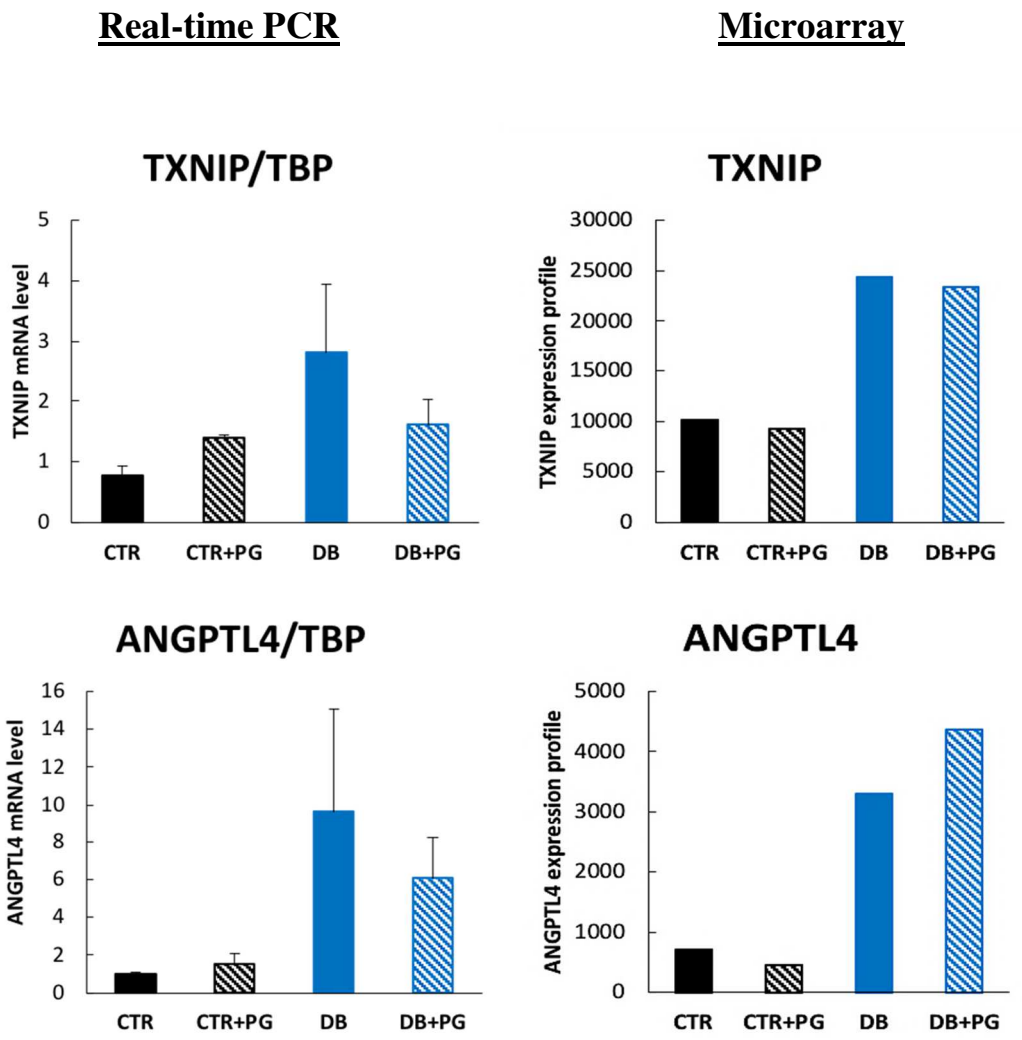

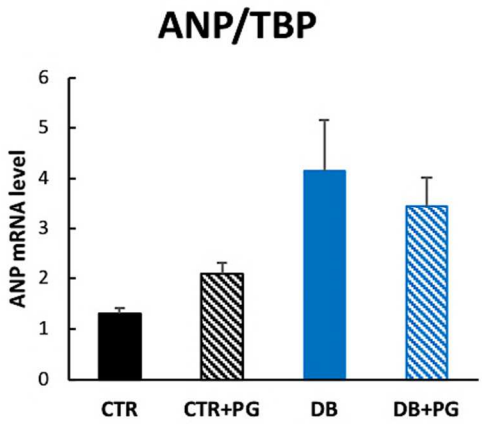
ANP/TBP
ANP mRNA level
0
1
2
3
4
5
6
CTR
CTR+PG
DB
DB+PG

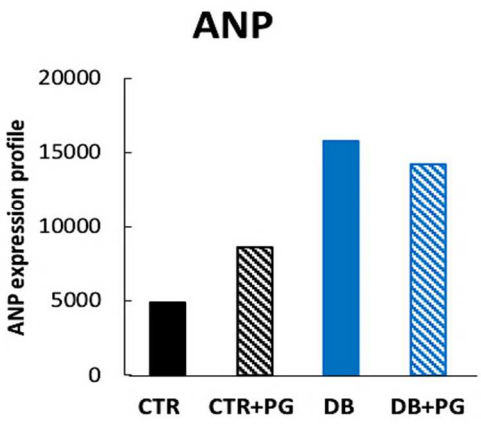
ANP
ANP expression profile
0
5000
10000
15000
20000
CTR
CTR+PG
DB
DB+PG

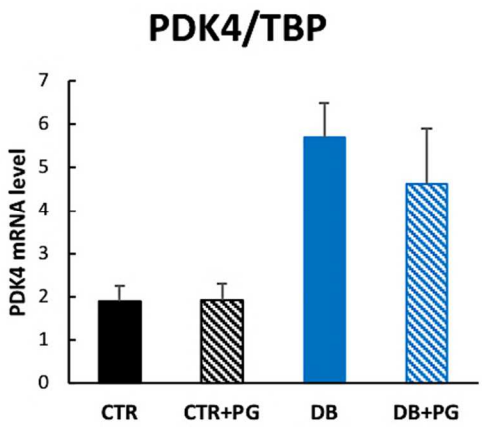
PDK4/TBP
PDK4 mRNA level
0
1
2
3
4
5
6
7
CTR
CTR+PG
DB
DB+PG

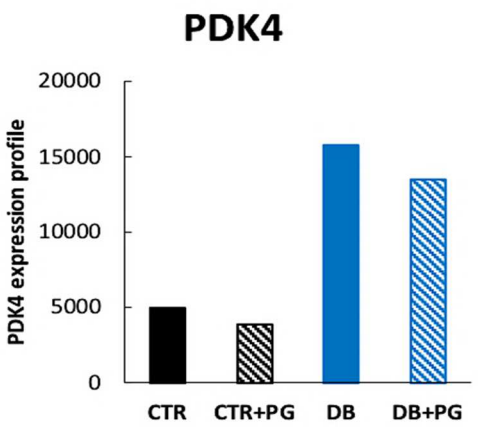
PDK4
PDK4 expression profile
0
5000
10000
15000
20000
CTR
CTR+PG
DB
DB+PG

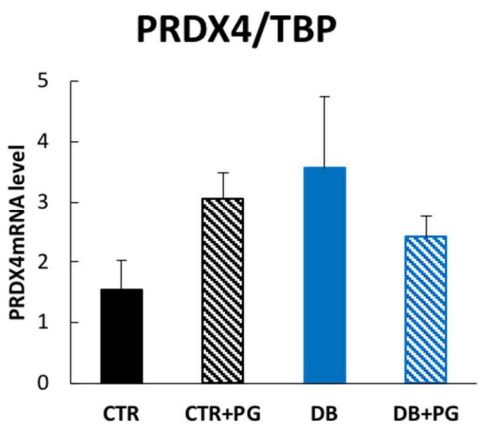
PRDX4/TBP
PRDX4mRNA level
0
1
2
3
4
5
CTR
CTR+PG
DB
DB+PG

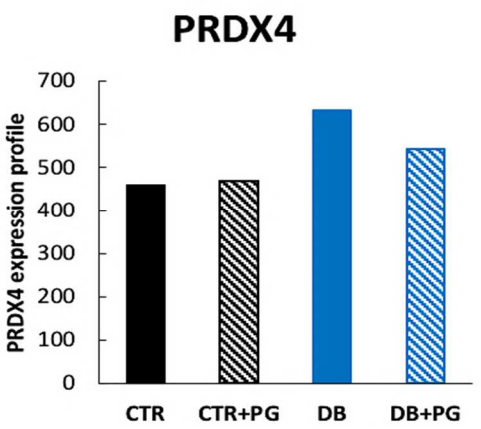
PRDX4
PRDX4 expression profile
0
100
200
300
400
500
600
700
CTR
CTR+PG
DB
DB+PG

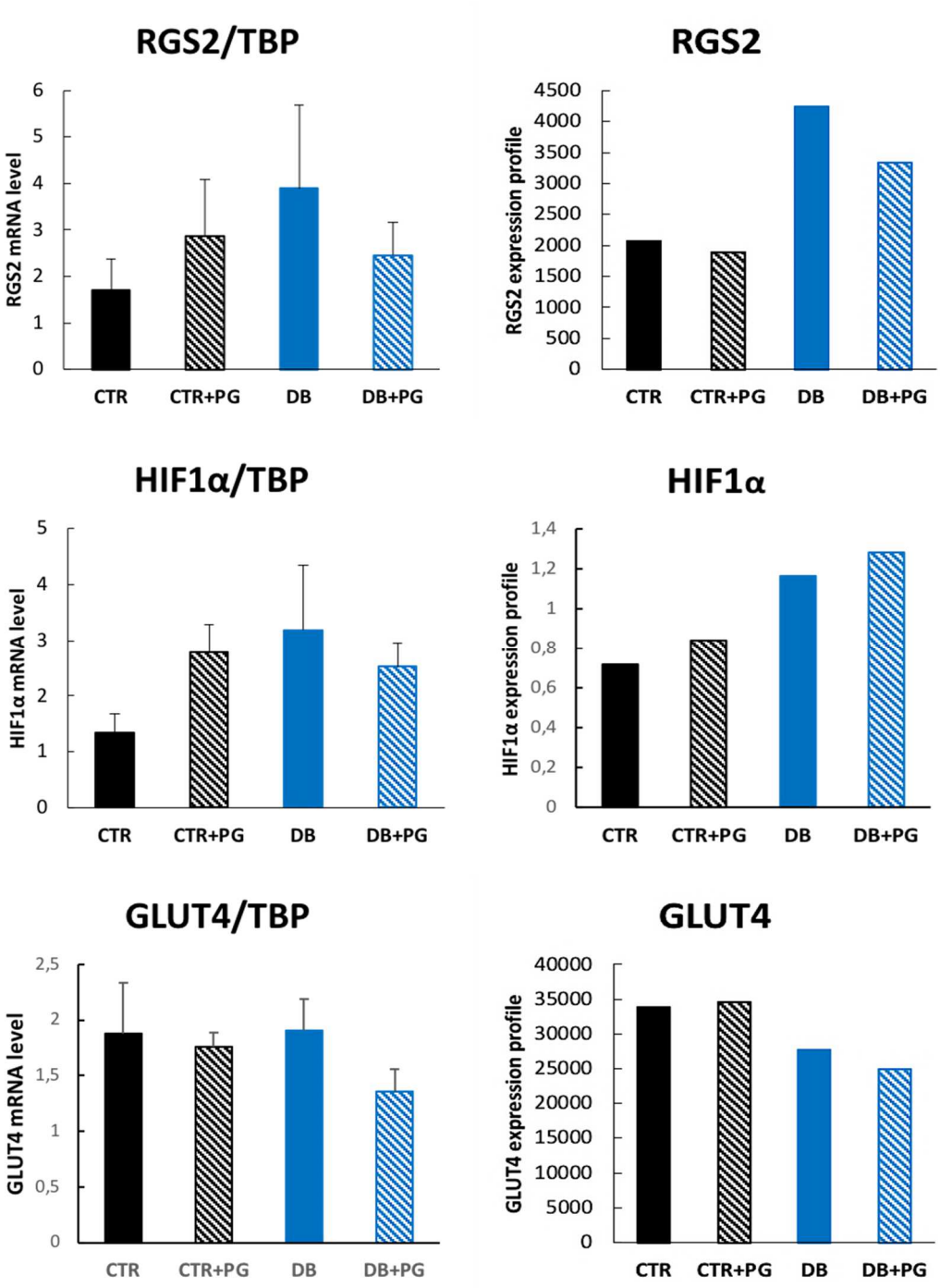

Figure 23: Validation of microarray by means of Real-time PCR. On the left panel, mRNA level was assessed by qRT-PCR; on the right panel, the expression profile was assessed through microarray. mRNA level is expressed as mean ± SEM. ANP: atrial natriuretic peptide, PDK4: pyruvate dehydrogenase lipoamide kinase isozyme 4, GLUT4: glucose transporter type 4, HIF1α: hypoxia-inducible factor 1α, TXNIP: thioredoxin-interacting protein, PRDX4: peroxiredoxin 4, ANGPTL4: angiopoietin-like 4, RGS2: regulator of G-protein signaling 2, TBP: TATA box binding protein.

4.7 Autophagy is increased in diabetic hearts

Following the successful validation of the microarray data and, considering that mitochondria and degradation processes were mostly affected in diabetic hearts in a MAO-dependent manner, we hypothesized that MAO activity might affect autophagy leading to mitochondrial and cellular derangements. To assess whether autophagy may be affected in our experimental groups, we measured protein levels of the mammalian LC3 in cardiac tissue (Figure 24). LC3-II protein is typically used as an autophagic marker, as its presence correlates with the number of autophagosomes. There was a significant increase in LC3-II in diabetic compared to the control hearts ($p<0,05$), suggesting that autophagy is increased in STZ hearts. Importantly, LC3-II protein levels were normalized in diabetic mice treated with pargyline.

An additional marker used to monitor autophagy is p62/SQSTM1[152] and an anticorrelation between LC3-II and p62 levels may reflect changes in the autophagy flux. In our conditions, in parallel with the reduction of LC3-II levels in the presence of the specific MAO inhibitor, there was a significant increase in p62 levels ($p<0,01$) suggesting a reduction in the autophagic flux (Figure 24).

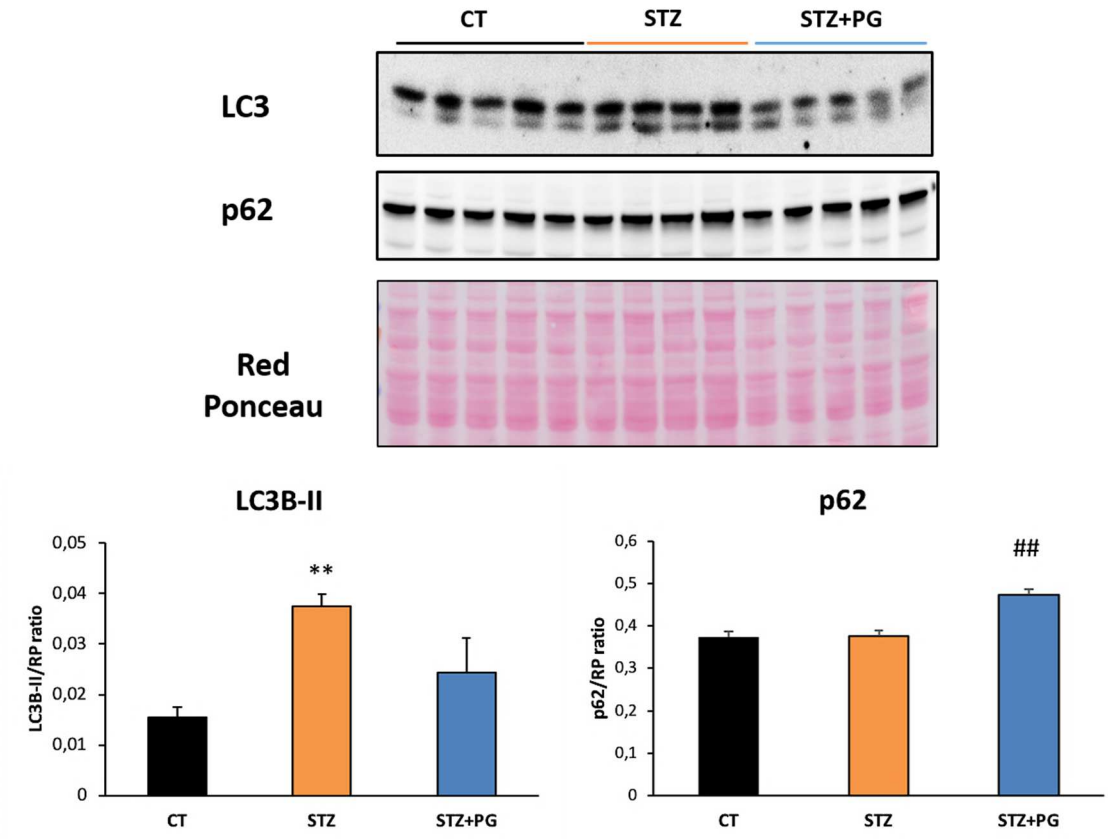

Figure 24: LC3B and p62 protein levels in cardiac tissue. Representative blots are shown for LC3B protein in control (n=5) and STZ-treated mice in absence (n=4) and presence of pargyline (n=5). The quantification of band intensity is shown normalized to total protein determined by Red Ponceau staining. Data were expressed as the mean ± SEM and analyzed by a non-paired two-tailed Student's *t* test (STZ *vs* CT **p<0,01; STZ+PG *vs* STZ ##p<0,01). LC3B: microtubule associated protein 1 light chain 3, CT: control mice, STZ: diabetic mice, STZ+PG: diabetic mice treated with pargyline.

4.8AMVMs exposed to HG and pargyline show reduced autophagy

An accurate assessment of the autophagic flux requires that all the experimental groups are paralleled by groups treated with inhibitors of lysosomal degradation. To evaluate changes in the autophagy flux due to T1D and/or MAO inhibition, an additional subset of experiments was performed in vitro employing AMVMs.

AMVMs were cultured with high glucose in the absence or presence of MAO inhibitor pargyline and/or inhibitor of lysosomal degradation chloroquine for the last 4h of treatment. Autophagy flux is calculated as the difference in LC3-II protein level in the absence or presence of lysosomal inhibitors. Cells cultured in presence of HG and pargyline displayed a dramatic reduction in the autophagy flux ($p<0.05$), evidenced by the lack of LC3-II accumulation following inhibition of lysosomal degradation with chloroquine for the last 4h (Figure 25). Autophagy flux was not significantly affected by pargyline in control conditions.

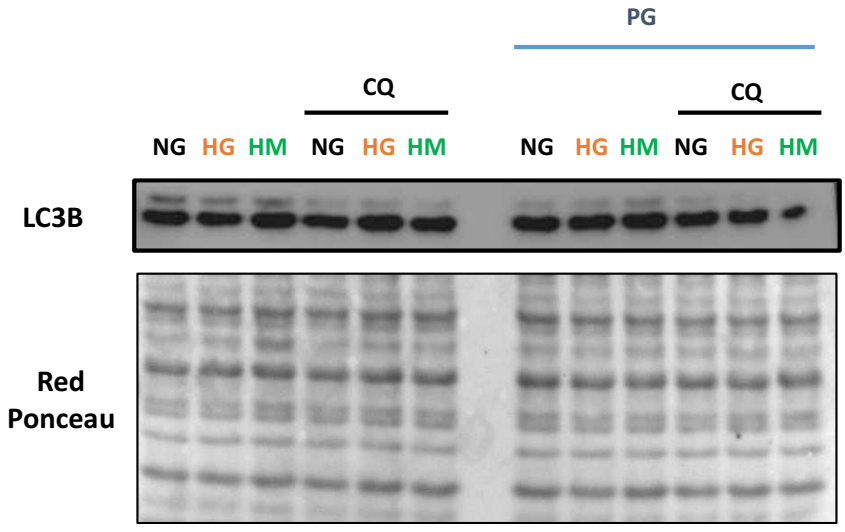

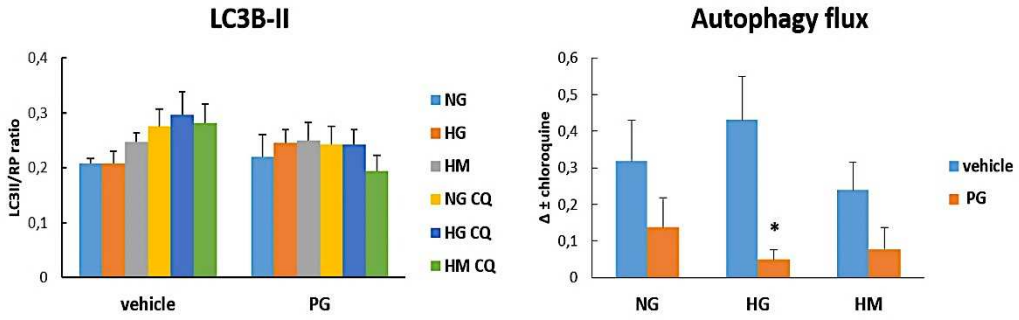

Figure 25: LC3B protein levels and autophagy flux in AMVMs. Representative blots are shown for LC3B-II protein in AMVMs cultured in HG in the absence or presence of pargyline. The quantification of band intensity is shown normalized to total protein determined by Red Ponceau staining (*n=5* for each group). LC3B-II levels were expressed as the mean ± SEM. Autophagic flux was calculated as the difference in LC3-II protein levels in the absence and presence of CQ. AMVMs were treated with CQ for 4h. Autophagic flux data were expressed as the mean ± SEM and analyzed a non-paired two-tailed Student's *t* test (*n*=5, *p<0,05). LC3B: LC3B: microtubule associated protein 1 light chain 3, CQ: chloroquine, PG: pargyline.

4.9 MAO-dependent ROS formation and AMPK activation

To explore the underlying signaling pathway that regulate autophagy, we tested AMPK pathway that is involved in autophagy and influenced by insulin. There was a trend to decrease of phosphorylated AMPKα (Thr-172), a well-known positive regulator of autophagy, in AMVMs treated with pargyline and exposed to HG (Figure 26). This result suggest that MAO-dependent ROS formation triggered by HG may impinge on this pathway to promote autophagy.

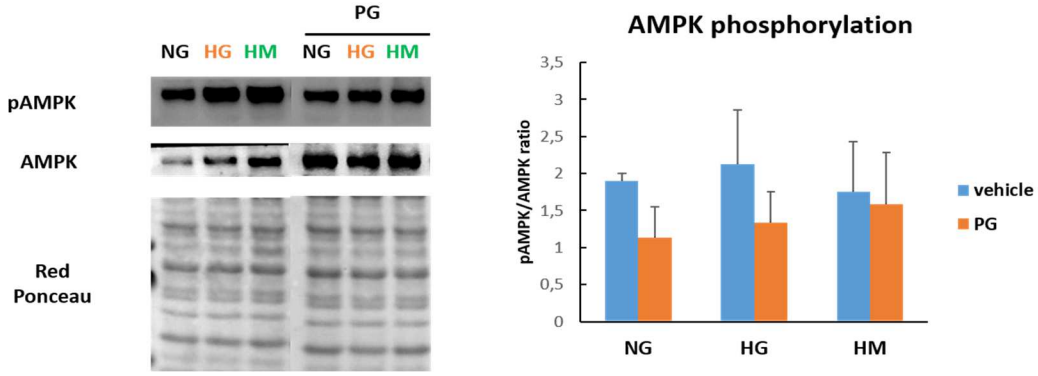

Figure 26: Phosphorylated AMPK levels in AMVMs. Representative blot is shown for phosphorylated AMPK proteins in AMVMs cultured in HG in the absence or presence of pargyline. The quantification of band intensity is shown normalized to total protein determined by Red Ponceau staining (*n=4* for each group). Data were expressed as the mean ± SEM. AMPK: AMP-activated protein kinase, PG: pargyline.

4.10 MAO inhibition might affect the cross-talk between mitochondrial dynamics and autophagy

Leading-edge analysis performed on the cluster of upregulated genes in diabetic condition in which pargyline prevented this effect, evidenced that several genes were enriched. Among these, MFF, a mitochondrial protein that functions as DRP1 receptor, was one of the genes enriched to the greatest extent in the mitochondrial compartment.

In the *in vitro* model, we observed an increase in MFF protein level in AMVMs exposed to HG. This event was dramatically reduced upon MAO inhibition with pargyline ($p<0.05$) confirming the trend observed for MFF expression profile obtained by microarray (Figure 27).

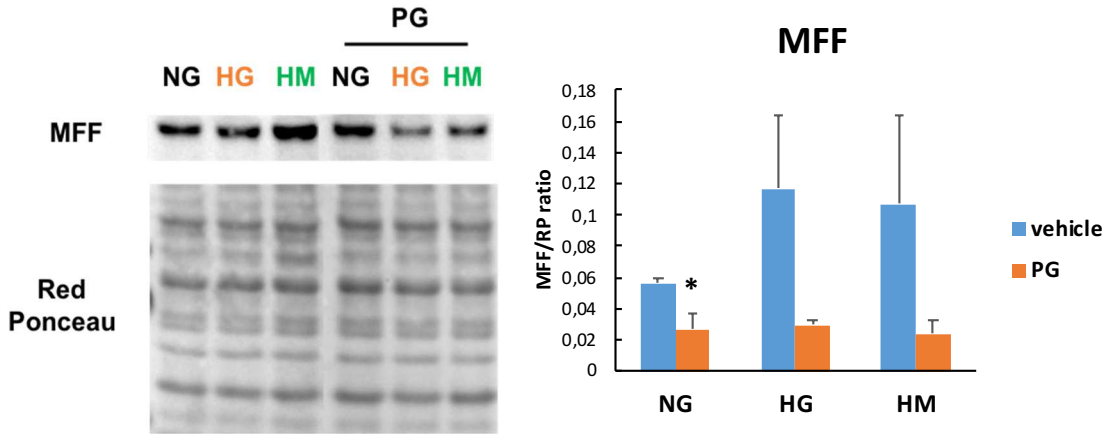

Figure 27: MFF protein levels. Representative blots are shown for MFF protein in AMVMs cultured in HG in the absence or presence of pargyline. The quantification of band intensity is shown normalized to total protein determined by Red Ponceau staining (*n=4* for each group). Data were expressed as the mean ± SEM and analyzed a non-paired two-tailed Student's *t* test (*p<0,05). MFF: mitochondrial fission factor, PG: pargyline.

Since MFF acts as a DRP1 receptor, we assessed the phosphorylation levels of DRP1 on Ser616, modification required for the translocation of the protein to mitochondria and organelle fission. A decreasing trend was observed upon treatment with pargyline in cells exposed to HG (Figure 28). These results suggest that mitochondrial fission might be reduced upon MAO inhibition in AMVMs exposed to HG. Further studies are necessary to confirm the role of MAO in mitochondrial fission. Interestingly, recent studies indicated that enhanced mitochondrial fission mediated by DRP1 in STZ-treated hearts is detrimental to cells and responsible for cardiac damage in diabetic hearts[153].

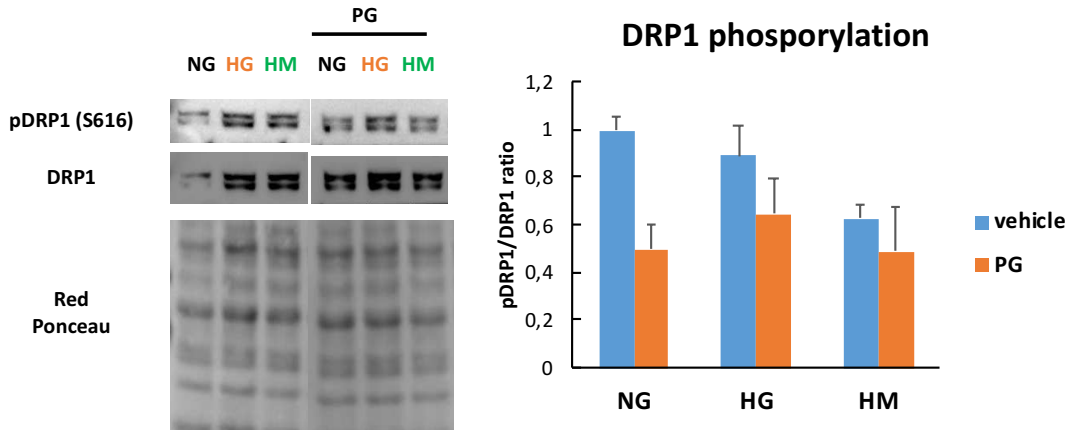

Figure 28: Phosphorylated DRP1 protein levels. Representative blots are shown for phosphorylated DRP1 protein in AMVMs cultured in HG in the absence or presence of pargyline. The quantification of band intensity is shown normalized to total protein determined by Red Ponceau staining (*n=4* for each group). Data were expressed as the mean ± SEM. DRP1: dynamin-related protein 1, PG: pargyline.

V. DISCUSSION AND CONCLUSIONS

This study shows that MAO-dependent ROS generation in diabetic hearts leads to profound transcriptomic changes, affecting the mitochondrial compartment, ECM, and catabolic processes in T1D mice in vivo. We also show that ROS produced by these flavoenzymes may act as a signal leading to autophagy activation and mitochondrial fragmentation in diabetic conditions. This provides an important link between MAO activity, transcriptomic changes, and autophagy in DCM. Interestingly, the occurrence of autophagy is reduced by the MAO inhibitor pargyline in a process that might underlie the cardioprotective role of MAO inhibition.

Many alterations of cellular and mitochondrial metabolism observed during the development and progression of DCM are associated with increased ROS levels and inflammation and not caused by hyperglycemia *per se*. Specifically, strong evidence provided by studies published in the laboratory of Prof. Di Lisa highlights that mitochondrial ROS formation and in particular MAO activity contribute to cardiac damage[43,86,87]. Indeed, diastolic and/or systolic dysfunction occurring in T1D mice and pressure overload is completely prevented upon MAO inhibition[43,86]. To further investigate the mechanisms underlying this cardioprotective effects, using microarray technology we evaluated changes in the gene expression profile induced by diabetes in relation to MAO activity in T1D hearts.

Microarray studies enable to evaluate the relative level of expression of practically all genes in a genome in order to determine the functional pathways influenced by a specific set of conditions. Thus, the microarray approach is useful for investigation of pathways and mechanisms involved in complex syndromes, such as diabetes. Indeed, several studies showed transcriptomic changes in blood samples[154], in the liver[155–157], kidney[158], placenta[159], skeletal muscle[160], adipose tissue[157,160], and hearts[161–163] of diabetic patients and in mouse models[164,165]. This suggests that genomics is important in the prediction, prevention, and diagnosis of the DCM. However, whether such changes in gene expression depend on oxidative stress in general, mitochondrial ROS formation or MAO activity has not been investigated yet. Thus, we studied this aspect based upon the efficient cardio-protection elicited by MAO inhibition in the setting of DCM[43,86,87]. Indeed, microarray analysis showed that the MAO inhibitor pargyline prevented the

changes in gene expression observed in diabetic hearts. This suggests that the cardioprotective effects afforded by MAO inhibition are likely contributed by changes in gene expression.

Microarray analyses have also been employed to examine the transcriptional profile in normal and pathological conditions in the heart[166,167]. Generally, studies performed binary or three-way comparisons of gene expression. Here, we focused our attention on differentially expressed genes between control and diabetic hearts, whose expression level was normalized by MAO inhibition. In this study, we have examined and proven the importance of genes upregulated in T1D hearts in relation to MAO activity. Nevertheless, it is equally important to study also downregulated genes and further investigation will be performed to have a clearer picture of transcriptional changes induced by diabetes and prevented by MAO inhibition.

To gain mechanistic insight into the potential function of the targets of deregulated mRNA, GO, GSEA and leading-edge analyses were performed. Our results showed mainly the upregulation of genes involved in mitochondrial compartment, ECM protein synthesis, and catabolic processes in diabetic hearts, events prevented by MAO inhibition. Our data are in accordance with other studies[168] that found upregulation of genes involved in ECM synthesis and mitochondrial components in Akita mouse hearts by means of microarray and NGS. Furthermore, here we unveil that these modifications are linked to mitochondrial ROS formation and, more specifically, MAO activity.

Transcriptomic data concerning ECM and mitochondria support and extend what has been previously observed[43,86,87]. Indeed, our laboratory has previously demonstrated that MAO activity is responsible for cardiac fibrosis in T1D mice and pressure overload. Collagen deposition and ECM remodeling result in the stiffening of the cardiac tissue and diastolic dysfunction[43,86]. MAO activity triggers mast cell degranulation in STZ-mice, thus providing a mechanistic link between these mitochondrial flavoenzymes, inflammation and fibrosis in DCM[43]. Our present results extend these previous observations and show that, in addition to the direct effects exerted by ROS on mast cells to promote fibrosis, MAO-dependent ROS generation can induce ECM remodeling by modulating the expression of genes involved in this process.

Our genomic data showed that processes related to protein degradation was highly affected by MAO-generated ROS in DCM. Thus, we hypothesized that MAO activity may be involved in the modulation of autophagy in diabetic hearts. Although, a growing

body of research identifies ROS as the principal intracellular signal transducers contributing to induction of autophagy, it is still unclear which species exactly drive the process and what are the exact ROS sources involved. So far, only Scherz-Shouval et al[129] demonstrated a redox-based mechanism essential for autophagy. They identified Atg4 as a direct target for oxidation by H_2O_2, thus providing a molecular mechanism for the redox regulation of the autophagic process.

In the present study, we observed an increase in LC3-II in STZ-treated mice. Interestingly, diabetic mice treated with the MAO inhibitor pargyline showed reduced protein level of LC3-II along with a parallel rise in p62/SQSTM1 levels. Therefore, we hypothesized that autophagy may be increased in diabetic hearts in a process prevented by MAO inhibition. In order to measure accurately the autophagic flux, all the experimental groups should be paralleled by groups of animals treated with inhibitors of lysosomal degradation. Thus, we employed AMVMs cultured in HG in the absence or presence of the MAO inhibitor pargyline and/or chloroquine. Chloroquine inhibits the last stage of autophagy impairing the basal autophagic flux by blocking autophagosome-lysosome fusion, and not by inhibiting lysosomal degradation capacity as previously assumed[169]. We observed a significant reduction in the LC3-II accumulation following chloroquine treatment in cells treated with HG and pargyline, suggesting that autophagy and autophagy flux are reduced by MAO inhibition. We also observed that phosphorylation of AMPK, an important factor involved in the regulation of autophagy, had a trend to decrease upon MAO inhibition in myocytes exposed to HG. These results suggest that MAO-dependent ROS formation triggered by HG impinges on AMPK pathway and promotes autophagy.

Pharmacological inhibition of MAO could regulate transcriptional changes of certain genes and autophagy also through ROS-independent mechanisms. Besides H_2O_2 formation, MAOs are also a source of reactive aldehydes and ammonia[43]. It cannot be excluded that products of MAO activity may also participate to the aforementioned processes. In addition to this, pharmacological inhibitors may present some off-target effects. In that regard, recent studies revealed that MAO inhibitors, including pargyline, are capable of inhibiting histone lysine-specific demethylase 1 (LSD1)[170,171]. LSD1 is a nuclear homolog of amine oxidases that generally functions as a histone demethylase and transcriptional corepressor[172]. This leads to transcriptional and epigenetic regulation of several genes, among which there are also some genes involved in the autophagic process[173]. However, our study excluded transcriptomic changes induced by pargyline

alone and focused only on changes induced by diabetes and prevented by the MAO inhibitor. It is thus unlikely that changes in the gene expression profile observed in this study are due to the non-specific effects of pargyline.

Previous studies showed that autophagy is downregulated in hearts of STZ-treated mice and OVE26 T1D mice, and restored after treatment with metformin resulting in improved cardiac function[174]. Conversely, other reports highlighted an increase in autophagy in hearts from STZ-T1D mice[120]. Interestingly, Xu et al. demonstrated that T1D-induced cardiac damage was rescued upon autophagy inhibition in either beclin 1- or Atg16-deficient mice[124]. This reduction in the canonical autophagy pathway was associated with the activation of the non-canonical alternative autophagy, thereby maintaining normal levels of mitophagy and limiting diabetic cardiac injury[124]. Although impaired autophagosome removal may be detrimental, we cannot exclude the involvement of LC3-independent autophagy mechanisms upon MAO inhibition in T1D that would allow for effective clearance and recycling of cytoplasmic components and organelles. Together with previously reported cardioprotective effects of MAO inhibition in preventing DCM[43,87], the present results support the hypothesis that reducing the levels of autophagy is beneficial for cardiac function in T1D. Nevertheless, further studies are necessary to elucidate whether activation of non-canonical, Rab9-dependent autophagy takes place in T1D hearts upon MAO inhibition to sustain cardiac function. In addition, the mechanisms underlying MAO-dependent effect on autophagy in relation to cardiac function warrant further, in depth investigation. The limitation of this study is that data on autophagy modulation by MAO in DCM in vivo are correlative at the moment and require a more robust validation. Future studies will definitively examine the impact of autophagy modulation on cardiac function in T1D in relation to MAO inhibition.

Among genes whose upregulation in diabetic condition was prevented by pargyline, transcriptomic analysis highlighted an enrichment of MFF that acts as a mitochondrial DRP1 receptor[175]. We observed an increase in MFF levels also in cells exposed to HG, and again MAO inhibition prevented this rise. In addition, phosphorylation of DRP1 on serine 616, an event that promotes mitochondrial fission, also showed a decreasing trend upon treatment with pargyline. These results suggest that mitochondrial fission may be reduced as a result of MAO inhibition in AMVMs exposed to HG, although further studies are necessary to fully characterize the role of MAO in diabetes-induced changes of mitochondrial dynamics.

As regards the tight link between autophagy and mitochondrial dynamics and the role Drp1 in cardiac autophagy[175–177], elucidating whether MAO-dependent ROS formation impacts on these events may prove of interest. Of note, mitochondrial dynamics is altered in HG-treated cardiomyocytes and in the diabetic hearts. For example, HG induces mitochondrial fragmentation in neonatal rat cardiomyocytes[122] and H9c2 cardiac myoblast cells[122,178–180], and this is dependent on the phosphorylation of Drp1 at serine 616[180]. Inhibition of mitochondrial fission attenuates HG-induced ROS production and cell death[179], suggesting that mitochondrial fragmentation contributes to HG toxicity. Moreover, increased mitochondrial fragmentation mediated by DRP1 in STZ-treated hearts is detrimental to cells and responsible for cardiac damage in diabetic hearts[153].

In conclusion, the present study demonstrates that profound transcriptomic changes observed in diabetic hearts occur in a MAO-dependent manner. In addition, MAO-dependent ROS formation triggered by HG acts as a signal that leads to autophagy activation. Taken together, our results provide novel evidence that mitochondrial ROS formation and specifically MAO activity modulates cardiac autophagy in DCM.

VI. REFERENCES

1. DS., B. *Diabetic Cardiomyopathy*. **26**, (2003).

2. International Diabetes Federation. *Eighth edition 2017*. *IDF Diabetes Atlas, 8th edition* (2017). doi:http://dx.doi. org/10.1016/S0140-6736(16)31679-8.

3. Riehle, C. & Bauersachs, J. Of mice and men: models and mechanisms of diabetic cardiomyopathy. *Basic Res. Cardiol.* **114**, 1–22 (2019).

4. Herrero, P. *et al.* Increased myocardial fatty acid metabolism in patients with type 1 diabetes mellitus. *J. Am. Coll. Cardiol.* **47**, 598–604 (2006).

5. Herrero, P. *et al.* PET detection of the impact of dobutamine on myocardial glucose metabolism in women with type 1 diabetes mellitus. *J. Nucl. Cardiol.* **15**, 791–799 (2008).

6. Peterson, L. R. *et al.* Effect of Obesity and Insulin Resistance on Myocardial Substrate Metabolism and Efficiency in Young Women. *Circulation* **109**, 2191–2196 (2004).

7. Peterson, L. R. *et al.* Type 2 diabetes, obesity, and sex difference affect the fate of glucose in the human heart. *Am. J. Physiol. Circ. Physiol.* **308**, H1510–H1516 (2015).

8. Yan, N. A Glimpse of Membrane Transport through Structures—Advances in the Structural Biology of the GLUT Glucose Transporters. *J. Mol. Biol.* **429**, 2710–2725 (2017).

9. Silverthorn, D. U. *Human Physiology: An Integrated Approach*. (Pearson, 2016).

10. Bryant, N. J., Govers, R. & James, D. E. Regulated transport of the glucose transporter GLUT4. *Nat. Rev. Mol. Cell Biol.* **3**, 267–277 (2002).

11. Klip, A., McGraw, T. E. & James, D. E. 30 sweet years of GLUT4. *J. Biol. Chem.* **294**, jbc.REV119.008351 (2019).

12. Jia, G., Hill, M. A. & Sowers, J. R. Diabetic cardiomyopathy: An update of mechanisms contributing to this clinical entity. *Circ. Res.* **122**, 624–638 (2018).

13. Tokarz, V. L., MacDonald, P. E. & Klip, A. The cell biology of systemic insulin function. *J. Cell Biol.* **217**, 1–17 (2018).

14. Merry, T. L. & McConell, G. K. Skeletal muscle glucose uptake during exercise: A focus on reactive oxygen species and nitric oxide signaling. *IUBMB Life* (2009). doi:10.1002/iub.179

15. Chang, L., Chiang, S. H. & Saltiel, A. R. Insulin signaling and the regulation of glucose transport. *Mol. Med.* **10**, 65–71 (2004).

16. Forbes, J. M. & Cooper, M. E. Mechanisms of diabetic complications. *Physiological Reviews* (2013). doi:10.1152/physrev.00045.2011

17. Yu, Y. & Chai, J. The function of miRNAs and their potential as therapeutic targets in burn-induced insulin resistance (Review). *Int. J. Mol. Med.* **35**, 305–310 (2015).

18. Rosano, G. *et al.* Type 2 diabetes mellitus and heart failure: a position statement from the Heart Failure Association of the European Society of Cardiology. *Eur. J. Heart Fail.* **20**, 853–872 (2018).

19. Qiulian Zhou, Dongchao Lv, Ping Chen, Tianzhao Xu, Siyi Fu, J. L. and Y. B. MicroRNAs in

diabetic cardiomyopathy and clinical perspectives. **5**, (2014).

20. Bugger, H. & Abel, E. D. Molecular mechanisms of diabetic cardiomyopathy. *Diabetologia* **57**, 660–671 (2014).

21. Jia, G., Demarco, V. G., Sowers, J. R. & Drive, O. H. Insulin resistance and hyperinsulinaemia in diabetic cardiomyopathy. *Nat Rev Endocrinol* **12**, 144–153 (2016).

22. Watanabe, K. *et al.* Role of Differential Signaling Pathways and Oxidative Stress in Diabetic Cardiomyopathy. *Curr. Cardiol. Rev.* **6**, 280–290 (2010).

23. Varga, Z. V. *et al.* Interplay of oxidative, nitrosative/nitrative stress, inflammation, cell death and autophagy in diabetic cardiomyopathy. *Biochim. Biophys. Acta - Mol. Basis Dis.* **1852**, 232–242 (2015).

24. Filomeni, G., De Zio, D. & Cecconi, F. Oxidative stress and autophagy: The clash between damage and metabolic needs. *Cell Death Differ.* **22**, 377–388 (2015).

25. Di Lisa, F., Kaludercic, N., Carpi, A., Menabò, R. & Giorgio, M. Mitochondrial pathways for ROS formation and myocardial injury: The relevance of p66Shc and monoamine oxidase. *Basic Res. Cardiol.* **104**, 131–139 (2009).

26. Johansen, J. S., Harris, A. K., Rychly, D. J. & Ergul, A. Oxidative stress and the use of antioxidants in diabetes: Linking basic science to clinical pratice. *Cardiovasc. Diabetol.* **4**, 1–11 (2005).

27. Furukawa, S. *et al.* Increased oxidative stress in obesity and its impact on metabolic syndrome Find the latest version : Increased oxidative stress in obesity and its impact on metabolic syndrome. *J. Clin. Invest.* **114**, 1752–1761 (2017).

28. Ye, G., Donthi, R. V., Metreveli, N. S. & Epstein, P. N. Cardiomyocyte dysfunction in models of type 1 and type 2 diabetes. *Cardiovasc. Toxicol.* **5**, 285–292 (2005).

29. Fiordaliso, F. *et al.* Antioxidant treatment attenuates hyperglycemia-induced cardiomyocyte death in rats. *J. Mol. Cell. Cardiol.* **37**, 959–968 (2004).

30. Vona, R., Gambardella, L., Cittadini, C., Straface, E. & Pietraforte, D. Biomarkers of Oxidative Stress in Metabolic Syndrome and Associated Diseases. *Oxid. Med. Cell. Longev.* **2019**, 8267234 (2019).

31. Hare, J. M., Beigi, F. & Tziomalos, K. Nitric Oxide and Cardiobiology-Methods for Intact Hearts and Isolated Myocytes. in *Methods in Enzymology* 369–392 (2008).

32. Ying, T., Jiangang, L. & JiankangLiu, Y. Hyperglycemia-Associated Oxidative Stress Induces Autophagy: Involvement of the ROS-ERK/JNK-p53 Pathway. in *Autophagy: Cancer, Other Pathologies, Inflammation, Immunity, Infection, and Aging* 105–115 (2014).

33. Osto, E. & Cosentino, F. The Role of Oxidative Stress in Endothelial Dysfunction and Vascular Inflammation. in *Nitric Oxide: Biology and Pathobiology* (ed. Edition, S.) 705–754 (2010).

34. Sirker, A., Zhang, M. & Shah, A. M. NADPH oxidases in cardiovascular disease: Insights from in vivo models and clinical studies. *Basic Res. Cardiol.* **106**, 735–747 (2011).

35. Rodiño-Janeiro, B. K. *et al.* Current status of NADPH oxidase researchin cardiovascular pharmacology. *Vasc. Health Risk Manag.* **9**, 401–428 (2013).

36. Maalouf, R. M. *et al.* Nox4-derived reactive oxygen species mediate cardiomyocyte injury in early type 1 diabetes. *Am. J. Physiol. - Cell Physiol.* (2012). doi:10.1152/ajpcell.00331.2011

37. Privratsky, J. R., Wold, L. E., Sowers, J. R., Quinn, M. T. & Ren, J. AT1 blockade prevents glucose-induced cardiac dysfunction in ventricular myocytes: Role of the AT1 receptor and NADPH oxidase. *Hypertension* (2003). doi:10.1161/01.HYP.0000082814.62655.85

38. Suriyajothi, M. A., Sangeetha, R. & Venkateswari, R. Activity of Xanthine oxidase in diabetics: Its correlation with aging. *Pharmacologyonline* (2011).

39. Rajesh, M. *et al.* Xanthine oxidase inhibitor allopurinol attenuates the development of diabetic cardiomyopathy. *J. Cell. Mol. Med.* **13**, 2330–2341 (2009).

40. Pacher, P., Nivorozhkin, A. & Szabó, C. Therapeutic effects of xanthine oxidase inhibitors: Renaissance half a century after the discovery of allopurinol. *Pharmacological Reviews* (2006). doi:10.1124/pr.58.1.6

41. Eddy, L. *et al.* Free radical-producing enzyme, xanthine oxidase, is undetectable in human hearts. *Am J Physiol.* **253**, H709-11 (1987).

42. Murphy, M. P. How mitochondria produce reactive oxygen species. *Biochem. J.* **417**, 1–13 (2009).

43. Deshwal, S. *et al.* Monoamine oxidase-dependent endoplasmic reticulum-mitochondria dysfunction and mast cell degranulation lead to adverse cardiac remodeling in diabetes. *Cell Death Differ.* **25**, 1671–1685 (2018).

44. Di Lisa, F. & Scorrano, L. Mitochondrial Morphology and Function, in Muscle. in *Fundamental biology and mechanisms of disease* (ed. Olson, J. A. H. and E. N.) 217–229 (2012).

45. Janssen-Heininger, Y. M. W. *et al.* Redox-based regulation of signal transduction: Principles, pitfalls, and promises. *Free Radic. Biol. Med.* **45**, 1–17 (2008).

46. Lodish, H., Berk, A. & Zipursky, S. *Molecular Cell Biology*. (New York: W. H. Freeman, 2000).

47. Ugun-Klusek, A. *et al.* Monoamine oxidase-A promotes protective autophagy in human SH-SY5Y neuroblastoma cells through Bcl-2 phosphorylation. *Redox Biol.* **20**, 167–181 (2019).

48. Dorn, G. W. Mitochondrial dynamism and heart disease: changing shape and shaping change. *EMBO Mol. Med.* **7**, 865–877 (2015).

49. Shah, M. S. & Brownlee, M. Molecular and cellular mechanisms of cardiovascular disorders in diabetes. *Circ. Res.* **118**, 1808–1829 (2016).

50. Roul, D. & Recchia, F. A. Metabolic Alterations Induce Oxidative Stress in Diabetic and Failing Hearts: Different Pathways, Same Outcome. *Antioxidants and Redox Signaling* (2015). doi:10.1089/ars.2015.6311

51. Ye, G. *et al.* Catalase Protects Cardiomyocyte Function in Models of Type 1 and Type 2 Diabetes. *Diabetes* (2004). doi:10.2337/diabetes.53.5.1336

52. Schriner, S. E. *et al.* Medecine: Extension of murine life span by overexpression of

catalase targeted to mitochondria. *Science (80-.).* (2005). doi:10.1126/science.1106653

53. Di Lisa, F., Giorgio, M., Ferdinandy, P. & Schulz, R. New aspects of p66Shc in ischaemia reperfusion injury and other cardiovascular diseases. *Br. J. Pharmacol.* **174**, 1690–1703 (2017).

54. Baysa, A. *et al.* The p66ShcA adaptor protein regulates healing after myocardial infarction. *Basic Res Cardiol.* **110**, (2015).

55. Migliaccio, E. *et al.* The p66shc adaptor protein controls oxidative stress response and life span in mammals. *Nature* **402**, 309–13 (1999).

56. Carpi, A. *et al.* The cardioprotective effects elicited by p66Shc ablation demonstrate the crucial role of mitochondrial ROS formation in ischemia/reperfusion injury. *Biochim. Biophys. Acta - Bioenerg.* **1787**, 774–780 (2009).

57. Orsini, F. *et al.* Mitochondrial regulation of p66Shc mitochondrial function. *Biol Chem* **387**, 1405–1410 (2006).

58. Graiani, G. *et al.* Genetic deletion of the p66Shc adaptor protein protects from angiotensin II-induced myocardial damage. *Hypertension* **46**, 433–440 (2005).

59. Ramsay, R. R. & Albreht, A. Kinetics, mechanism, and inhibition of monoamine oxidase. *J. Neural Transm.* **125**, 1659–1683 (2018).

60. Deshwal, S., Di Sante, M., Di Lisa, F. & Kaludercic, N. Emerging role of monoamine oxidase as a therapeutic target for cardiovascular disease. *Curr. Opin. Pharmacol.* **33**, 64–69 (2017).

61. Kaludercic, N., Mialet-Perez, J., Paolocci, N., Parini, A. & Di Lisa, F. Monoamine oxidases as sources of oxidants in the heart. *J Mol Cell Cardiol* 34–42 (2014).

62. Shih, J. C., Chen, K. & Ridd, M. J. MONOAMINE OXIDASE: From Genes to Behavior. *Annu. Rev. Neurosci.* **22**, 197–217 (1999).

63. Abell, C. W. & Kwan, S.-W. Molecular characterization of monoamine oxidases A and B. *Prog. Nucleic Acid Res. Mol. Biol.* **65**, 129–132 (2001).

64. Edmondson, D. E., Mattevi, A., Binda, C., Li, M. & Hubalek, F. Structure and Mechanism of Monoamine Oxidase. *Curr. Med. Chem.* **11**, 1983–1993 (2004).

65. Iacovino, L. G., Magnani, F. & Binda, C. The structure of monoamine oxidases: past, present, and future. *J. Neural Transm.* **125**, 1567–1579 (2018).

66. Youdim, M., Edmondson, D. & Tipton, K. The therapeutic potential of monoamine oxidase inhibitors. *Nat Rev Neurosci.* **7**, 295–309 (2006).

67. Binda, C., Newton-Vinson, P., Hubálek, F., Edmondson, D. & Mattevi, A. Structure of human monoamine oxidase B, a drug target for the treatment of neurological disorders. *Nat. Struct. Biol.* **9**, 22–26 (2002).

68. Li, M., Hubálek, F., Newton-Vinson, P. & Edmondson, D. High-Level Expression of Human Liver Monoamine Oxidase A in Pichia pastoris: Comparison with the Enzyme Expressed in Saccharomyces cerevisiae. *Protein Expr. Purif.* **24**, 152–162 (2002).

69. Newton-Vinson, P., Hubalek, F. & Edmondson, D. High-level expression of human liver

monoamine oxidase B in Pichia pastoris. *Protein Expr. Purif.* **20**, 334–345 (2000).

70. Son, S.-Y. *et al.* Human monoamine oxidase A: structure and control of opening the entry for substrates/inhibitors. *Acta Crystallogr. Sect. A Found. Crystallogr.* **64**, C457–C457 (2008).

71. Ma, J. *et al.* Structure of Rat Monoamine Oxidase A and Its Specific Recognitions for Substrates and Inhibitors. *J Mol Biol.* **338**, 103–114 (2004).

72. De Colibus, L. *et al.* Three-dimensional structure of human monoamine oxidase A (MAO A): Relation to the structures of rat MAO A and human MAO B. *Proc. Natl. Acad. Sci. U. S. A.* **102**, 12684–12689 (2005).

73. Tipton, K. F. 90 years of monoamine oxidase: some progress and some confusion. *J. Neural Transm.* **125**, 1519–1551 (2018).

74. Mialet-Perez, J., Santin, Y. & Parini, A. Monoamine oxidase-A, serotonin and norepinephrine: synergistic players in cardiac physiology and pathology. *J. Neural Transm.* **125**, 1627–1634 (2018).

75. Akiyama, T. & Yamazaki, T. Myocardial interstitial norepinephrine and dihydroxyphenylglycol levels during ischemia and reperfusion. *Cardiovasc. Res.* **49**, 78–85 (2001).

76. Saura, J. *et al.* Localization of monoamine oxidases in human peripheral tissues. *Life Sci.* **59**, 1341–1349 (1996).

77. Saura, J., Richards, J. & Mahy, N. Differential age-related changes of mao-a and mao-b in mouse brain and pe peripheral organs. *Neurobiol Aging* **15**, 399–408 (1994).

78. KATAYAMA, M., KOBAYASHI, S., OGUCHI, K. & YASUHARA, H. Properties of Monoamine Oxidase in Monkey Heart. *Japan. J. Pharmacol.* **35**, 425–431 (1984).

79. Krakoff, L., Buccino, R., Spann, J. J. & De Champlain, J. Cardiac catechol O-methyltransferase and monoamine oxidase activity in congestive heart failure. *Am J Physiol.* **215**, 549–52 (1968).

80. DE CHAMPLAIN, J., KRAKOFF, L. R. & AXELROD, J. Increased Monoamine Oxidase Activity during the Development of Cardiac Hypertrophy in the Rat. *Circ. Res.* **23**, 361–369 (1968).

81. Kaludercic, N., Carpi, A., Menabò, R., Di Lisa, F. & Paolocci, N. Monoamine oxidases (MAO) in the pathogenesis of heart failure and ischemia/reperfusion injury. *Biochim. Biophys. Acta - Mol. Cell Res.* **1813**, 1323–1332 (2011).

82. Anderson, E. J. *et al.* Monoamine oxidase is a major determinant of redox balance in human atrial myocardium and is associated with postoperative atrial fibrillation. *J. Am. Heart Assoc.* **3**, 1–12 (2014).

83. Hauptmann, N., Grimsby, J., Shih, J. & Cadenas, E. The Metabolism of Tyramine by Monoamine Oxidase A/B Causes Oxidative Damage to Mitochondrial DNA. *Arch. Biochem. Biophys.* **335**, 295–304 (1996).

84. Bianchi, P. *et al.* Oxidative stress by monoamine oxidase mediates receptor-independent cardiomyocyte apoptosis by serotonin and postischemic myocardial injury. *Circulation* **112**, 3297–3305 (2005).

85. Pchejetski, D. *et al.* Oxidative stress-dependent sphingosine kinase-1 inhibition mediates monoamine oxidase A-associated cardiac cell apoptosis. *Circ. Res.* **100**, 41–49 (2007).

86. Kaludercic, N. *et al.* Monoamine oxidase a-mediated enhanced catabolism of norepinephrine contributes to adverse remodeling and pump failure in hearts with pressure overload. *Circ. Res.* **106**, 193–202 (2010).

87. Kaludercic, N. *et al.* Monoamine Oxidase B Prompts Mitochondrial and Cardiac Dysfunction in Pressure Overloaded Hearts. *Antioxid. Redox Signal.* **20**, 267–280 (2013).

88. Umbarkar, P. *et al.* Monoamine oxidase-A is an important source of oxidative stress and promotes cardiac dysfunction, apoptosis, and fibrosis in diabetic cardiomyopathy. *Free Radic. Biol. Med.* **87**, 263–273 (2015).

89. Mialet-Perez, J., Bianchi, P., Kunduzova, O. & Parini, A. New insights on receptor-dependent and monoamine oxidase-dependent effects of serotonin in the heart. *J. Neural Transm.* **114**, 823–827 (2007).

90. Vindis, C., Séguélas, M. H., Bianchi, P., Parini, A. & Cambon, C. Monoamine oxidase B induces ERK-dependent cell mitogenesis by hydrogen peroxide generation. *Biochem. Biophys. Res. Commun.* **271**, 181–185 (2000).

91. Lairez, O. *et al.* Genetic deletion of MAO-A promotes serotonin-dependent ventricular hypertrophy by pressure overload. *J Mol Cell Cardiol* **26**, 587–595 (2009).

92. Kunduzova, Bianchi, Parini & Cambon. Hydrogen peroxide production by monoamine oxidase during ischemia/reperfusion. *Eur. J. Pharmacol.* **448**, 225–230 (2002).

93. Villeneuve, C. *et al.* p53-PGC-1α Pathway Mediates Oxidative Mitochondrial Damage and Cardiomyocyte Necrosis Induced by Monoamine Oxidase-A Upregulation: Role in Chronic Left Ventricular Dysfunction in Mice. *Antioxid. Redox Signal.* **18**, 5–18 (2012).

94. Laban, T. S. & Saadabadi, A. *Monoamine Oxidase Inhibitors (MAOI)*. (StatPearls Publishing, 2019).

95. Rapaport, M. H. Dietary restrictions and drug interactions with monoamine oxidase inhibitors: The state of the art. *J. Clin. Psychiatry* **68**, 42–46 (2007).

96. Culpepper, L. Reducing the Burden of Difficult-to-Treat Major Depressive Disorder: Revisiting Monoamine Oxidase Inhibitor Therapy. *Prim Care Companion CNS Disord* **15**, (2013).

97. Dao, V. T. V. *et al.* Pharmacology and Clinical Drug Candidates in Redox Medicine. *Antioxidants and Redox Signaling* (2015). doi:10.1089/ars.2015.6430

98. Dikic, I. & Elazar, Z. Mechanism and medical implications of mammalian autophagy. *Nat. Rev. Mol. Cell Biol.* **19**, 349–364 (2018).

99. Choi, A. M. K., Ryter, S. W. & Levine, B. Autophagy in human health and disease. *N. Engl. J. Med.* **368**, 651–62 (2013).

100. Lamb, C. A., Yoshimori, T. & Tooze, S. A. The autophagosome: Origins unknown, biogenesis complex. *Nat. Rev. Mol. Cell Biol.* **14**, 759–774 (2013).

101. Levine, B. & Kroemer, G. Biological Functions of Autophagy Genes: A Disease Perspective. *Cell* **176**, 11–42 (2019).

102. Levine, B. & Kroemer, G. Autophagy in the pathogenesis of disease. *Cell* **132**, 27–42 (2008).

103. Kroemer, G. Autophagy_druggable_rev_JCI2015. *J. Clin. Invest.* **125**, 8–11 (2015).

104. Kaludercic, N. *et al.* Comprehensive autophagy evaluation in cardiac diseases models. *Cardiovasc. Res.* (2019). doi:https://doi.org/10.1093/cvr/cvz233

105. Sebastiano Sciarretta, Yasuhiro Maejima, Daniela Zablocki, and J. S. The Role of Autophagy in the Heart. *Annu. Rev. Physiol.* 1–7.26 (2018).

106. Nishida, Y. *et al.* Discovery of Atg5/Atg7-independent alternative macroautophagy. *Nature* **461**, 654–658 (2009).

107. Saito, T. & Sadoshima, J. Molecular mechanisms of mitochondrial autophagy/mitophagy in the heart. *Circ. Res.* **116**, 1477–1490 (2015).

108. Shirakabe, A., Ikeda, Y., Sciarretta, S., Zablocki, D. K. & Sadoshima, J. Aging and Autophagy in the Heart. *Circ. Res.* **118**, 1563–1576 (2016).

109. Kageyama, Y. *et al.* Parkin-independent mitophagy requires D rp1 and maintains the integrity of mammalian heart and brain . *EMBO J.* (2014). doi:10.15252/embj.201488658

110. McWilliams, T. G. *et al.* Basal Mitophagy Occurs Independently of PINK1 in Mouse Tissues of High Metabolic Demand. *Cell Metab.* (2018). doi:10.1016/j.cmet.2017.12.008

111. Nakai, A. *et al.* The role of autophagy in cardiomyocytes in the basal state and in response to hemodynamic stress. *Nat. Med.* **13**, 619–624 (2007).

112. Zhai, P., Sciarretta, S., Galeotti, J., Volpe, M. & Sadoshima, J. Differential roles of gsk-3β during myocardial ischemia and ischemia/reperfusion. *Circ. Res.* **109**, 502–511 (2011).

113. Matsui, Y. *et al.* Distinct Roles of Autophagy in the Heart During Ischemia and Reperfusion. *Circ. Res.* **100**, 914–922 (2007).

114. Ma, X. *et al.* Impaired autophagosome clearance contributes to cardiomyocyte death in ischemia/reperfusion injury. *Circulation* **125**, 3170–3181 (2012).

115. Fernández, Á. *et al.* Disruption of the beclin 1-BCL2 autophagy regulatory complex promotes longevity in mice. *Nature* **558**, 136–140 (2018).

116. Levine, B. *et al.* Cardiac autophagy is a maladaptive response to hemodynamic stress. *J. Clin. Invest.* **117**, 1782–1793 (2007).

117. Sun, N. *et al.* Measuring In Vivo Mitophagy. *Mol. Cell* **60**, 685–696 (2015).

118. Shirakabe, A. *et al.* Drp1-dependent mitochondrial autophagy plays a protective role against pressure overload-induced mitochondrial dysfunction and heart failure. *Circulation* **133**, 1249–1263 (2016).

119. Saito, T., Kundu, M. & Sadoshima, J. An alternative mitophagy pathway mediated by Rab9 protects the heart against ischemia Graphical abstract The Journal of Clinical Investigation. *J Clin Invest* **129**, 802–819 (2019).

120. Kanamori, H. *et al.* Autophagic adaptations in diabetic cardiomyopathy differ between type 1 and type 2 diabetes. *Autophagy* **11**, 1146–1160 (2015).

121. Kobayashi, S. & Liang, Q. Autophagy and mitophagy in diabetic cardiomyopathy. *Biochimica et Biophysica Acta - Molecular Basis of Disease* (2015). doi:10.1016/j.bbadis.2014.05.020

122. Liang, Q. & Kobayashi, S. Mitochondrial quality control in the diabetic heart. *J. Mol. Cell. Cardiol.* **95**, 57–69 (2016).

123. Munasinghe, P. E. *et al.* Type-2 diabetes increases autophagy in the human heart through promotion of Beclin-1 mediated pathway. *Int. J. Cardiol.* (2016). doi:10.1016/j.ijcard.2015.08.111

124. Xu, X. *et al.* Diminished autophagy limits cardiac injury in mouse models of type 1 diabetes. *J. Biol. Chem.* **288**, 18077–18092 (2013).

125. Tong, M. *et al.* Mitophagy Is Essential for Maintaining Cardiac Function During High Fat Diet-Induced Diabetic Cardiomyopathy. *Circ. Res.* **124**, (2019).

126. Sciarretta, S., Volpe, M. & Sadoshima, J. Mammalian target of rapamycin signaling in cardiac physiology and disease. *Circ. Res.* **114**, 549–564 (2014).

127. Sciarretta, S. *et al.* Rheb is a critical regulator of autophagy during myocardial ischemia: Pathophysiological implications in obesity and metabolic syndrome. *Circulation* **125**, 1134–1146 (2012).

128. Kim, J., Kundu, M., Viollet, B. & Guan, K.-L. AMPK and mTOR regulate autophagy through direct phosphorylation of Ulk1. *Nat. Cell Biol.* **13**, 132–41 (2011).

129. Scherz-Shouval, R. *et al.* Reactive oxygen species are essential for autophagy and specifically regulate the activity of Atg4. *EMBO J.* **26**, 1749–1760 (2007).

130. Sciarretta, S. *et al.* Activation of NADPH oxidase 4 in the endoplasmic reticulum promotes cardiomyocyte autophagy and survival during energy stress through the protein kinase RNA-activated-like endoplasmic reticulum kinase/eukaryotic initiation factor 2α/activating transcripti. *Circ. Res.* **113**, 1253–1264 (2013).

131. Santin Y, Sicard P, Vigneron F, Guilbeau-Frugier C, D. M. *et al.* Oxidative stress by monoamine oxidase-A impairs transcription factor EB activation and autophagosome clearance, leading to cardiomyocyte necrosis and heart failure. *Antioxid. Redox Signal.* **25**, 10–27 (2016).

132. Ucar, A. *et al.* The miRNA-212/132 family regulates both cardiac hypertrophy and cardiomyocyte autophagy. *Nat. Commun.* **3**, 1011–1078 (2012).

133. Sun, T., Li, M.-Y., Li, P.-F. & Cao, J.-M. MicroRNAs in Cardiac Autophagy: Small Molecules and Big Role. *Cells* (2018). doi:10.3390/cells7080104

134. Kim, E. Insulin resistance at the crossroads of metabolic syndrome: Systemic analysis using microarrays. *Biotechnology Journal* (2010). doi:10.1002/biot.201000048

135. Keller, M. P. & Attie, A. D. Physiological Insights Gained from Gene Expression Analysis in Obesity and Diabetes. *Annu. Rev. Nutr.* (2010). doi:10.1146/annurev.nutr.012809.104747

136. Nilsson, E. *et al.* Altered DNA methylation and differential expression of genes influencing metabolism and inflammation in adipose tissue from subjects with type 2 diabetes. *Diabetes* (2014). doi:10.2337/db13-1459

137. Planas, R., Pujol-Borrell, R. & Vives-Pi, M. Global gene expression changes in type 1 diabetes: Insights into autoimmune response in the target organ and in the periphery. *Immunology Letters* (2010). doi:10.1016/j.imlet.2010.08.001

138. Lu, J. M. *et al.* System network analysis of genomics and transcriptomics data identified type 1 diabetes-associated pathway and genes. *Genes Immun.* (2018). doi:10.1038/s41435-018-0045-9

139. Babu, M. M. An Introduction to Microarray Data Analysis. In Computational Genomics: Theory and Application. in (ed. P., R.) 225–249 (2004).

140. Bolstad, B., Irizarry, R., Astrand, M. & Speed, T. A comparison of normalization methods for high density oligonucleotide array data based on variance and bias. *Bioinformatics* **19**, 185–193 (2003).

141. Pereira, A. *Plant Reverse Genetics*. **678**, (2011).

142. Dunn, O. J. Multiple Comparisons among Means. *J. Am. Stat. Assoc.* **56**, 52–64 (1961).

143. Dopazo, J. & Carazo, J. M. Phylogenetic reconstruction using an unsupervised growing neural network that adopts the topology of a phylogenetic tree. *J. Mol. Evol.* **44**, 226–233 (1997).

144. Herrero, J., Valencia, A. & Dopazo, J. An hierarchical unsupervised growing neural network form clustering gene expression patterns. *Bioinformatics* **17**, 126–136 (2001).

145. Saeed, A. I. *et al.* TM4: A free, open-source system for microarray data management and analysis. *Biotechniques* (2003).

146. Zeeberg, B. R. *et al.* GoMiner: a resource for biological interpretation of genomic and proteomic data. *Genome Biol.* **4**, R7 (2003).

147. Subramanian, A. *et al.* Gene set enrichment analysis: A knowledge-based approach for interpreting genome-wide expression profiles. *PNAS* **102**, 15545–15550 (2005).

148. Cordero, F., Botta, M. & Calogero, R. A. Microarray data analysis and mining approaches. *Briefings Funct. Genomics Proteomics* **6**, 265–281 (2007).

149. Maere, S., Heymans, K. & Kuiper, M. BiNGO: A Cytoscape plugin to assess overrepresentation of Gene Ontology categories in Biological Networks. *Bioinformatics* **21**, 3448–3449 (2005).

150. Mootha, V. *et al.* PGC-1alpha-responsive genes involved in oxidative phosphorylation are coordinately downregulated in human diabetes. *Nat Genet* **34**, 267–73 (2003).

151. Shipp, M. A. *et al.* Molecular profiling of diffuse large B-cell lymphoma identifies robust subtypes including one characterized by host inflammatory response. *Blood* **105**, 1851–1861 (2005).

152. Katsuragi, Y., Ichimura, Y. & Komatsu, M. P62/SQSTM1 functions as a signaling hub and an autophagy adaptor. *FEBS J.* **282**, 4672–4678 (2015).

153. Ding, M. *et al.* Inhibition of dynamin-related protein 1 protects against myocardial ischemia-reperfusion injury in diabetic mice. *Cardiovasc. Diabetol.* (2017). doi:10.1186/s12933-017-0501-2

154. Das, U. N. & Rao, A. A. Gene expression profile in obesity and type 2 diabetes mellitus. *Lipids Health Dis.* (2007). doi:10.1186/1476-511X-6-35

155. Shen, J. & Zhu, B. Integrated analysis of the gene expression profile and DNA methylation profile of obese patients with type 2 diabetes. *Mol. Med. Rep.* (2018). doi:10.3892/mmr.2018.8804

156. Zhang, F. *et al.* Gene Expression Profile Analysis of Type 2 Diabetic Mouse Liver. *PLoS One* (2013). doi:10.1371/journal.pone.0057766

157. Lan, H. *et al.* Gene expression profiles of nondiabetic and diabetic obese mice suggest a role of hepatic lipogenic capacity in diabetes susceptibility. *Diabetes* (2003). doi:10.2337/diabetes.52.3.688

158. Fan, Q. *et al.* Gene expression profile in diabetic KK/Ta mice. *Kidney Int.* **64**, Gene expression profile in diabetic KK/Ta mice (2003).

159. Zhang, Y., Zhang, T. & Chen, Y. Comprehensive Analysis of Gene Expression Profiles and DNA Methylome reveals Oas1, Ppie, Polr2g as Pathogenic Target Genes of Gestational Diabetes Mellitus. *Sci. Rep.* (2018). doi:10.1038/s41598-018-34292-z

160. Yang, Y. L. *et al.* Gene expression profile of human skeletal muscle and adipose tissue of Chinese Han patients with type 2 diabetes mellitus. *Biomed. Environ. Sci.* (2009). doi:10.1016/S0895-3988(10)60012-8

161. Appa Rao, A., M, S. & Gedela, S. Microarray Analysis of Differentially Expressed Genes Between Diabetes vs Healthy. *J. Proteomics Bioinform.* **s1**, 55–65 (2008).

162. Li, H. *et al.* Identification of biomarkers and mechanisms of diabetic cardiomyopathy using microarray data. *Cardiol. J.* (2013). doi:10.5603/cj.a2018.0113

163. Li, N., Wu, H., Geng, R. & Tang, Q. Identification of core gene biomarkers in patients with diabetic cardiomyopathy. *Dis. Markers* (2018). doi:10.1155/2018/6025061

164. Zeng, L. Q. *et al.* Systematic profiling of mRNA and miRNA expression in the pancreatic islets of spontaneously diabetic Goto-Kakizaki rats. *Mol. Med. Rep.* (2015). doi:10.3892/mmr.2014.2723

165. Shen, Z., Zhang, S., Zou, C. C., Gu, W. Z. & Shang, S. Q. DNA microarray analysis of the gene expression profile of kidney tissue in a type 2 diabetic rat model. *Mol. Med. Rep.* (2010). doi:10.3892/mmr.2010.367

166. Cook, S. A., Rosenzweig, A. & Tomaselli, G. F. DNA microarrays: Implications for cardiovascular medicine. *Circulation Research* (2002). doi:10.1161/01.RES.0000036019.55901.62

167. Kittleson, M. M. & Hare, J. M. Molecular signature analysis: Using the myocardial transcriptome as a biomarker in cardiovascular disease. *Trends in Cardiovascular Medicine* (2005). doi:10.1016/j.tcm.2005.05.007

168. Kesherwani, V., Shahshahan, H. R. & Mishra, P. K. Cardiac transcriptome profiling of diabetic Akita mice using microarray and next generation sequencing. *PLoS One* **12**, 1–17 (2017).

169. Mauthe, M. *et al.* Chloroquine inhibits autophagic flux by decreasing autophagosome-

lysosome fusion. *Autophagy* (2018). doi:10.1080/15548627.2018.1474314

170. Yang, M. *et al.* Structural Basis for CoREST-Dependent Demethylation of Nucleosomes by the Human LSD1 Histone Demethylase. *Mol. Cell* (2006). doi:10.1016/j.molcel.2006.07.012

171. Yang, M. *et al.* Structural basis for the inhibition of the LSD1 histone demethylase by the antidepressant trans-2-phenylcyclopropylamine. *Biochemistry* (2007). doi:10.1021/bi700664y

172. Shi, Y. *et al.* Histone demethylation mediated by the nuclear amine oxidase homolog LSD1. *Cell* (2004). doi:10.1016/j.cell.2004.12.012

173. Baek, S. H. & Kim, K. Il. Epigenetic Control of Autophagy: Nuclear Events Gain More Attention. *Molecular Cell* (2017). doi:10.1016/j.molcel.2016.12.027

174. Xie, Z. *et al.* Improvement of cardiac functions by chronic metformin treatment is associated with enhanced cardiac autophagy in diabetic OVE26 mice. *Diabetes* (2011). doi:10.2337/db10-0351

175. Shirihai, O. S., Song, M. & Dorn, G. W. How mitochondrial dynamism orchestrates mitophagy. *Circulation Research* (2015). doi:10.1161/CIRCRESAHA.116.306374

176. Song, M., Mihara, K., Chen, Y., Scorrano, L. & Dorn, G. W. Mitochondrial fission and fusion factors reciprocally orchestrate mitophagic culling in mouse hearts and cultured fibroblasts. *Cell Metab.* (2015). doi:10.1016/j.cmet.2014.12.011

177. Ikeda, Y. *et al.* Endogenous Drp1 mediates mitochondrial autophagy and protects the heart against energy stress. *Circ. Res.* **116**, 264–278 (2015).

178. Yu, T., Robotham, J. L. & Yoon, Y. Increased production of reactive oxygen species in hyperglycemic conditions requires dynamic change of mitochondrial morphology. *Proc. Natl. Acad. Sci. U. S. A.* (2006). doi:10.1073/pnas.0511154103

179. Yu, T., Sheu, S. S., Robotham, J. L. & Yoon, Y. Mitochondrial fission mediates high glucose-induced cell death through elevated production of reactive oxygen species. *Cardiovasc. Res.* (2008). doi:10.1093/cvr/cvn104

180. Yu, T., Jhun, B. S. & Yoon, Y. High-glucose stimulation increases reactive oxygen species production through the calcium and mitogen-activated protein kinase-mediated activation of mitochondrial fission. *Antioxidants Redox Signal.* (2011). doi:10.1089/ars.2010.3284